



SSI report

# SSI Rapport 2008:07

Rapport från Statens strålskyddsinstitut  
tillgänglig i sin helhet via [www.ssi.se](http://www.ssi.se)

## SKI Rapport 2008:24

### *Modelling of long term geochemical evolution and study of mechanical perturbation of bentonite buffer of a KBS-3 repository*

François Marsal, Laurent de Windt, Delphine Pellegrini,  
Frédéric Deleruyelle and Christophe Serres

**SKi** STATENS KÄRNKRAFTINSPEKTION  
Swedish Nuclear Power Inspectorate



*Statens strålskyddsinstitut*  
Swedish Radiation Protection Authority

# SSI's Activity Symbols



## Ultraviolet, solar and optical radiation

Ultraviolet radiation from the sun and solariums can result in both long-term and short-term effects. Other types of optical radiation, primarily from lasers, can also be hazardous. SSI provides guidance and information.

---



## Solariums

The risk of tanning in a solarium are probably the same as tanning in natural sunlight. Therefore SSI's regulations also provide advice for people tanning in solariums.

---



## Radon

The largest contribution to the total radiation dose to the Swedish population comes from indoor air. SSI works with risk assessments, measurement techniques and advises other authorities.

---



## Health care

The second largest contribution to the total radiation dose to the Swedish population comes from health care. SSI is working to reduce the radiation dose to employees and patients through its regulations and its inspection activities.

---



## Radiation in industry and research

According to the Radiation Protection Act, a licence is required to conduct activities involving ionising radiation. SSI promulgates regulations and checks compliance with these regulations, conducts inspections and investigations and can stop hazardous activities.

---



## Nuclear power

SSI requires that nuclear power plants should have adequate radiation protection for the general public, employees and the environment. SSI also checks compliance with these requirements on a continuous basis.

---



## Waste

SSI works to ensure that all radioactive waste is managed in a manner that is safe from the standpoint of radiation protection.

---



## Mobile telephony

Mobile telephones and base stations emit electromagnetic fields. SSI is monitoring developments and research in mobile telephony and associated health risks.

---



## Transport

SSI is involved in work in Sweden and abroad to ensure the safe transportation of radioactive substances used in the health care sector, industrial radiation sources and spent nuclear fuel.

---



## Environment

"A safe radiation environment" is one of the 15 environmental quality objectives that the Swedish parliament has decided must be met in order to achieve an ecologically sustainable development in society. SSI is responsible for ensuring that this objective is reached.

---



## Biofuel

Biofuel from trees, which contains, for example from the Chernobyl accident, is an issue where SSI is currently conducting research and formulating regulations.

---



## Cosmic radiation

Airline flight crews can be exposed to high levels of cosmic radiation. SSI participates in joint international projects to identify the occupational exposure within this job category.

---



## Electromagnetic fields

SSI is working on the risks associated with electromagnetic fields and adopts countermeasures when risks are identified.

---



## Emergency preparedness

SSI maintains a round-the-clock emergency response organisation to protect people and the environment from the consequences of nuclear accidents and other radiation-related accidents.

---



## SSI Education

is charged with providing a wide range of education in the field of radiation protection. Its courses are financed by students' fees.

**EDITORS / REDAKTÖRER :** François Marsal<sup>1)</sup>, Laurent de Windt<sup>2)</sup>, Delphine Pellegrini<sup>1)</sup>, Frédéric Deleruyelle<sup>1)</sup> and Christophe Serres<sup>1)</sup>

1) French Institute for Radiological Protection and Nuclear Safety (IRSN)

2) Paris School of Mines (ENSMP)

**TITLE / TITEL:** Modelling of long term geochemical evolution and study of mechanical perturbation of bentonite buffer of a KBS-3 repository / Modellering av långsiktigt geokemisk utveckling samt studie av mekanisk störning i bentonitbuffert i ett KBS-3 slutförvar.

**DEPARTMENT / AVDELNING:** Department of Nuclear Facilities and Waste Management / Avdelningen för kärnteknik och avfall

**SUMMARY:** PART I: The Swedish Nuclear Fuel and Waste Management Co. (SKB) has recently completed a safety assessment project named SR-Can, related to the KBS-3 disposal concept. In this concept, the waste packages are surrounded by a buffer made of either MX-80 or Deponit CA-N bentonite. Interactions between the buffer and groundwater may modify the buffer composition and thus its containment properties. The Swedish Radiation Protection Authorities (SSI) requested the French Institute for Radiological Protection and Nuclear Safety (IRSN) to perform the present study in support of SSI review of the SR-Can report. The purpose is to assess the geochemical evolution of both potential buffer materials due to the intrusion of different types of groundwater, with a similar modelling layout to that reported in SR-Can and detailed in Arcos et al. (2006). Three main categories of water inflows via a fracture intersecting a deposition hole are considered: the Forsmark reference groundwater, a high-salinity groundwater to account for up-rise of deep-seated brines and a diluted water representing ice-melting derived-groundwater. In addition to this, the redox buffering capacity of Deponit CA-N bentonite and the thermal effect on MX-80 bentonite geochemistry have been assessed. This modelling work has been performed using the reactive transport modelling code HYTEC.

The main outcome of the present study is that the intrusion of the considered groundwaters should not affect drastically the geochemistry of neither the Deponit CA-N nor the MX-80 bentonite on the long-term (100,000 y). Bentonite pH may reach high values (up to 10.5) in some cases but does not reach SKB criterion value related to bentonite chemical stability. Dissolution-precipitation of accessory minerals is not significant enough to induce important porosity changes (rise by maximum 2 %). Globally, the montmorillonite exchanger undergoes Na by Ca partial replacement, which may decrease the swelling pressure of the bentonite. The simulated intrusion of oxidizing waters lead to a limited perturbation, i.e. localized within bentonite near the fracture plane level. Actually, the calculated evolutions are relatively slow, so that in some cases the buffer remains in a transient stage over the whole simulation period and thus could turn heterogeneous in geochemical properties. Regarding the effect of temperature, a heterogeneous evolution is again observed, with moderate to slight dissolution-precipitation reactions either on the inner or outer border of the buffer (warmer and cooler zones) depending on the accessory minerals. These main trends in bentonite geochemical evolutions are in good agreement with the results presented in SR-Can and in Arcos et al. (2006), though some discrepancies have been pointed out, that can be explained by differences in modelling input data (mainly regarding log K values). Finally, issues in terms of processes and data would worth being further investigated as they might have a significant influence on bentonite evolutions, such as the thermo-hydraulic coupling of processes during the initial transient phase or the stability of montmorillonite.

PART II: Elements of the SR-Can project relative to piping and erosion phenomena of bentonite components of a KBS-3 repository are analysed with regard to the experience feedback available at IRSN and consisting in experimental results obtained on samples at the UJF-Grenoble between 2000 and 2004. A synthesis of these tests is presented, with a closer attention to the Argillite/Bentonite tests during which phenomena of erosion occurred. The reference evolution of a KBS-3 repository, the resaturation and swelling kinetics of backfills and buffers and the possibility for a buffer to swell upwards the backfill have been considered. According to the reviewed documents, IRSN notes that the SR-Can project tackles the piping and erosion phenomena with local modellings and "rough estimates", the latter being based on 3 "key" parameters: the water inflow in an underground opening, the concentration of bentonite in pipe water and the duration of the phenomena. IRSN considers that the reviewed elements do not evidence enough the conservatism of the parameters value, especially for the duration of the phenomena. Additional experimental results, at small and large scale, may be necessary.

SSI rapport: 2008:07

mars 2008

ISSN 0282-4434

*The conclusions and viewpoints presented in the report are those of the authors and do not necessarily coincide with those of the SSI.*

Författarna svarar själva för innehållet i rapporten.



Statens strålskyddsinstitut  
Swedish Radiation Protection Authority



STATENS KÄRNKRAFTINSPEKTION  
Swedish Nuclear Power Inspectorate

**SAMMANFATTNING:** DEL I: Svensk Kärnbränslehantering AB (SKB) har nyligen genomfört en säkerhetsanalys, SR-Can, som baseras på KBS-3 metoden. Viktiga komponenter utgörs av kopparkapslar som omges av en buffert som består av kompakterad lera (antigen MX-80 bentonit eller Deponit CA-N bentonit). Växelverkan mellan bufferten och grundvattnet kan modifiera buffertens kemiska sammansättning och påverka dess isoleringsförmåga. På SSI:s och SKI:s begäran har IRSN (Institut de Radioprotection et de Sûreté Nucléaire) utfört denna studie som ett stöd för myndigheternas granskning av SR-Can. Syftet är att utvärdera den geokemiska utveckling av bufferten som orsakas av inträngande grundvatten med olika kemiska sammansättningar. Modellkonceptet som används i denna studie är likartad den metod som används i SKB:s motsvarande modellering (Arcos et al., 2006). Tre typer av grundvatten har beaktats: ett referensgrundvatten från Forsmark; ett saltvatten som representerar uppströmmande djupt belägna grundvattnen, samt ett utspätt grundvatten som bildas från glaciala smältvatten. Dessutom har redoxbuffringskapacitet i Deponit CA-N bentonit samt termisk inverkan på MX-80 utvärderats. Denna modellering har utförts med hjälp av den numeriska koden HYTEC.

Huvudslutsatsen är att inträngningen av olika typer av grundvatten inte ens på lång sikt (upp till 100 000 år) kommer att väsentligt påverka buffertens geokemiska egenskaper för vare sig MX-80 bentonit eller Deponit CA-N bentonit. Bentonitens pH kan möjligen i vissa fall öka väsentligt (upp till pH 10,5) men pH förblir ändå lägre än SKB:s gränsvärde för buffertens kemiska stabilitet. Upplösning/utfällning av accessoriska mineral är inte tillräckligt omfattande för att åstadkomma betydelsefull porositetsförändring i bufferten (porositeten ökar maximalt med 2 %). Modelleringsresultaten visar att det pågår en jonbytesprocess på montmorillonit mineralens yta då Na utbyts med Ca. Detta kan möjligen minska bentonitens svälltryck. Numerisk simulering av inträngningen av oxiderande grundvatten leder till en begränsad störning i bentoniten nära inflödespunkten för en korsande sprickan. Den beräknade kemiska utvecklingen är i detta fall relativt långsam. För vissa egenskaper är bufferten fortfarande i ett transient skede genom hela simuleringssperioden och heterogenitet i buffertens geokemiska egenskaper kan då förekomma. Temperaturenns påverkan leder också till heterogen utveckling med måttlig eller obetydlig upplösning/utfällning av accessoriska mineral på både in- och utsidan av bufferten (varmare och kallare zoner). Dessa huvudsakliga tendenser för den geokemiska utvecklingen överensstämmer med SKB:s resultat (Arcos et al., 2006). Vissa avvikelser förekommer dock som kan förklaras med att andra termodynamiska indata (huvudsakligen log K) har använts i den föreliggande studien. Slutligen påpekas att mera studier behövs för att utvärdera betydelsen av indata och den exakta formuleringen av processerna i modelleringen. De har stor inverkan på bentonitens utveckling såsom den kopplade termisk-hydrauliska utvecklingen i det initiala transienta skedet och stabiliteten för montmorillonit.

DEL II: Fenomenet piping/erosion som redovisas i SKB:s SR-Can projekt har analyserats med hjälp av tidigare erfarenheter från IRSN:s experimentella försök mellan 2000 och 2004 på Université Joseph Fourier i Grenoble (UJG). En sammanfattning av försöken presenteras med fokus på de försök där erosion av argillit/bentonit har förekommit. Referensutvecklingen för ett KBS-3 förvar, återmättnad och svällningskinetik för buffert/återfyllning samt förekomsten av en uppåtgående svällning i bufferten har beaktats. Genom granskning av de dokument som ingår i SR-Can redovisningen noterar IRSN att SKB har hanterat piping/erosionen med lokala modeller och ”grov uppskattning”. Det sistnämnda angreppssättet är baserat på 3 nyckelparametrar: vatteninflödet in i en öppen förvarsanläggning innan förslutning, koncentrationen av bentonitpartiklar i grundvatten vid kanalbildning, samt varaktigheten av fenomenet. IRSN anser att det resonemanget i SR-Can inte ger tillräckligt stöd för de konservativa parametervärdena som valts i SR-Can, särskilt när det gäller varaktigheten av piping/erosion. Ytterligare experimentella försök i både liten och stor skala behöver genomföras.

## Foreword

The work presented in this report is part of the Swedish Nuclear Power Inspectorate's (SKI) and the Swedish Radiation Protection Authority's (SSI) SR-Can review project.

The Swedish Nuclear Fuel and Waste Management Co (SKB) plans to submit a license application for the construction of a repository for spent nuclear fuel in Sweden 2010. In support of this application SKB will present a safety report, SR-Site, on the repository's long-term safety and radiological consequences. As a preparation for SR-Site, SKB published the preliminary safety assessment SR-Can in November 2006. The purposes were to document a first evaluation of long-term safety for the two candidate sites at Forsmark and Laxemar and to provide feedback to SKB's future programme of work.

An important objective of the authorities' review of SR-Can is to provide guidance to SKB on the complete safety reporting for the license application. The authorities have engaged external experts for independent modelling, analysis and review, with the aim to provide a range of expert opinions related to the sufficiency and appropriateness of various aspects of SR-Can. This report is one of those external experts' review reports, compiled by consultants at the French Institute for Radiological Protection and Nuclear Safety (IRSN). The report consists of two parts: Part I presents modelling of the long-term geochemical evolution of the bentonite buffer independent of SKB's approach. In Part II issues of mechanical perturbation such as piping/erosion have been reviewed.

The conclusions and judgements in this report are those of the authors and may not necessarily coincide with those of SKI and SSI. The authorities own review will be published separately (SKI Report 2008:23, SSI Report 2008:04 E).

Björn Dverstorp (project leader SSI)

Bo Strömberg (project leader SKI)

## Förord

Denna rapport är en underlagsrapport till Statens kärnkraftinspektion (SKI) och Statens strålskyddsinstitut (SSI) gemensamma granskning av Svensk Kärnbränslehantering AB:s (SKB) säkerhetsredovisning SR-Can.

SKB planerar att lämna in en ansökan om uppförande av ett slutförvar för använt kärnbränsle i Sverige under 2010. Som underlag till ansökan kommer SKB presentera en säkerhetsrapport, SR-Site, som redovisar slutförvarets långsiktiga säkerhet och radiologiska konsekvenser. Som en förberedelse inför SR-Site publicerade SKB den preliminära säkerhetsanalysen SR-Can i november 2006. Syftena med SR-Can är bl.a. att redovisa en första bedömning av den långsiktiga säkerheten för ett KBS-3-förvar vid SKB:s två kandidatplatser Laxemar och Forsmark och att ge återkoppling till SKB:s fortsatta arbete.

Myndigheternas granskning av SR-Can syftar till att ge SKB vägledning om förväntningarna på säkerhetsredovisningen inför den planerade tillståndsansökan. Myndigheterna har i sin granskning tagit hjälp av externa experter för oberoende modellering, analys och granskning. Denna rapport är en del av den externa expertgranskningen. Rapporten har skrivits av experter på Institut de Radioprotection et de Sûreté Nucléaire (IRSN) i Frankrike. Det finns två delar i rapporten. Del I redovisar oberoende modellering av den långsiktiga geokemiska utvecklingen av bufferten i slutförvaret. I del II granskas SKB:s redovisning i SR-Can av mekaniska processer såsom kanalbildning (piping/erosion) i bufferten.

Slutsatserna i denna rapport är författarnas egna och överensstämmer inte nödvändigtvis med SKI:s eller SSI:s ställningstaganden. Myndigheternas egen granskning publiceras i en annan rapport (SKI Rapport 2008:19; SSI Rapport 2008:04).

Björn Dverstorp (projektledare SSI)

Bo Strömberg (projektledare SKI)

## ABSTRACT

The Swedish Nuclear Fuel and Waste Management Co. (SKB) has recently completed a safety assessment project named SR-Can, related to the KBS-3 disposal concept. In this concept, the waste packages are surrounded by a buffer made of either MX-80 or Deponit CA-N bentonite. Interactions between the buffer and groundwater may modify the buffer composition and thus its containment properties. The Swedish Radiation Protection Authorities (SSI) requested the French Institute for Radiological Protection and Nuclear Safety (IRSN) to perform the present study in support of SSI review of the SR-Can report. The purpose is to assess the geochemical evolution of both potential buffer materials due to the intrusion of different types of groundwater, with a similar modelling layout to that reported in SR-Can and detailed in Arcos *et al.* (2006). Three main categories of water inflows via a fracture intersecting a deposition hole are considered: the Forsmark reference groundwater, a high-salinity groundwater to account for up-rise of deep-seated brines and a diluted water representing ice-melting derived-groundwater. In addition to this, the redox buffering capacity of Deponit CA-N bentonite and the thermal effect on MX-80 bentonite geochemistry have been assessed. This modelling work has been performed using the reactive transport modelling code HYTEC.

The main outcome of the present study is that the intrusion of the considered groundwaters should not affect drastically the geochemistry of neither the Deponit CA-N nor the MX-80 bentonite on the long-term (100,000 y). Bentonite pH may reach high values (up to 10.5) in some cases but does not reach SKB criterion value related to bentonite chemical stability. Dissolution-precipitation of accessory minerals is not significant enough to induce important porosity changes (rise by maximum 2 %). Globally, the montmorillonite exchanger undergoes Na by Ca partial replacement, which may decrease the swelling pressure of the bentonite. The simulated intrusion of oxidizing waters lead to a limited perturbation, i.e. localized within bentonite near the fracture plane level. Actually, the calculated evolutions are relatively slow, so that in some cases the buffer remains in a transient stage over the whole simulation period and thus could turn heterogeneous in geochemical properties. Regarding the effect of temperature, a heterogeneous evolution is again observed, with moderate to slight dissolution-precipitation reactions either on the inner or outer border of the buffer (warmer and cooler zones) depending on the accessory minerals. These main trends in bentonite geochemical evolutions are in good agreement with the results presented in SR-Can and in Arcos *et al.* (2006), though some discrepancies have been pointed out, that can be explained by differences in modelling input data (mainly regarding log K values). Finally, issues in terms of processes and data would worth being further investigated as they might have a significant influence on bentonite evolutions, such as the thermo-hydraulic coupling of processes during the initial transient phase or the stability of montmorillonite.



# TABLE OF CONTENTS

ABSTRACT .....	1
LIST OF FIGURES .....	4
LIST OF TABLES .....	6
1 INTRODUCTION .....	7
2 MODELLING FEATURES .....	9
2.1 REACTIVE TRANSPORT CODE HYTEC.....	9
2.1.1 Main concepts and equations.....	9
2.1.2 Discretization and coupling schemes.....	9
2.1.3 Kinetics of geochemical processes .....	10
2.1.4 Cation exchange and surface complexation .....	10
2.2 THERMODYNAMIC AND KINETIC DATA .....	12
2.2.1 Aqueous chemistry and dissolution/precipitation reactions.....	12
2.2.2 Cation exchange and surface complexation .....	13
2.3 GEOMETRICAL DESIGN: KBS-3 CONCEPT AND SIMULATION GRIDS .....	14
2.4 GEOCHEMISTRY AND MINERALOGY.....	15
2.4.1 Groundwaters .....	15
2.4.2 Deponit CA-N bentonite .....	17
2.4.3 MX-80 bentonite .....	18
2.4.4 Waste package and host rock.....	18
2.5 FLOW AND SOLUTE TRANSPORT PARAMETERS .....	21
2.5.1 Bentonites and fracture .....	21
3 DEPONIT CA-N BENTONITE/GROUNDWATER LONG-TERM INTERACTIONS .....	22
3.1 REFERENCE CASE, THE FORSMARK GROUNDWATER .....	22
3.2 HIGH-SALINITY WATER INTRUSION, THE LAXEMAR GROUNDWATER .....	29
3.3 ICE-MELTING WATER INTRUSION, THE GRIMSEL GROUNDWATER .....	35
3.4 SENSITIVITY ANALYSIS .....	38
3.4.1 Gypsum equilibrium constants .....	38
3.4.2 Activity correction models.....	40
3.4.3 Numerical considerations .....	40
4 MX-80 BENTONITE/GROUNDWATER LONG-TERM INTERACTIONS.....	43
4.1 REFERENCE CASE, THE FORSMARK GROUNDWATER .....	43
4.2 HIGH-SALINITY WATER INTRUSION, THE LAXEMAR GROUNDWATER .....	48
4.3 ICE-MELTING WATER INTRUSION, THE GRIMSEL GROUNDWATER .....	53
5 DURABILITY OF THE DEPONIT CA-N REDOX BUFFERING CAPACITY.....	57
5.1 CONTEXT.....	57
5.2 INTRUSION OF ICE-MELTING WATER WITH INCREASING OXYGEN CONTENTS.....	58
6 THERMAL EFFECT ON MX-80 BENTONITE.....	64
7 SUMMARY AND CROSS-COMPARISON OF SIMULATED CASES .....	71
8 CONCLUSION .....	74
9 REFERENCES.....	76
APPENDIX.....	78

# LIST OF FIGURES

Figure 2-1. Simplified representation of a montmorillonite clay structure. ....	11
Figure 2-2. Schematic view of the KBS-3 disposal concept (SKB, 2006) and representation of the simulated subsystem with an hypothetical fracture plane. ....	16
Figure 2-3. Calculation grid representative for the cross-section at the level of the fracture plane.....	17
Figure 2-4. Calculation grid representative for the cylindrical geometry (rotation around the z axis, perpendicularly to the fracture plane). ....	17
Figure 2-5. Advective flow (Darcy velocity) in the fracture plane; coarser grid for a better visualization of the flow field. ....	21
Figure 3-1. Reference case with Deponit CA-N bentonite: evolution of pH and pe over 100,000 y. ....	24
Figure 3-2. Reference case with Deponit CA-N bentonite: evolution of exchangeable Ca (top), Na (middle) and Mg (bottom) populations over 100,000 y. ....	25
Figure 3-3. Reference case with Deponit CA-N bentonite: evolution of gypsum (top), dolomite (middle) and calcite (bottom) contents over 100,000 y. ....	26
Figure 3-4. Pourbaix/pe-pH diagram of iron (Fe, HCO <sub>3</sub> and SO <sub>4</sub> concentrations identical to those of the initial pore water of the Deponit CA-N). ....	27
Figure 3-5. Reference case with Deponit CA-N bentonite: evolution of the porosity over 100,000 y. ....	27
Figure 3-6. Reference case with Deponit CA-N bentonite: evolution of pH and pe over the first 10,000 y. ....	28
Figure 3-7. Reference case with Deponit CA-N bentonite: evolution of exchangeable Na and Ca populations over the first 10,000 y. ....	28
Figure 3-8. High-salinity water intrusion in Deponit CA-N bentonite: evolution of pH and pe over 100,000 y. ....	31
Figure 3-9. High-salinity groundwater intrusion in Deponit CA-N bentonite: evolution of pyrite (top) and siderite (bottom) contents over 100,000 y. ....	32
Figure 3-10. High-salinity water intrusion in Deponit CA-N bentonite: evolution of DPN-OH <sub>2</sub> <sup>+</sup> site concentration (top) and exchangeable Ca population (bottom) over 100,000 y. ....	33
Figure 3-11. High-salinity groundwater intrusion in Deponit CA-N bentonite: evolution of pore water chemistry, cation exchange population and mineralogy in the bentonite, 50 cm above the fracture level. ....	34
Figure 3-12. Evolution with time of cumulative flux of carbonate, chloride and sulfate ions in the full volume of the bentonite buffer and in the zone around the canister (5 cm width). ....	34
Figure 3-13. Ice-melting water intrusion in Deponit CA-N bentonite: evolution of pH and pe over 100,000 y. ....	36
Figure 3-14. Ice-melting water intrusion in Deponit CA-N bentonite: evolution of exchangeable Ca (top) and Na (bottom) populations over 100,000 y. ....	37
Figure 3-15. Ice-melting water intrusion in Deponit CA-N bentonite: evolution of calcite (top) and dolomite (bottom) over 100,000 y. ....	38
Figure 3-16. Influence of the Log K value selected for gypsum on the stability of this mineral: evolution of gypsum concentration at 10,000 and 50,000 y for the reference case with Deponit CA-N Bentonite. ....	39
Figure 3-17. Highly-saline groundwater intrusion, modelling results obtained with an iterative sequential coupling and an adaptative time step (left) and with a non iterative sequential coupling and a fixed time step of 1 y (right). ....	41

Figure 3-18. Illustration of mass distributions for FV and FE approaches. Too much mass is defined for uncorrected FE approach. ....	41
Figure 3-19. Highly-saline groundwater intrusion, the number of nodes is increased by a factor 4 between the top and bottom graphs. ....	42
Figure 4-1. Reference case with MX-80 bentonite: evolution of pH and pe over 100,000 y. ....	44
Figure 4-2. Reference case with MX-80 bentonite: evolution of exchangeable Ca (top) and Na (bottom) populations over 100,000 y. ....	45
Figure 4-3. Reference case with MX-80 bentonite: evolution of exchangeable Na and Ca populations as a function of time over 100,000 y at two points, located at 0.5 and 3.9 m above the fracture level as defined in the figure on the right. ....	46
Figure 4-4. Reference case with MX-80 bentonite: evolution of gypsum content over 5,000 y. ....	46
Figure 4-5. Reference groundwater intrusion in with MX-80 bentonite with carbonate minerals: evolution of pH and calcite content over 100,000 y. ....	47
Figure 4-6. Reference groundwater intrusion in with MX-80 bentonite with carbonate minerals: evolution of aqueous carbonate concentration (top) and pH (bottom) at two points, located at 0.5 and 3.9 m above the fracture level as defined in Figure 4-3. ....	48
Figure 4-7. High-salinity water intrusion in MX-80 bentonite: evolution of pH and pe over 100,000 y. ....	50
Figure 4-8. High-salinity water intrusion in MX-80 bentonite: evolution of exchangeable Ca (top), Na (middle) and Mg (bottom) populations over 100,000 y. ....	51
Figure 4-9. High-salinity water intrusion in MX-80 bentonite with carbonate minerals: evolution of pH over 100,000 y. ....	52
Figure 4-10. High-salinity water intrusion in MX-80 bentonite with carbonate minerals: evolution of calcite and siderite contents as a function of time over 100,000 y at two points, located at 0.5 m (left) and 3.9 m (right) above the fracture level as defined in Figure 4-3. ....	52
Figure 4-11. Ice-melting water intrusion in MX-80 bentonite: evolution of pH and pe over 100,000 y. ....	54
Figure 4-12. Ice-melting water intrusion in MX-80 bentonite: evolution of exchangeable Ca (top), Na (bottom) populations over 100,000 y. ....	55
Figure 4-13. Ice-melting water intrusion in MX-80 bentonite with carbonate minerals: evolution of pH (top), calcite content (middle) and exchangeable Ca (bottom) over 100,000 y. ....	56
Figure 5-1. Titration of a siderite/pyrite buffer by dissolved oxygen assuming thermodynamic equilibrium (left); kinetic rate of oxygen consumption by siderite and pyrite according to pH and oxygen fugacity (right). ....	58
Figure 5-2. Ice-melting groundwater intrusion in Deponit CA-N bentonite ( $fug O_2 = 0.04$ ), evolution of pH (top), pe and the dissolved oxygen content over 90,000 y. ....	60
Figure 5-3. Ice-melting groundwater intrusion in Deponit CA-N bentonite ( $fug O_2 = 0.04$ ), cross-section through the bentonite buffer showing the interdependency between the redox state (pe) and the redox-poising minerals. ....	61
Figure 5-4. Ice-melting groundwater intrusion in Deponit CA-N bentonite ( $fug O_2 = 0.04$ ), progressive dissolution of pyrite and siderite yielding precipitation of secondary ferrihydrite (at 90,000 y). ....	61
Figure 5-5. Ice-melting groundwater intrusion in Deponit CA-N bentonite ( $fug O_2 = 0.04$ ), pyrite, siderite and secondary iron-mineral contents calculated at 90,000 y considering either ferrihydrite (top) or goethite precipitation. ....	62
Figure 5-6. Ice-melting groundwater intrusion in Deponit CA-N bentonite, extension of the pyrite dissolution front at 90,000 y as a function of the oxygen fugacity. ....	63

Figure 6-1. Thermal evolution of the near field (Arcos *et al.*, 2006). .....64

Figure 6-2. Constant temperature field modelled over 1,000 y. The temperature of the bentonite inner border is set at 80°C while that at its outer border is set at 65°C. ....65

Figure 6-3. Thermal effect on MX-80 bentonite without initial carbonate minerals: evolution of pH and aqueous carbonate contents over 1,000 y. ....67

Figure 6-4. Thermal effect on MX-80 bentonite without initial carbonate minerals: evolution of exchangeable Ca (top) and Na (bottom) populations over 1,000 y. ....68

Figure 6-5. Thermal effect on MX-80 bentonite without initial carbonate minerals: evolution of dolomite (top), anhydrite (middle) and quartz (bottom) contents over 1,000 y. Note that for a better observation, scale bars have been limited to a very narrow range. ....69

Figure 6-6. Thermal effect on MX-80 bentonite with carbonate minerals in its initial composition: evolution of siderite (top) and pyrrhotite (bottom) contents over 1,000 y. ....70

## LIST OF TABLES

Table 2-1. Cation exchange and surface complexation data. ....14

Table 2-2. Chemical composition of the groundwaters and bentonite pore waters. ....19

Table 2-3. Saturation indices calculated for groundwaters and bentonite pore waters. ....20

Table 2-4. Flow and transport parameters selected for bentonite and fracture zones. ....21

Table 3-1. Gypsum formation constant ( $\text{Ca}^{2+} + \text{SO}_4^{2-} + \text{H}_2\text{O} \rightarrow \text{CaSO}_4 \cdot \text{H}_2\text{O}$ ) from various thermodynamic databases..39

Table 6-1. Chemical composition of MX-80 bentonite pore water at 80°C and 15°C. ....65

# 1 INTRODUCTION

The Swedish Nuclear Fuel and Waste Management Co. (SKB) has recently completed a safety assessment project named SR-Can, as a preparatory stage for the next assessment SR-Site that will be used in support of SKB's application for a final deep underground disposal of high-level long-lived radioactive waste. The Swedish Radiation Protection Authorities (SSI), which reviews the SR-Can report, requested the French Institute for Radiological Protection and Nuclear Safety (IRSN) to perform independent study and technical appraisal on some geochemical and mechanical aspects of the SR-Can report in support of SSI review process. The present document focuses on geochemical issues, as described hereafter. A second document (IRSN, DSU/SSIAD n°2) is issued on mechanical concerns.

The safety assessment project SR-Can (SKB, 2006) relates to the KBS-3 disposal concept, in which copper canisters containing spent nuclear fuel are emplaced in a granitic rock at a depth of approximately 500 m, in vertical holes equipped with a surrounding engineered component made of bentonite clay. The primary safety function of the KBS-3 concept is to completely isolate the waste and should isolation be breached, the secondary safety function is to retard a potential release from the repository. The bentonite buffer contributes to these main safety functions of isolation and retardation through subordinate functions, among which:

- to prevent advective transport in the deposition hole, so as to limit the inflow of dissolved copper corroding agents to the canister, thereby providing canister protection against corrosion (isolation function);
- to slow transport of potential radionuclide releases from the canister, by avoiding advection, providing sorption and ensuring that radionuclide release will be limited by their solubility (retardation function).

Another important issue related to the buffer is to preserve reducing conditions so as to provide a chemical environment favourable to low canister corrosion rates, to a stable fuel matrix and to low radionuclide solubility.

Interactions between the buffer and groundwater may modify the buffer composition and thus its chemical and hydraulic containment properties. The evaluation of the potential geochemical evolutions due to such interactions is therefore required for safety assessment purpose. Arcos *et al.* (2006) developed a numerical model with this aim, which addresses the influence on near-field geochemistry of the intrusion of various types of water for a range of conditions and assumptions, using the reactive transport code PHAST.

In the frame of the SR-Can review, SSI requested IRSN to perform a geochemical modelling of the buffer evolution with the same or similar layout to that presented in Arcos *et al.* (2006), completed with a specific point related to the handling of ion exchange reactions with solute transport and the assessment of the durability of the reducing capacity of the buffer.

The present work thus addresses the geochemical perturbations due to the intrusion of waters into the bentonite buffer, via a fracture in the Host-rock intersecting a deposition hole, on the basis of reactive transport modelling using the code HYTEC. In the following, the section 2 is devoted to the presentation of the modelling features

(code HYTEC, thermodynamic and kinetic data, geometrical design, geochemical and hydraulic parameters). Simulations results are reported in next sections, in terms of calculated changes in geochemical master-characteristics which control the chemical and hydraulic containment properties of the bentonite, namely pH and pe (stability of bentonite and radionuclide solubility), exchanged ion populations and mineralogy (hydraulic properties related to swelling pressure and porosity). A particular attention is given to the processes that control the evolution of these characteristics. When appropriate, the variations in concentration of aqueous species in bentonite pore water are also commented, in a first attempt, especially with regards to corrosion. More precisely, section 3 documents the simulations performed considering the interaction of Deponit CA-N bentonite with three categories of inflowing waters, i.e. the Forsmark reference groundwater, a high-salinity groundwater to account for up-rise of deep-seated brines and diluted water for ice-melting derived-groundwater. This section also describes some sensitivity analysis calculations to modelling features. Section 4 presents the same kind of simulations but with a different buffer, i.e. MX-80 bentonite. The redox buffering capacity of Deponit CA-N bentonite is assessed in section 5, whereas section 6 focuses on the influence of the transient thermal phase in the case where MX-80 bentonite interacts with the reference groundwater. A summary of the whole sets of calculation results is given in section 7 together with a cross-comparison, between the simulation cases treated in the present study on the one hand and with respect to the outcomes from Arcos *et al.* (2006) on the other hand. At last, the main outlines of each simulation case are recapitulated as a summarizing table in an appendix.

## 2 MODELLING FEATURES

### 2.1 REACTIVE TRANSPORT CODE HYTEC

#### 2.1.1 MAIN CONCEPTS AND EQUATIONS

HYTEC (van der Lee *et al.* (2003); van der Lee (2005)) is a reactive transport code commonly used for transport in porous media under saturated and unsaturated conditions. This numerical code simulates advective and diffusive transport of solutes coupled with chemical reactions (aqueous chemistry, dissolution/precipitation of minerals, cation exchange and surface complexation) at equilibrium or with kinetic control. Transport is coupled to chemistry according to the following equation in a saturated medium:

$$\frac{\partial \omega c_i}{\partial t} = \nabla \cdot (D_d \nabla c_i - c_i U) - \frac{\partial \omega \bar{c}_i}{\partial t},$$

where the dispersive/diffusive coefficient,  $D_d = D_e + \alpha U$ ,  $D_e$  is the effective diffusion coefficient,  $\alpha$  the dispersivity,  $U$  the Darcy velocity,  $\omega$  is the porosity. The velocity field  $U$  can be obtained from the hydraulic conductivity  $K$  and Darcy's law. Note that the porosity is explicitly included in the equation since this entity is subject to change in time and space due to geochemical processes such as precipitation, dissolution or clogging of pores by colloidal retention. The terms  $c_i$  and  $\bar{c}_i$  are respectively the mobile and immobile concentrations of a species per unit volume of solution. The fixed or solid fraction is evaluated on the basis of chemical calculations, whereas the aqueous fraction is a function of chemical and transport processes.

#### 2.1.2 DISCRETIZATION AND COUPLING SCHEMES

HYTEC code solves the multi-component transport problem according to operator splitting method combined with a sequential iterative approach and a severe, normalized convergence criterion. Transport and chemistry are solved one after the other within a single time-step. Since both parts are dependent on each other, an accurate solution is obtained only after several iterations within the time-step. Different studies demonstrate the importance of iterative improvement when applying the sequential approach (see references in van der Lee *et al.*, 2003). HYTEC recovers from diverging or slowly converging situations by reducing the current time-step. Inversely, the code increases the time-step when possible. Hence HYTEC adapts the time step to the numerical stiffness of the problem.

HYTEC is strongly coupled, e.g. hydraulic conductivity and diffusion parameters might evolve when mineral precipitation or dissolution changes the local porosity. Therefore, HYTEC allows accounting for clogging by precipitation, or to the contrary, for porosity increase by leaching of minerals (De Windt *et al.*, 2004). This option has not been used for the present study since the porosity appeared to be almost constant throughout preliminary simulations.

Chemistry is solved by the "basis component" method according to an improved Newton-Raphson algorithm enhanced by a polishing factor to improve its global convergence capacity. The corresponding chemical module is

called JCHESS (van der Lee and De Windt, 2002). The R2D2 hydrodynamic code (Lagneau, 2003) (computing flow and advective-dispersive-diffusive transport) is coupled with JCHESS in the HYTEC platform. R2D2 is based on a finite volume (FV) approach which is particularly useful for treatment of the variable porosity problem. This code uses a flexible grid based on Thiesen polygons and hence is easily adapted to complex geometries, albeit currently limited to 2D cylindrical or Cartesian coordinates.

### 2.1.3 KINETICS OF GEOCHEMICAL PROCESSES

HYTEC is structured with respect to the local thermodynamic equilibrium approach but kinetics can be optionally introduced for dissolution and precipitation of solid phases, microbiology-mediated reactions and sorption/desorption processes. The following kinetic formula for a solid (mineral, colloidal) species,  $S$ , is for the present study:

$$\frac{d[M]}{dt} = k \cdot A_v \prod_i (A_i)^{a_i} \left( \left( \frac{Q}{K_s} \right)^p - 1 \right)$$

where  $k$  denotes a kinetic constant in mol/m<sup>2</sup>/s;  $A_v$  is the volumetric surface area expressed in m<sup>2</sup>/m<sup>3</sup>;  $p$  is an arbitrary power-constant used to fit the law to experimental data;  $Q/K_s$  is the saturation state;  $a_i$  is a factor including reaction-catalyzing ( $a_i > 0$ ) or inhibiting ( $a_i < 0$ ) species and may be different for precipitation and dissolution. An example will be given below in the case of pyrite dissolution (subsections 2.2 and 5.1).

### 2.1.4 CATION EXCHANGE AND SURFACE COMPLEXATION

Figure 2-1 gives a simplified representation of a montmorillonite clay structure. This mineral represents the main component of bentonites (about 80 %wt of the Deponit CA-N and about 87 %wt of the MX-80 bentonite). It undergoes two distinct sorption mechanisms. Cation exchange takes place in the interlayer space to balance ionic charge disequilibrium in the clay skeleton. This exchange mechanism buffers the bentonite hydrochemistry, in particular for Ca<sup>2+</sup> or Na<sup>+</sup> ions. Surface complexation on the clay surface is another important process with respect to water/rock interactions: acid/base reactions take place at the clay/solution interface and control, to some extent, the pH of the bentonite pore water. HYTEC accounts simultaneously for interlayer cation exchange and surface complexation, either in thermodynamic equilibrium or kinetic paths. However, since the kinetic of sorption is much faster than mass diffusion in the case of compacted bentonite, kinetic of sorption will not be considered in this study.

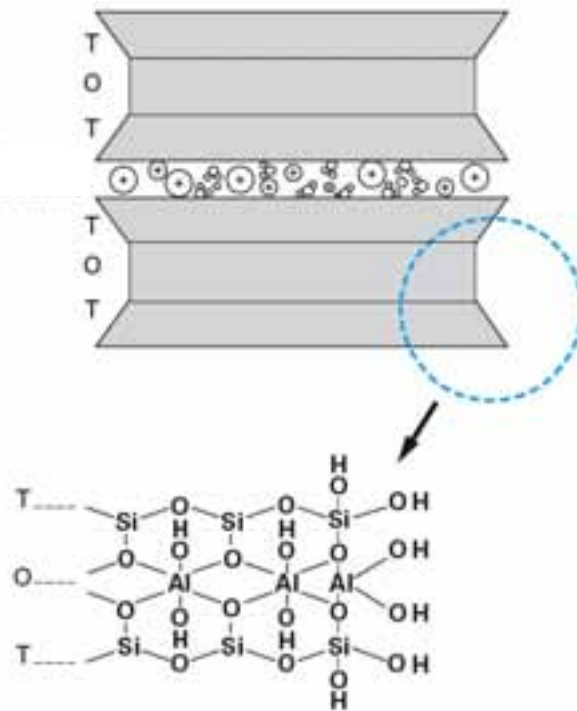


Figure 2-1. Simplified representation of a montmorillonite clay structure.

#### 2.1.4.1 Cation exchange

Any cation exchange reaction can be written in terms of a mass-action law, for instance:

$$2 \bar{A}^+ + B^{2+} \rightleftharpoons \bar{B}^{2+} + 2 A^+, \quad K = \frac{(\bar{B}^{2+})(A^+)^2}{(A^+)^2(\bar{B}^{2+})}$$

where the bar stands for an ion in the interlayer space and the parenthesis for the ion activity either in the solution or in the interlayer space. HYTEC, PHAST, and most of the other reactive transport codes use this equation to simulate cation exchange reactions.

The calculation of the ion activity in the interlayer space is still a debated question. One of the simplest and most common approaches is the Gaines-Thomas formalism (Helfferich, 1995):

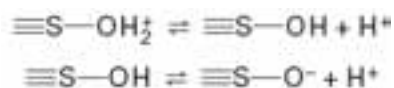
$$K_{GT} = \frac{f_B(A^+)^2}{f_A^2(B^{2+})}$$

$K_{GT}$ , which is known as the “selectivity coefficient”, can be experimentally measured and easily (automatically) re-expressed as a mass-balance constant  $K$  required for the reactive transport code (see Bradbury and Baeyens, 1998). An implicit assumption in the calculations is that selectivity coefficients are constants over the ranges of considered cation occupancies. The equivalent fraction  $f_A$  can be written as a function of the cation exchange capacity (CEC):

$$f_A = \frac{|\bar{A}^+|}{|\bar{A}^+| + |\bar{B}^+|} = \frac{|\bar{A}^+|}{\text{CEC}}$$

#### 2.1.4.2 Surface complexation

The interruption of the crystal network at the surface of the clay pellet leads to hydroxyl groups such as silanol Si-OH and aluminol Al-OH ones, which affinity depends on their location on the surface (basal or edge sites). These functional groups are generally amphoteric, that is to say they can take or give a proton to the solution:



and be characterized by two pKa values.

In addition to protons, the other cations and some anions can also react with the clay surface groups. At the overall balance of the site concentrations corresponds an electrical state of the surface and, accordingly, an electrical potential field propagating more or less within the pore volume. HYTEC uses the double layer theory, which takes into account the intrinsic acid/base and ion complexation constants.

## 2.2 THERMODYNAMIC AND KINETIC DATA

### 2.2.1 AQUEOUS CHEMISTRY AND DISSOLUTION/PRECIPITATION REACTIONS

In the present study, local thermodynamic equilibrium assumption is assumed for all the aqueous reactions including the electron transfer (redox) mechanisms. The dissolution/precipitation kinetic of carbonates (calcite, dolomite) and sulfates (gypsum) are fast (Savage *et al.*, 2002), at least significantly faster than diffusion mass transfer and were also modelled at a local equilibrium level. The equilibrium constants (log K) come from the EQ3/6 (Wolery, 1992) thermodynamic database (TDB), version 8.6, but:

- for dolomite, the constant was taken from the Nagra TDB (Pearson and Berner, 1991), as commented in section 2.4.2. Bradbury and Baeyens (1998) also used this optional constant for dolomite in their modelling work of Opalinus Clay pore water;
- for gypsum, the constant from the EQ3/6 TDB has been identified to be lower than that contained in other TDBs. A sensitivity analysis to this parameter value has therefore been performed for one of the calculation cases treated in the present study, so as to assess the potential influence of this mineral stability (see section 3.4).

As in Arcos *et al.* (2006), montmorillonite dissolution is assumed in any case to be too low to be coupled to the chemical evolution of the system over the 100,000 y duration. This hypothesis is supported by the following grounds: i) montmorillonite is only slightly under-saturated in most of the chemical conditions considered in this study except for the Grimsel diluted groundwater, ii) the kinetic dissolution constant is relatively low (around  $1 \times 10^{-14}$  -  $3 \times 10^{-14}$  mol/m<sup>2</sup>/s at 25 °C in a pH range of 6 to 10, see for instance Köhler *et al.*, 2003, Read *et al.* 2001, Savage *et al.* 2002) iii) the expected temperature increase within the near-field, which would accelerate the dissolution rate (about 30 times at 70 °C), drops below 50 °C after 1,000 y and this transient period should therefore be too short to have a major influence, iv) a transformation of montmorillonite into non-swelling clays such as illite appears, in a first assessment step, unlikely in the geochemical conditions considered for the present study (low potassium content of the waters, low temperature values on the long-term). Nevertheless, this

assumption of non-dissolution of montmorillonite ought to be further assessed, in particular in the case of diluted groundwaters such as ice-melting ones.

Pyrite and siderite are assumed to be either in equilibrium with the solution in the reference and high-salinity water cases or kinetically controlled in the scenario of (oxidizing) ice-melting water intrusion. In the later situation, the kinetic laws used for pyrite (see Williamson and Rimstidt, 1994) and siderite (see Duckworth and Martin, 2004) were respectively:

$$\frac{d[FeS_2]}{dt} = k_1 A_v (H^+)^{-0.1} (O_2(aq))^{0.8}$$

and

$$\frac{d[FeCO_3]}{dt} = k_2 A_v (H^+)^{0.75} + k_3 A_s$$

with  $k_1 = 6.5e-9$  mol/m<sup>2</sup>/s,  $k_2 = 2.5e-5$  mol/m<sup>2</sup>/s and  $k_3 = 2e-9$  mol/m<sup>2</sup>/s. It is worth noting that the kinetic rate law of pyrite is not suitable for simulating pyrite dissolution in a reduced environment where the dissolved oxygen concentration is zero. In such a case, other laws should be taken into account, e.g. similar to the present kinetic equation of pyrite dissolution (though a thermodynamic equilibrium approach is usually justified by the very low solubility of pyrite in such conditions).

### 2.2.2 CATION EXCHANGE AND SURFACE COMPLEXATION

In the lack of specific data available for the Deponit CA-N bentonite, the ionic exchange and surface complexation data are the same as those taken for the MX-80 bentonite from Wersin *et al.* (2003), since the same type of clay mineral (montmorillonite) is massively present in the two bentonites. The data reported in Table 2-1 correspond to the main clay reactions involved in this study, that is to say ionic exchanges between the major cations Na<sup>+</sup>, Ca<sup>2+</sup>, K<sup>+</sup> and Mg<sup>2+</sup>, as well as the acid/base buffering capacity of the clay surface groups by proton exchange. Those data are equals to those selected in Arcos *et al.* (2006).

Table 2-1. Cation exchange and surface complexation data.

Reaction	Log K (25 °C)
<i>Cation exchange<sup>(*)</sup></i>	
$K^+ + NaX \rightarrow Na^+ + KX$	0.60
$Ca^{2+} + 2 NaX \rightarrow 2 Na^+ + CaX_2$	0.41
$Mg^{2+} + 2 NaX \rightarrow 2 Na^+ + MgX_2$	0.34
CEC <sub>Deponit CA-N</sub> = 70 meq/100g	
CEC <sub>MX-80</sub> = 75 meq/100g	
<i>Surface complexation (**)</i>	
$S_1-OH + H^+ \rightarrow S_1-OH_2^+$	4.5
$S_1-OH \rightarrow S_1-O^- + H^+$	-7.9
$S_2-OH + H^+ \rightarrow S_2-OH_2^+$	6.0
$S_2-OH \rightarrow S_2-O^- + H^+$	-10.5
Site density $S_1$ x specific surface <sub>Deponit CA-N</sub> = 3.5e-5 eq/g	
Site density $S_1$ x specific surface <sub>MX-80</sub> = 3.75e-5 eq/g	

(\*) Gaines-Thomas formalism; (\*\*) Proton exchange only.

## 2.3 GEOMETRICAL DESIGN: KBS-3 CONCEPT AND SIMULATION GRIDS

This modelling study deals with a system representative for an individual deposition hole of the KBS-3 concept, with its canister and buffer, as shown in Figure 2-2. The deposition hole is 1.75 m in diameter for a height of about 7.8 m. The canister is surrounded by several decimeters of bentonite buffer (0.35 m thick around, 0.5 m height below and 1.5 m above). The concrete bottom plate, as well as the backfill at the top of the deposition hole and in the deposition tunnel is not accounted for in the present study. The spent fuel package is assumed neither to be porous nor to be chemically reactive.

A fracture network can be formed in the crystalline rock due to geological history, and fractures may be intersected during the excavation of deposition holes. As in Arcos *et al.* (2006), a hydraulically active fracture plane is therefore assumed in the considered system, at about mid-height of the deposition hole. Solute migration will thus be driven by advective flow in the fracture and mostly by diffusion within the bentonite buffer.

Such a system presents a cylindrical geometry which is broken by the asymmetric flow field in the fracture plane. Since HYTEC cannot manage three dimensional grids, the system has been split into two complementary simulation grids:

- a first one, reported in Figure 2-3, corresponds to a horizontal cross-section at the level of the fracture plane with water flowing from left to right in the fracture plane. The cross-section does not

take into account the buffer in its full height but only a fraction equal to the fracture width (0.1 m). With this respect, the chemical and mineralogical evolutions of the simulated part of the buffer will be overestimated (geochemical changes propagate further for a given time period) since the fracture water cannot diffuse up and down, within the entire buffer volume;

- a second simulation grid accounts for the cylindrical symmetry (2D-cylindrical grid equivalent to a 3D grid) without explicit flow within the fracture (see Figure 2-4). A constant concentration constraint is used as a boundary condition in the fracture plane instead. This is correct for the upstream part of the fracture, but less for the downstream region, where species concentrations may change due to groundwater/bentonite interactions. One therefore may expect that the chemical and mineralogical evolutions in the buffer with time are slightly increased with this constant concentration assumption.

To summarize, the geochemical evolution is overestimated by the calculations based on the cross-section grid. Overestimation means here an acceleration of the propagation of the chemical perturbations within the bentonite buffer, perturbation intensity itself being correctly estimated. This point is illustrated in section 3.1. The time periods resulting from simulations with the cylindrical grid should be closer to what could be expected and, except when that is mentioned, the time indications in the following text refer to the cylindrical grid.

In the cross-section grid, the average node size is about 0.05 m. In the cylindrical configuration, the node size in the bentonite zone is 0.05 m in the X coordinates (the width of the buffer) and 0.1 m in the Y coordinates (the height of the buffer).

## 2.4 GEOCHEMISTRY AND MINERALOGY

### 2.4.1 GROUNDWATERS

Interactions between the buffer and three distinct kinds of water have been investigated, as in Arcos *et al.* (2006): a reference groundwater (Forsmark), a high-salinity groundwater (Laxemar) and an ice-melting groundwater (Grimsel). In addition, a fourth type of water was considered, i.e. a dilute groundwater (similar to the ice-melting one) with various oxygen contents. An equivalent approach to that presented in Arcos *et al.* (2006) was followed in the present study to compute the composition of these groundwaters. Saturation indices were first determined with JCHESS from experimental data, and then partly adapted to modelling constraints.

The Forsmark groundwater considered in the reference scenario is a Na-Ca-Cl water type, as reported in Table 2-2, with a pH value close to neutrality and a reducing redox potential. Table 2-3 shows that the groundwater is close to saturation (equilibrium) with respect to calcite, dolomite, chalcedony/quartz, goethite and Ca-montmorillonite. The water is slightly undersaturated with respect to gypsum as well as siderite, whereas a noticeable undersaturation state is calculated for pyrite. Calcite and quartz are experimentally observed as minerals infilling the fractures; siderite which is close to the equilibrium with the water is likely to be present in the fracture (Arcos *et al.* (2006)). Consequently, the Forsmark groundwater was pre-equilibrated with those three minerals prior to be considered as a boundary condition at the fracture level. The recalculated chemistry remains obviously very close to the experimentally determined one, as shown in Table 2-2.

The high-salinity groundwater composition is modelled from Laxemar experimental data. This Na-Cl water presents a more alkaline and strongly more reducing signature than the Forsmark water, and is in close equilibrium with calcite and chalcedony-quartz, which are common secondary minerals found in fractures. For this reason, the modelled groundwater was set in perfect equilibrium with calcite and quartz. The water is strongly oversaturated with respect to pyrite and undersaturated with respect to gypsum. Reduced sulfur is the predominant species at such low pe values. However, according to Arcos *et al.* (2006), analytical data from Laxemar indicates that the dominant aqueous sulfur species are rather sulfate species. Therefore, it seems more realistic to redefine the pe of the system by forcing equilibrium with pyrite. The calculated chemical composition is detailed in Table 2-2.

Diluted water may circulate in the fracture network during extended ice-melting periods. A possible chemical composition based on Grimsel data is found in Table 2-2. On the one hand, the ionic strength is two to three orders of magnitude below that of the previous groundwater ones. This is a clear indication of shallow origin. On the other hand, the pH is significantly more alkaline (around 9.6). Calcite and quartz were set in equilibrium with the recalculated groundwater.

The fourth type of water is derived from the previous dilute one, adding dissolved oxygen so as to assess the redox buffering capacity of the buffer versus an oxidative perturbation. The fugacity in oxygen is fixed to an intermediate value of 0.04, which assumes a 80 % consumption of the oxygen dissolved in a shallow water equilibrated with atmosphere. Two other alternative values, 0.001 and 0.2 (water fully saturated in oxygen) are also considered in the purpose of a sensitivity analysis. More details on this ‘oxidative case’ are given in section 5.1.

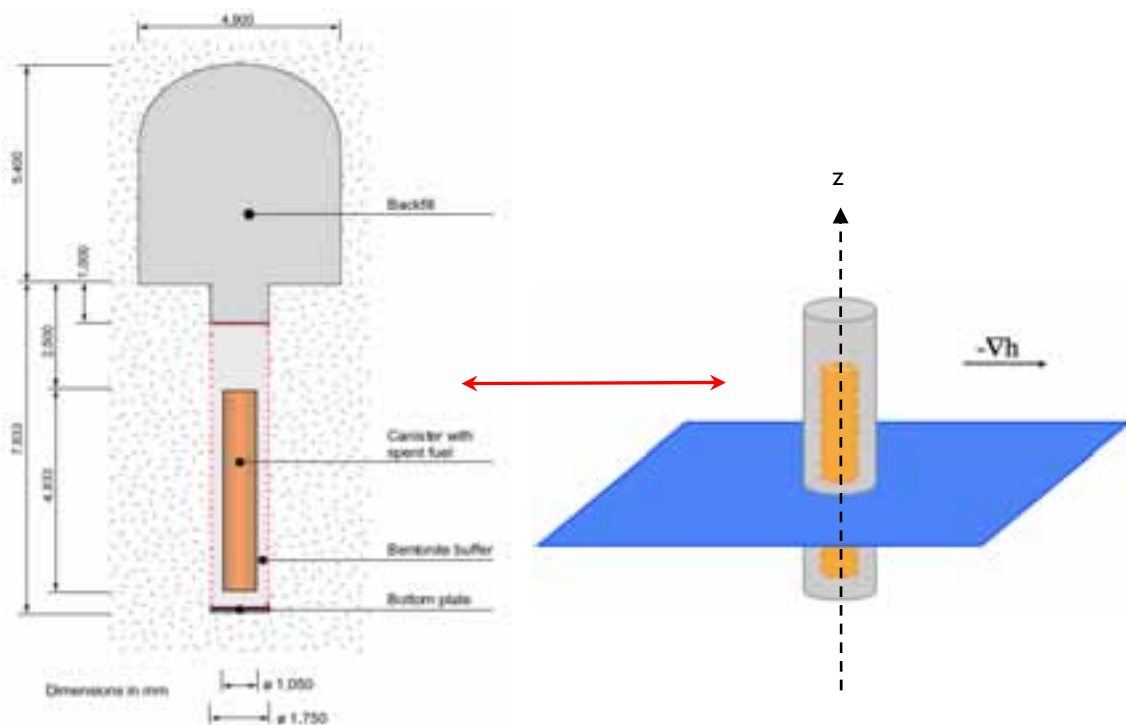


Figure 2-2. Schematic view of the KBS-3 disposal concept (SKB, 2006) and representation of the simulated subsystem with an hypothetical fracture plane.

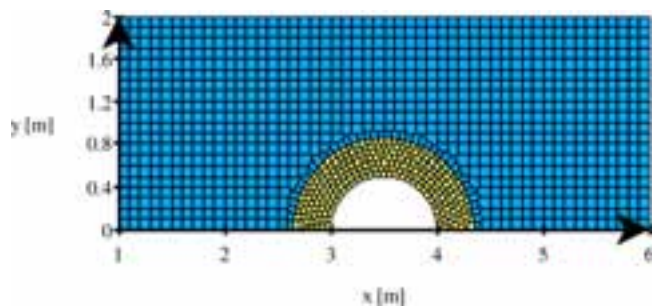


Figure 2-3. Calculation grid representative for the cross-section at the level of the fracture plane.

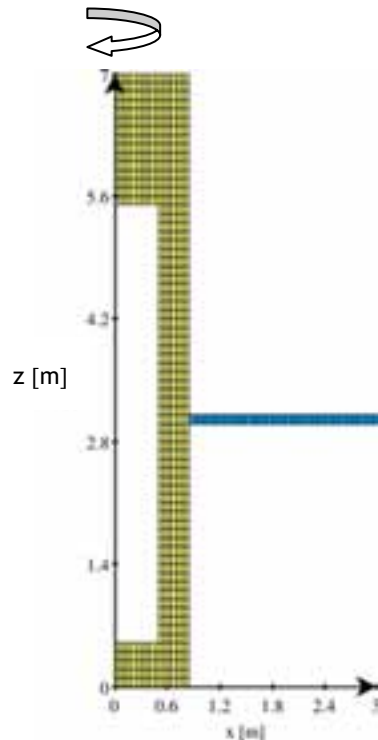


Figure 2-4. Calculation grid representative for the cylindrical geometry (rotation around the z axis, perpendicularly to the fracture plane).

#### 2.4.2 DEPOSIT CA-N BENTONITE

The mineral composition of the Deponit CA-N bentonite (SKB, 2004) taken into account in the calculations is, by decreasing order of weight content, montmorillonite (81%), calcite-siderite (10%), dolomite (3%), gypsum (1.8%), quartz (2%) and pyrite (0.5%). It's worth noting that this bentonite contains accessory minerals which strongly affect its pore water chemistry, especially at high solid/liquid (S/L) ratios. One should also specify that i) the amount of quartz includes the cristobalite content and ii) that the calcite-siderite amount was divided in 8 % of calcite for 2 % of siderite, which probably overestimates the siderite percentage.

The calculated pore water of the Deponit CA-N bentonite is reported in Table 2-2. Temperature was set to 15 °C, the long-term value considered by SKB (SKB, 2006). This initial state considers a pre-equilibrium phase with the Forsmark groundwater. The equilibrium of the pore water is imposed with respect to calcite, dolomite, siderite, gypsum, quartz and pyrite. This leads to a Na-Ca-Cl water type, with a pH value close to neutrality and reducing conditions, similar though different from the Forsmark water. The pore water composition is in good agreement with the composition obtained by Arcos *et al.* (2006).

The pore water is also in equilibrium with the exchangeable cations of montmorillonite. The subsequent modelled occupancy ranges as Ca (41% in equivalent), Mg (33%), Na (24%) and K (2%). This distribution has to be compared to the experimental one (SKB, 2004), i.e. Ca (46%), Mg (29%), Na (24%) and K (2%). The equilibrium of dolomite, which is strictly imposed in the calculations, explains the moderate difference in the Ca/Mg ratio. The discrepancy of the modelling with the measured values becomes significantly worse if the EQ3/6 log K value of dolomite is used instead of the Nagra TDB one. Therefore, the choice of Nagra TDB log K for dolomite has been maintain throughout this study, leading to faster dissolution of this mineral with respect to the results presented in Arcos *et al.* (2006).

To summarize, the dissolution and precipitation of the following set of minerals are considered in all the simulations dealing with the Deponit CA-N bentonite: the carbonates calcite, dolomite, magnesite and siderite; the sulfate gypsum; the silica oxide quartz; the iron minerals pyrite and alternatively ferrihydrite or goethite.

### 2.4.3 MX-80 BENTONITE

MX-80 bentonite is modelled from the data provided by SKB (SKB, 2004) with montmorillonite (87%), quartz-cristobalite (5%), gypsum (0.7%) and pyrrhotite (0.07%). Pyrrhotite (FeS) was considered instead of pyrite (FeS<sub>2</sub>) in the reactive transport calculations for convergence reasons. The consequence on the geochemical evolutions of MX-80 bentonite when interacting with the different waters considered in the present study is found to be insignificant, except for pe. Actually, the equilibrium of bentonite water with pyrrhotite instead of with pyrite diminishes the pe values by about 0.5 unit (-3.15 to be compared with -2.6 derived from pyrite).

Because of their incidence on the bentonite capacity to buffer geochemical perturbations, even if in small concentrations, and the relative uncertainties concerning their presence, calcite (0.7 %) and siderite (0.7 %) are considered in the context of a sensitivity analysis, as in Arcos *et al.* (2006). This induces changes in the aqueous iron and carbonate contents of bentonite pore water, as reported in Table 2-2.

The composition of the pore water of MX-80 bentonite is calculated with JCHESS (see Table 2-2). Temperature was set to 15 °C, as for Deponit CA-N. The equilibrium is imposed with respect to gypsum, quartz and pyrrhotite and leads to a Na-Ca-Cl type of water, with a pH close to 7 and reducing conditions. This composition is in good agreement with that calculated by Arcos *et al.* (2006), except for the Na concentration, which is a little higher than in Arcos' work (2.1e-1 mol/l vs. 1.6e-1 mol/l).

The modelled occupancy distribution of exchangeable cations is given as follows: Na (72%), Ca (18%), Mg (8%), K (1.5%). This distribution is strictly identical to the experimental ratio.

The simulations reported in the following chapters take into account the dissolution/precipitation of carbonates (calcite, dolomite and siderite), sulfate (gypsum), quartz and iron minerals (pyrrhotite and ferrihydrite).

### 2.4.4 WASTE PACKAGE AND HOST ROCK

As written above, the waste package was not explicitly taken into account in the calculations. This implies that, neither the uranium dioxide, nor the copper containers, is considered as solid phases present in the near-field environment. Similarly, the Host-rock minerals are not assumed to react with the different groundwaters and the bentonite pore water. Indeed, the rock-forming minerals are characterized by very low intrinsic dissolution kinetic constants as well as tiny reactive surface area, even in the damaged state induced by spalling.

Table 2-2. Chemical composition of the groundwaters and bentonite pore waters.

		Reference case groundwater		High-salinity groundwater		Ice-melting groundwater			Bentonite pore water		
		Experimental	Modelling	Experimental	Modelling	Experimental	Modelling (reducing conditions)	Modelling (oxidative conditions)	Deponit CA-N	MX-80 (without carbonates)	MX-80 (with carbonates)
Temp.	°C	-	15	-	15	-	15	15	15	15	15
pH	-	7.2	7.2	7.9	7.9	9.6	9.6	9.6	7.0	7.0	7.0
pe	-	-2.4	-2.7	-5.1	-3.9	-3.4	-3.15(**)	11.6(***)	-2.6	-3.15	-3.15
Eh	V	-0.15	-0.16	-0.29	-0.22	-0.20	-0.31	0.66	-0.15	-0.18	-0.18
I	mol/L	0.19	0.20	1.7	1.7	0.001	0.001	0.001	0.25	0.29	0.29
Na	mol/L	8.9e-2	8.9e-2	3.5e-1	3.5e-1	6.9e-4	6.9e-4	6.9e-4	7.3e-2	2.1e-1	2.1e-1
K	mol/L	8.8e-4	8.8e-4	7.0e-4	7.0e-4	5.0e-6	5.0e-6	5.0e-6	1.6e-3	1.4e-3	1.4e-3
Ca	mol/L	2.3e-2	2.4e-2	4.6e-1	4.7e-1	1.4e-4	8.0e-5	8.0e-5	2.9e-2	1.0e-2	1.0e-2
Mg	mol/L	9.3e-3	9.3e-3	1.0e-4	1.0e-4	6.2e-7	5.0e-6	5.0e-6	3.2e-2	5.6e-3	5.6e-3
Al <sup>(+)</sup>	mol/L	2e-10	7.5e-9	2.0e-9	1.0e-8	-	-	-	5e-9	-	-
Fe	mol/L	3.3e-5	2.9e-4	8.0e-6	8.0e-6	3.0e-9	3.0e-9	3.0e-9	3.7e-4	1.1e-5	1.0e-4
SiO <sub>2</sub>	mol/L	1.9e-4	6.0e-5	8.0e-5	4.4e-5	2.1e-4	8.0e-5	8.0e-5	6.0e-5	6.0e-5	6.0e-5
HCO <sub>3</sub> <sup>-</sup>	mol/L	2.2e-3	1.5e-3	1.0e-4	4.8e-5	4.5e-4	4.7e-4	4.7e-4	2.3e-3	1.5e-3	4.0e-3
Cl <sup>-</sup>	mol/L	1.5e-1	1.5e-1	1.28	1.28	1.6e-4	1.6e-4	1.6e-4	1.5e-1	1.5e-1	1.5e-1
SO <sub>4</sub> <sup>2-</sup>	mol/L	6.8e-3	6.8e-3	9.0e-3	6.0e-3	6.1e-5	6.1e-4	6.1e-4	2.6e-2	3.8e-2	3.8e-2

(\*) Set in equilibrium with K-Feldspar; (\*\*) fixed value; (\*\*\*) O<sub>2</sub> fugacity set to 0.04.

Table 2-3. Saturation indices calculated for groundwaters and bentonite pore waters.

	Reference case groundwater		High-salinity groundwater		Ice-melting groundwater			Bentonite pore water	
	Experimental	Modelling	Experimental	Modelling	Experimental	Modelling (reducing conditions)	Modelling (oxidative conditions)	Deponit CA-N	MX-80
Calcite	0.2	0.0	0.3	0.0	0.2	0.0	0.0	0.0	0.55
Dolomite <sup>(**)</sup>	1.0	-	-1.8	-	-0.7	-	-	-	-
Dolomite_ng <sup>(**)</sup>	-0.1	-0.4	-3.0	-3.5	-1.9	-2.1	-2.1	0.0	0.0
Magnesite	-0.8	-	-3.8	-	-2.7	-	-	-	-
Siderite	-0.8	0.0	-2.5	-2.8	-3.3	-5.1	-17.9	0.0	0.0
Gypsum	-0.5	-0.5	-2.8	0.0	-3.7	-4.0	-4.0	0.0	0.0
Ferrihydrite	-4.0	-3.3	-5.3	-4.0	-2.2	-4.0	-1.7	-3.6	-7.1
Goethite	0.0	0.7	-1.3	-0.4	1.8	1.8	2.2	0.36	
Hematite	1.0	-	-1.7	-	4.5	-	-	-	-
Pyrite	-7.1	-1.6	12.0	0.0	-39	-40	-263	0.0	0.0
Pyrrhotite	-8.4	-4.9	3.5	-3.8	-25	-27	-160	-4.2	-5.3
Chalcedony	0.2	-	0.0	-	0.1	-	-	-	-
Quartz	0.5	0.0	0.26	0.0	0.4	0.0	0.0	0.0	0.0
Albite	-1.2	-	-0.5	-	-	-	-	-	-
K-feldspar <sup>(*)</sup>	0.0	-	0.0	-	-	-	-	-	-
Illite	-1.7	-	-1.9	-	-	-	-	-	-
Nontronite	3.9	-	0.9	-	-	-	-	-	-
Montmor.	-0.4	-	-0.8	-	-	-	-	-	-
Saponite	-1.4	-	-3.8	-	-	-	-	-	-

(\*) K-Feldspar equilibrium is set in the calculations. (\*\*) Dolomite, log K from EQ3/6 TDB, Dolomite\_ng, logK from the Nagra TDB.

## 2.5 FLOW AND SOLUTE TRANSPORT PARAMETERS

### 2.5.1 BENTONITES AND FRACTURE

The whole system was assumed to be fully (water) saturated since the beginning of the calculations, i.e. the transient saturation stage of the buffer was not simulated.

The flow and transport properties used for calculations are those selected in Arcos *et al.* (2006), detailed in Table 2-4. Although groundwater advection occurs in the fracture network, diffusion is the predominant transport process in both compacted bentonites because of their very low hydraulic conductivities ( $K = 1e-13$  m/s, six orders of magnitude lower than in fracture). The selected effective diffusion coefficients are those of neutral or cationic species. For the cylindrical grid, the total exchange of the buffer pore water is found to be in around 2,000 y.

Table 2-4. Flow and transport parameters selected for bentonite and fracture zones.

		Bentonite (Deponit CA-N and MX-80)	Fracture
Porosity $\omega$	-	0.43	0.20
$D_{eff}$	$m^2/s$	$1.2e-10$	$1.0e-10$
$K$	$m/s$	$1e-13$	$5e-7$
$\alpha$	$m$	0.1	0.1

The calculated steady-state flow field is reported in Figure 2-5 for a hydraulic gradient of 0.002 m/m (value from Arcos *et al.*, 2006). The bentonite ring behaves as expected as a hydraulic barrier, with an average velocity close to zero, diverting the water around. There is accordingly a local maximum in the Darcy velocity at the (3.5, 1 m) coordinates in the fracture plane. However, the Darcy velocity remains low, i.e. less than 0.1 meter per year.

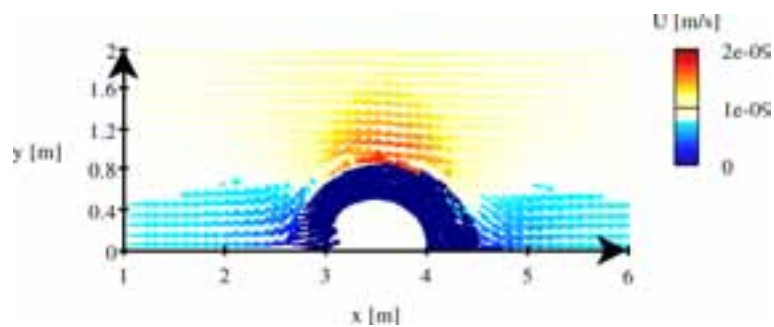


Figure 2-5. Advective flow (Darcy velocity) in the fracture plane; coarser grid for a better visualization of the flow field.

### 3 DEPOSIT CA-N BENTONITE/GROUNDWATER LONG-TERM INTERACTIONS

#### 3.1 REFERENCE CASE, THE FORSMARK GROUNDWATER

In the reference case, i.e. Forsmark groundwater entering the Deponit CA-N bentonite buffer, the Forsmark water slowly imposes its chemistry within the entire cylindrical volume of the bentonite buffer, from the bentonite zone around the fracture level to the other parts of the buffer. This interaction induces moderate changes in pH and pe values over the 100,000 y of simulation, as shown in Figure 3-1, pH increasing by 0.3 unit at the most and pe decreasing by 0.3 unit accordingly.

During this 100,000 y period, the exchangeable Na and Ca populations (Figure 3-2) both increase of approximately 10 % (respectively 24 to 35 % and 41 to 50 %) at the expense of the Mg and K cations. The K occupancy, which is whatever low comparatively to the others, moves from 2 to 1 %, whereas the initial Mg occupancy drops from 33 to 13 %.

Regarding mineral modifications (Figure 3-3), one observes in the entire bentonite volume a progressive but complete dissolution of gypsum in 25,000 y and of dolomite in 85,000 y, while calcite content increases. It is worth emphasizing that dolomite dissolution probably results from the modelling approach, i.e. recalculation of Forsmark groundwater (Table 1-3), and the selection of an alternative log K value (section 2.4.2), and should be considered with some caution. The experimental data of the Forsmark groundwater indicates a supersaturation state for dolomite, arguing for the long-term stability of this mineral in the Deponit CA-N buffer. Dolomite dissolution occurs in a two-step process. Gypsum dissolution which is faster than dolomite dissolution yields a first concomitant decrease of one third of the dolomite content over the whole buffer in 25,000 y. This is followed by a second stage of dolomite dissolution, slower, leading to a complete depletion at 85,000 y. Siderite, pyrite and quartz contents are unchanged (i.e. stable on the long-term). Note that the dissymmetry (up versus bottom) within the bentonite core is transient and results from the asymmetrical distribution of bentonite around the waste package and the fracture plane.

The processes responsible for these changes are mainly induced by the difference in aqueous sulfate and magnesium content between the Forsmark groundwater and the bentonite pore water. The aqueous sulfate concentration is lower (about 3.8 times) in the fracture than in the bentonite pore water. This concentration gradient induces a diffusion of sulfates out from the bentonite, and consequently gypsum dissolution as a supply in aqueous sulfates. Similarly, the lower aqueous magnesium content (about 3.4 times) in the fracture with respect to bentonite generates the out-diffusion of this species from bentonite. The depletion in magnesium within the bentonite leads to the dissolution of dolomite, which raises the aqueous carbonate and calcium concentrations and thus yields calcite precipitation. This last process results in the observed rise in pH, which in turns leads to a decrease in pe, as predicted by the Pourbaix pe-pH diagram of iron given in Figure 3-4 without any consequence on the content in redox sensitive minerals. These dissolution-precipitation reactions and the associated modifications in the aqueous chemistry of the bentonite pore water, i.e. aqueous Mg decrease and Ca supply, explain the

calculated re-organization of the cation occupancy in the montmorillonite exchanger. The Mg by Na replacement completes that by Ca, due to a slight in-diffusion of Na from the fracture to the bentonite. The dissolution of the accessory minerals does not yield to any significant changes in the porosity of the system, as indicated by Figure 3-5. The increase of porosity is less than 2 % and is essentially due to the dissolution of gypsum since most of the dissolved dolomite reprecipitates as calcite. The diffusion coefficient should not significantly change accordingly.

Globally, the chemical evolution of the bentonite buffer - driven by diffusion of the Forsmark groundwater - slowly occurs over the full bentonite height and reaches a quasi-steady state at the end of the simulation time. It is worth emphasizing that the chemical evolution within the buffer is smoothed down progressively, in a typical diffusion process manner, as the concentration gradients between the fracture and the buffer decrease (not thoroughly represented in the present report).

At last, the evolutions in pH, pe and exchanged cation populations calculated using the cross-section grid (Figure 3-6 and Figure 3-7) are given for illustration purpose. As mentioned in the previous section, the modifications are similar to those obtained with the cylindrical grid, although in shorter simulation times.

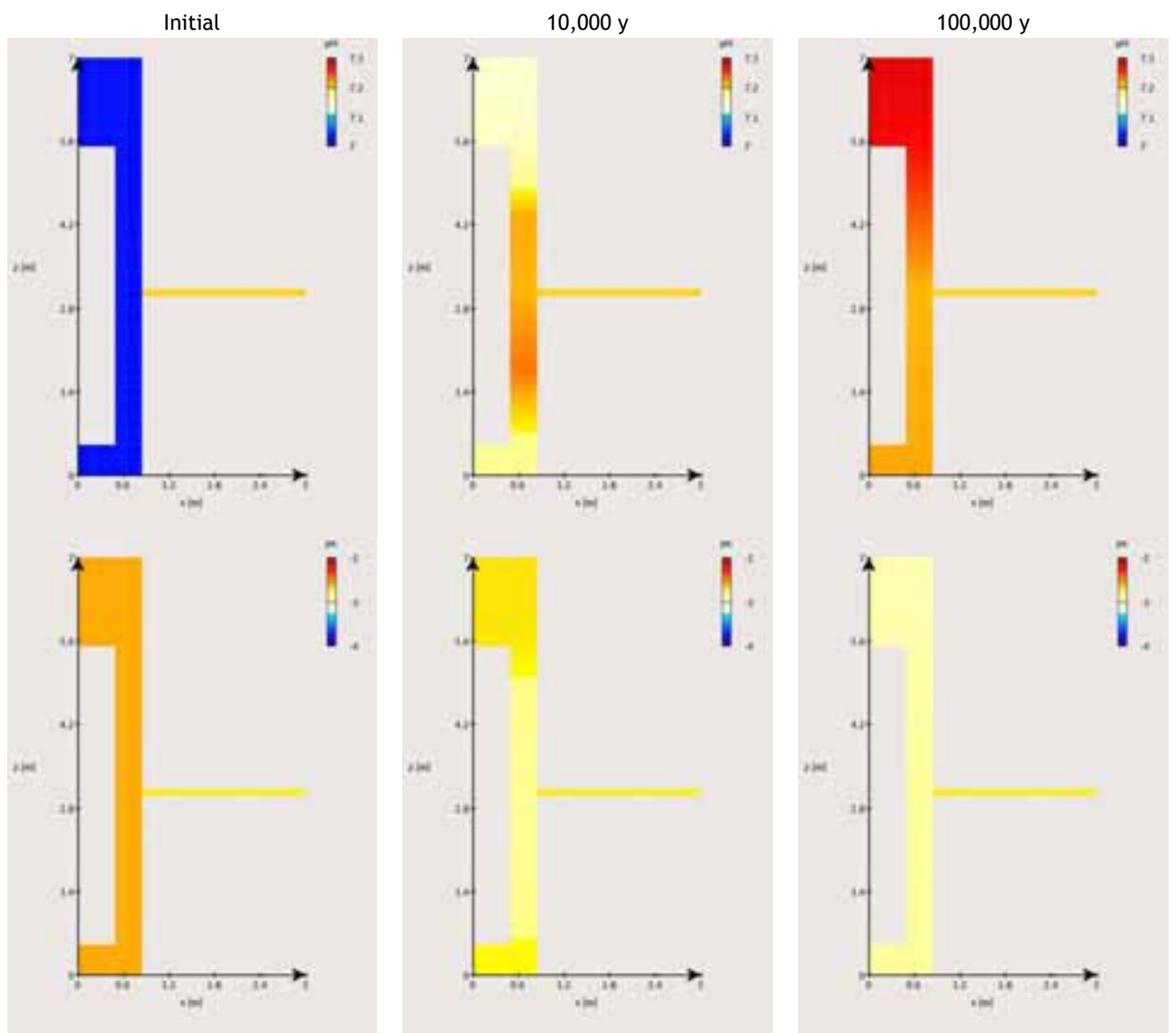


Figure 3-1. Reference case with Deponit CA-N bentonite: evolution of pH and pe over 100,000 y.

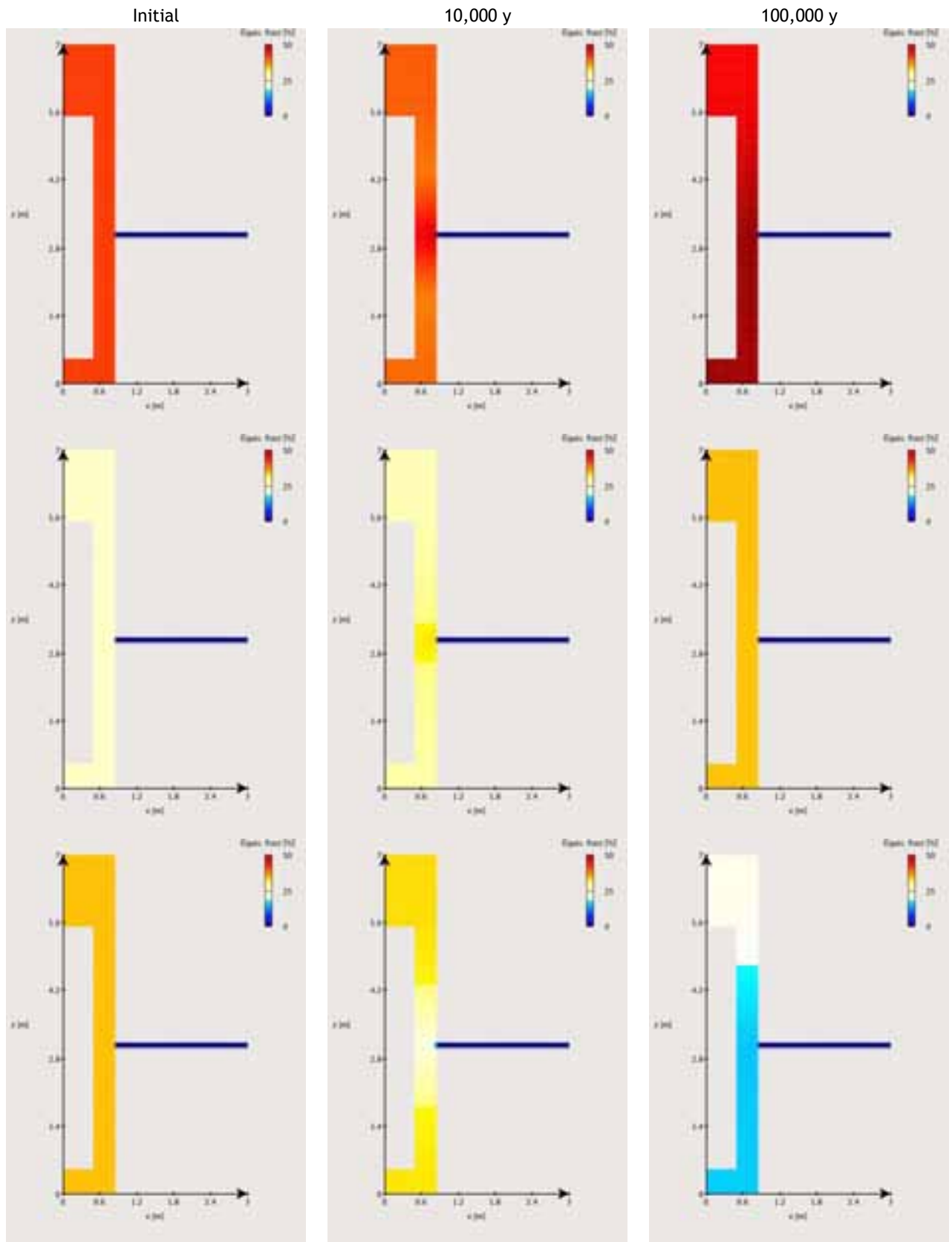


Figure 3-2. Reference case with Deponit CA-N bentonite: evolution of exchangeable Ca (top), Na (middle) and Mg (bottom) populations over 100,000 y.

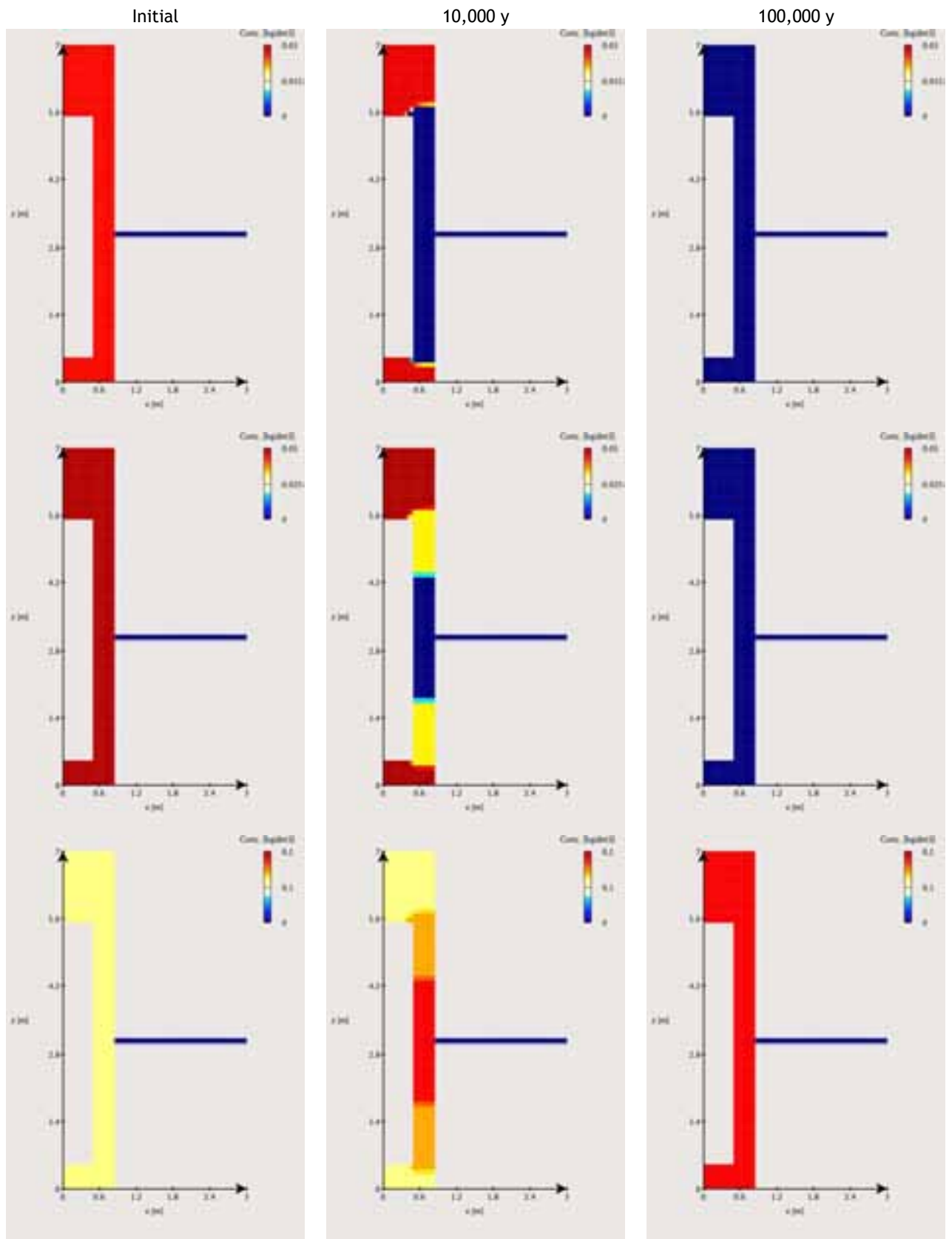


Figure 3-3. Reference case with Deponit CA-N bentonite: evolution of gypsum (top), dolomite (middle) and calcite (bottom) contents over 100,000 y.

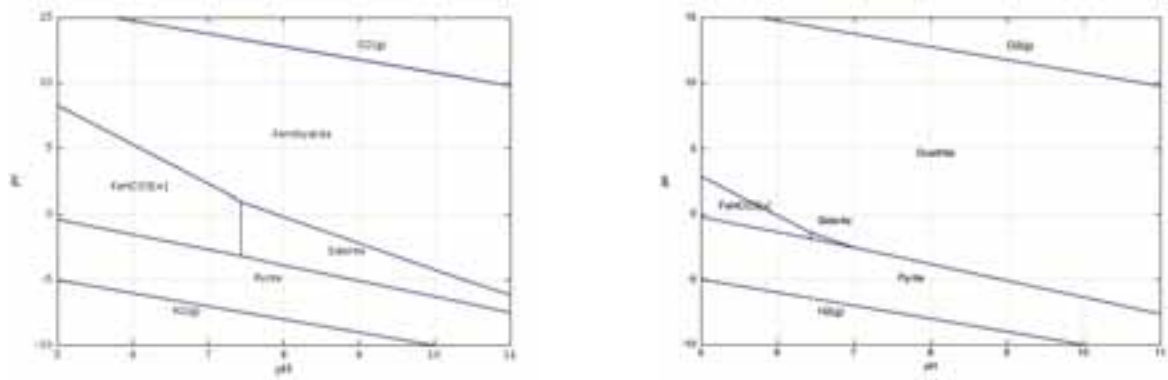


Figure 3-4. Pourbaix/pe-pH diagram of iron (Fe, HCO<sub>3</sub> and SO<sub>4</sub> concentrations identical to those of the initial pore water of the Deponit CA-N).

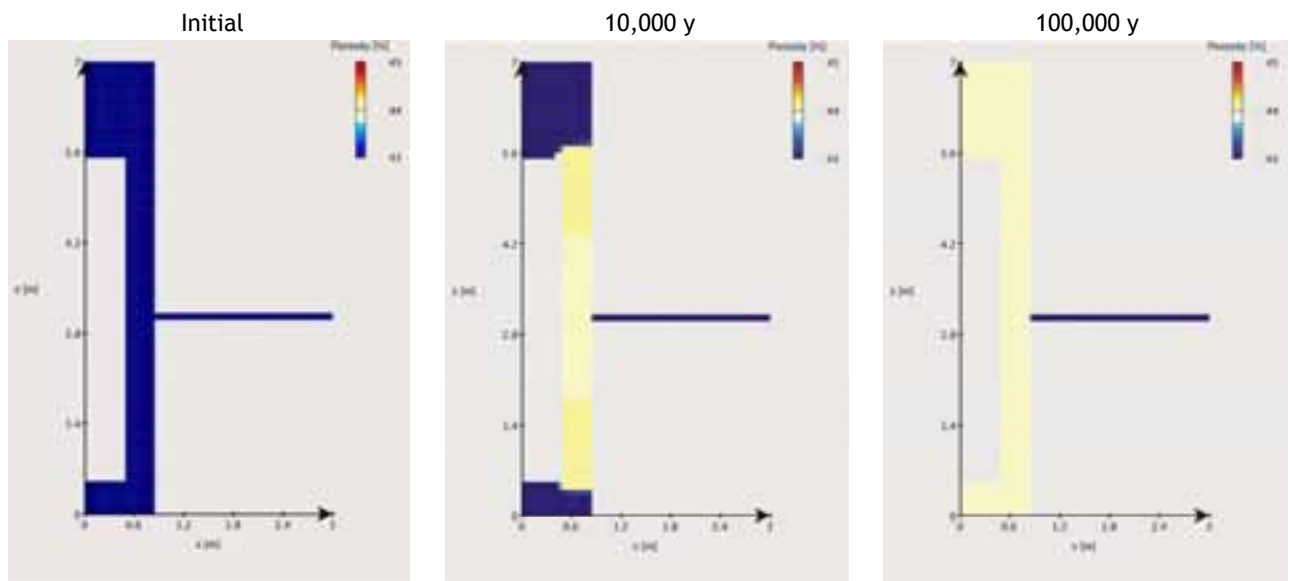


Figure 3-5. Reference case with Deponit CA-N bentonite: evolution of the porosity over 100,000 y.

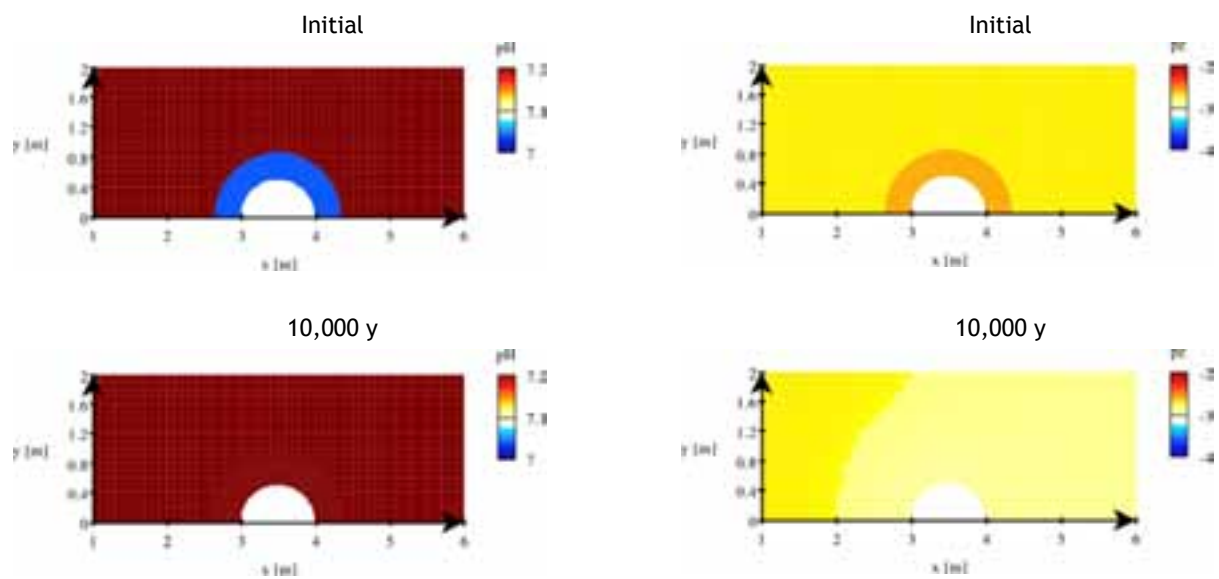


Figure 3-6. Reference case with Deponit CA-N bentonite: evolution of pH and pe over the first 10,000 y.

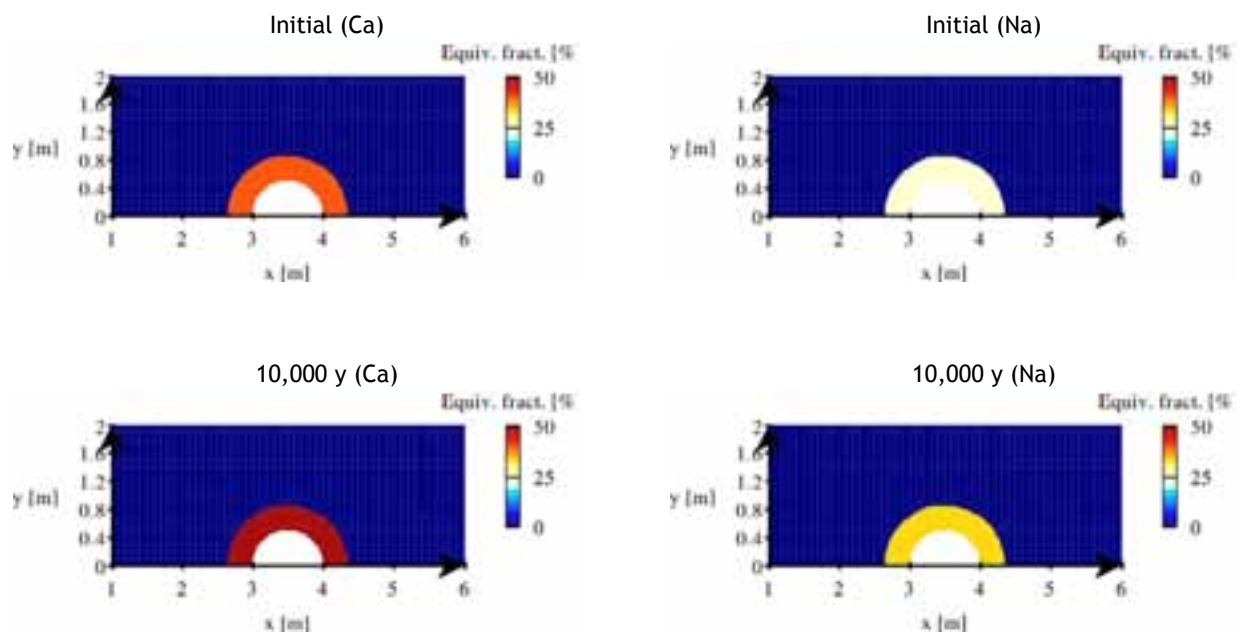


Figure 3-7. Reference case with Deponit CA-N bentonite: evolution of exchangeable Na and Ca populations over the first 10,000 y.

## 3.2 HIGH-SALINITY WATER INTRUSION, THE LAXEMAR GROUNDWATER

The first 10,000 y of the system evolution are strictly identical to the Forsmark reference case (the so called “Forsmark stage”), then the Laxemar groundwater starts to interact with the Deponit CA-N buffer.

As a consequence, the pH in the buffer pore water progressively increases, shifting from 7.0 to 7.9 after 100,000 y at the fracture plane level, whereas the pe values drops from -2.6 to -3.5 in strict relation with the pH ( $\Delta\text{pH} = -\Delta\text{pe}$ ), as shown in Figure 3-8. The evolution driven by diffusion is smoothed down progressively. However, equilibrium with respect to these parameters is not reached in the whole buffer at the end of the simulation. The average pH and pe values within the bentonite buffer after 100,000 y are about 7.4 and -3.0 respectively.

The Laxemar groundwater is sharply depleted in Mg cations compared to the initial Deponit CA-N pore water (almost two orders of magnitude) and, accordingly, the Mg exchange occupancy converges towards a value of 0.1 % after 25,000 y at the favor of Na occupancy (from 24 % to 35 %) and Ca occupancy (from 41 % to 65 %). The potassium exchangeable population remains below 2 %.

As in the reference case, dolomite is completely dissolved in agreement with a strong undersaturation state of the Laxemar groundwater with respect to this mineral. Dolomite dissolution yields a concomitant increase in calcite content. Quartz is still unaltered since both the groundwater and the bentonite pore water are in equilibrium with this mineral. Gypsum, which is almost dissolved during the first 10,000 y of Forsmark water intrusion, precipitates as Laxemar water enters the buffer. The siderite stability drops as a consequence of the pe excursion towards a more reducing state due to the Laxemar water intrusion, whereas pyrite is further stabilized (see pe-pH diagram in Figure 3-4). The strong undersaturation state of siderite is experimentally measured for the Laxemar water type (see Table 1-3). Accordingly, siderite disappears in terms of sharp dissolution fronts which slowly migrate on both sides of the fracture while pyrite is not altered (Figure 3-9). Siderite dissolution is recycled in terms of calcite precipitation. The dissolution of dolomite and siderite is thus counterbalanced by precipitation of secondary calcite and gypsum. Therefore, there is only a small increase (less than 2 %) of the bentonite porosity.

The deprotonation reaction, which takes place at the montmorillonite surface, buffers or at least slows down the penetration of a more alkaline pH wave in the buffer. This is illustrated by the evolution of the  $\text{DPN-OH}_2^+$  site concentration in Figure 3-10, which has to be compared to the evolution of pH profiles in Figure 3-8. In Figure 3-10, one also notes that the cation exchange reactions proceed much faster than the pH front with a steady state reached in approximately 25,000 , whilst the pH front is slowed down by buffering processes.

Figure 3-11 reports the evolution with time of some interdependent chemical parameters, 50 cm above the fracture level. The aqueous concentrations of Na and Ca, which are significantly higher in the high-salinity water, increase quickly in the bentonite by diffusion. On the opposite, the aqueous concentration of Mg is smaller in the highly-saline water than in the bentonite buffer. As a consequence, the exchangeable Mg population progressively decreases at the benefit of the Na and Ca occupancies. The re-equilibrium of the exchangeable ion population takes about 20,000 y to be completed. The equilibrium of the solution with respect to calcite combined to the increase of dissolved Ca concentration imposes a decrease of bicarbonate aqueous concentrations (i.e. a solubility

product constraint:  $(\text{Ca}^{2+}) \times (\text{CO}_3^{2-}) = K_s$ ). Gypsum is dissolved first, since the Forsmark groundwater is undersaturated with respect to this mineral, but precipitates as a secondary phase during a short period when the Laxemar water enters in the system and then remains stable. The precipitation is due to the sudden increase of dissolved Ca while sulfates in the bentonite are still in higher concentrations than in the Laxemar groundwater. The pre-equilibration of the Laxemar groundwater with respect to gypsum explains the long-term stability of this mineral.

The intrusion of highly saline groundwater within the buffer also modifies the concentrations in anionic species. With respect to corrosion processes, chlorides and sulfides, as well as carbonates and sulfates in a second extent, are the main potential corrosion-enhancing species usually found in natural waters. The sulfide concentration is very low in the Deponit CA-N pore water, about  $5 \cdot 10^{-10}$  mol/L, and further decreases during the highly saline intrusion stage. Such a range of values is unlikely to yield sulfide-specific corrosion. The bicarbonate content shifts from an initial value of  $2 \cdot 10^{-3}$  to  $2 \cdot 10^{-4}$  mol/L approximately after 20,000 y (Figure 3-11) and should not be active either. The sulfate concentration slightly decreases during the Laxemar in-diffusion and remains around a moderate value of  $10^{-2}$  mol/L. Contrarily to the other anions, chloride concentration increases by one order of magnitude to 1.3 mol/L; i.e. one half of the corrosive threshold concentration of 3 mol/L.

The change in ionic aqueous concentrations is relatively uniform within the whole volume of the buffer. However, this is not the single factor of interest for corrosion. The flux of elements available for chemical reactions is another important one. Figure 3-12 shows the evolution with time of the cumulative mass of carbonate, chloride and sulfate ions which results from mass diffusion between the fracture and the full volume of the bentonite buffer, as well as through a 5 cm thick layer around the canister. The "Forsmark stage" does not yield any chloride net change since the chloride content is similar in both the bentonite and the groundwater. The sulfate concentration slows down a little bit. The main effect of highly saline water diffusion is to raise the chloride mass in the buffer and around the canister. The evolution is particularly sharp since chloride behaves like a non reactive tracer.

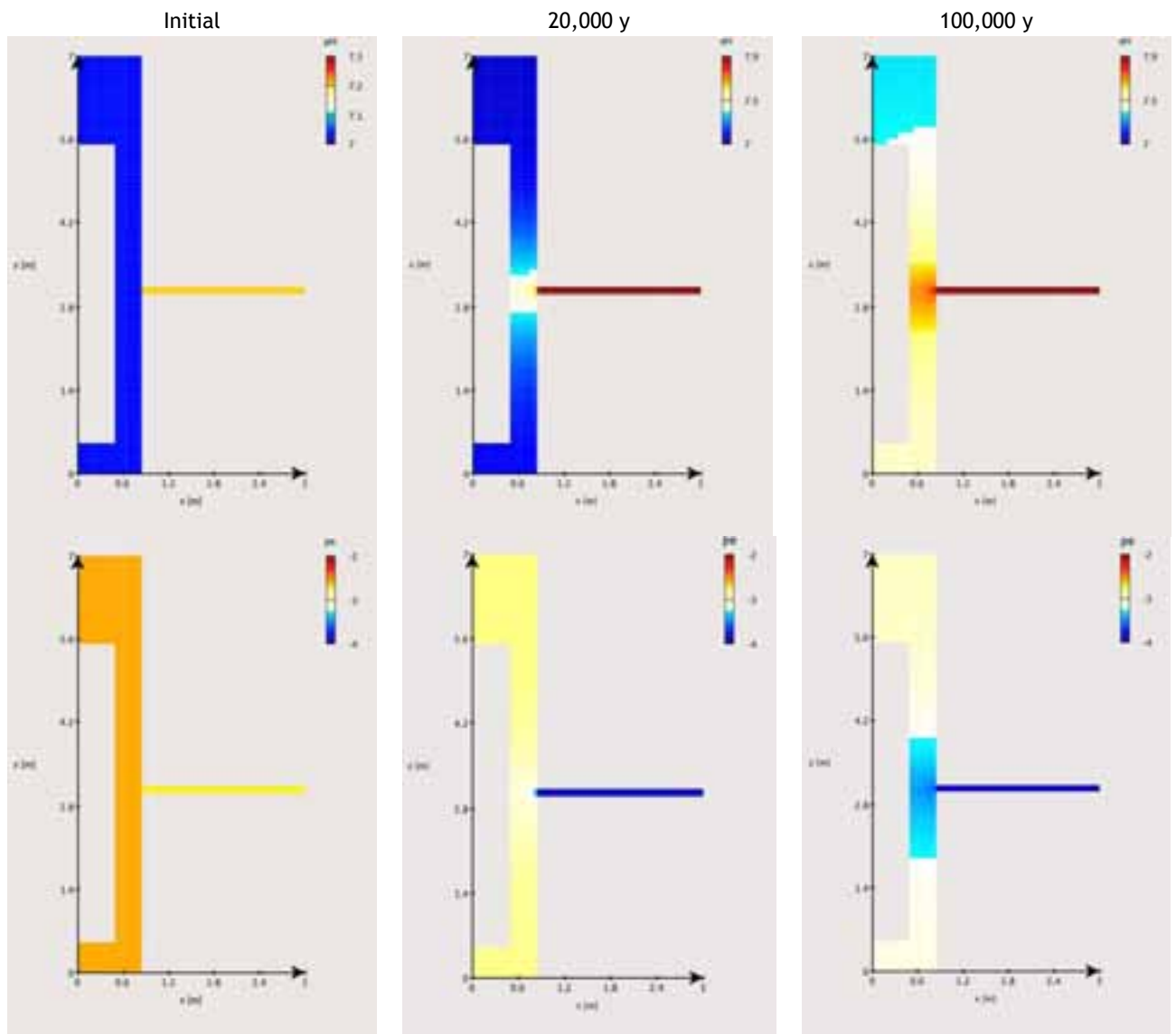


Figure 3-8. High-salinity water intrusion in Deponit CA-N bentonite: evolution of pH and pe over 100,000 y.

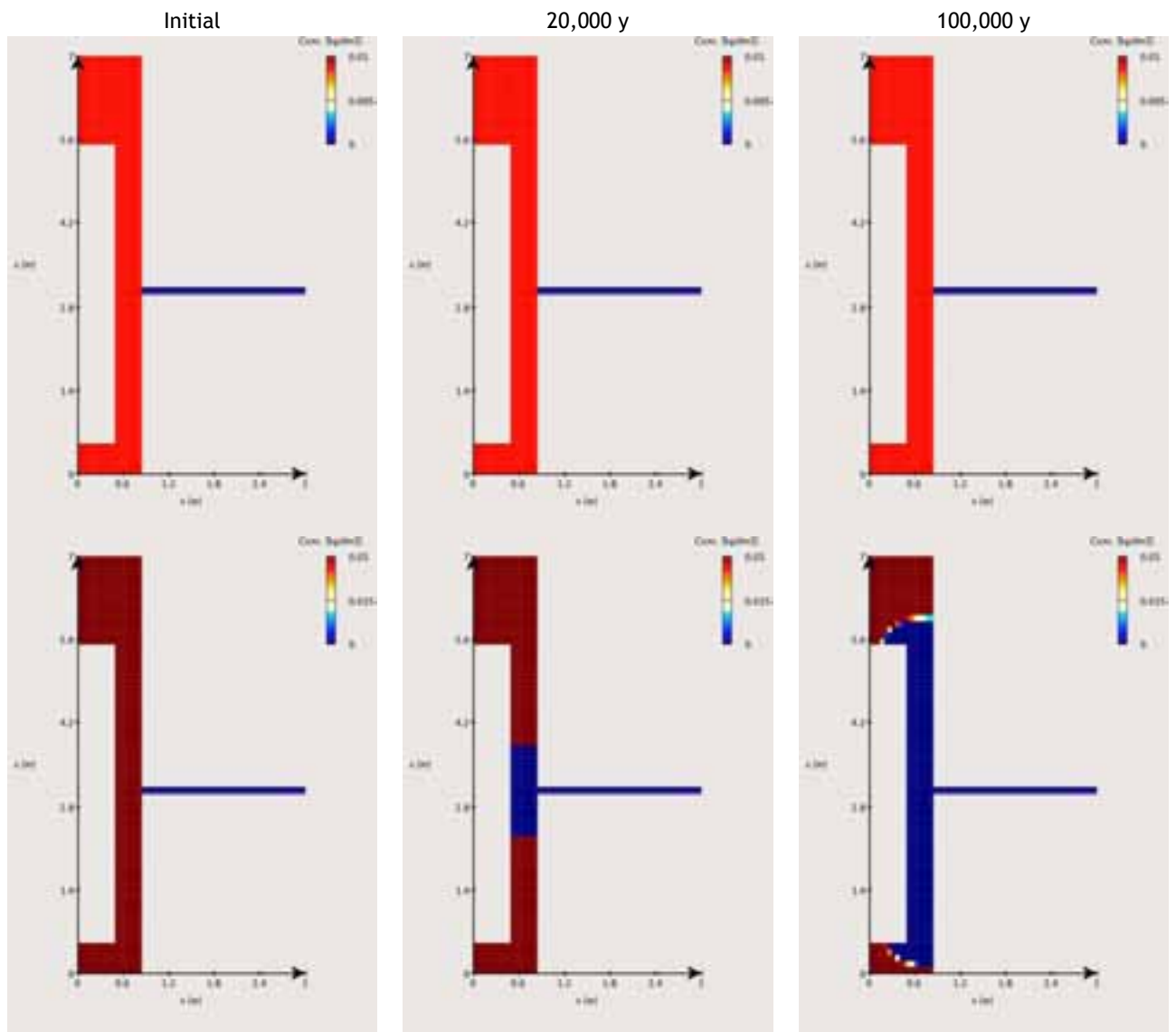


Figure 3-9. High-salinity groundwater intrusion in Deponit CA-N bentonite: evolution of pyrite (top) and siderite (bottom) contents over 100,000 y.

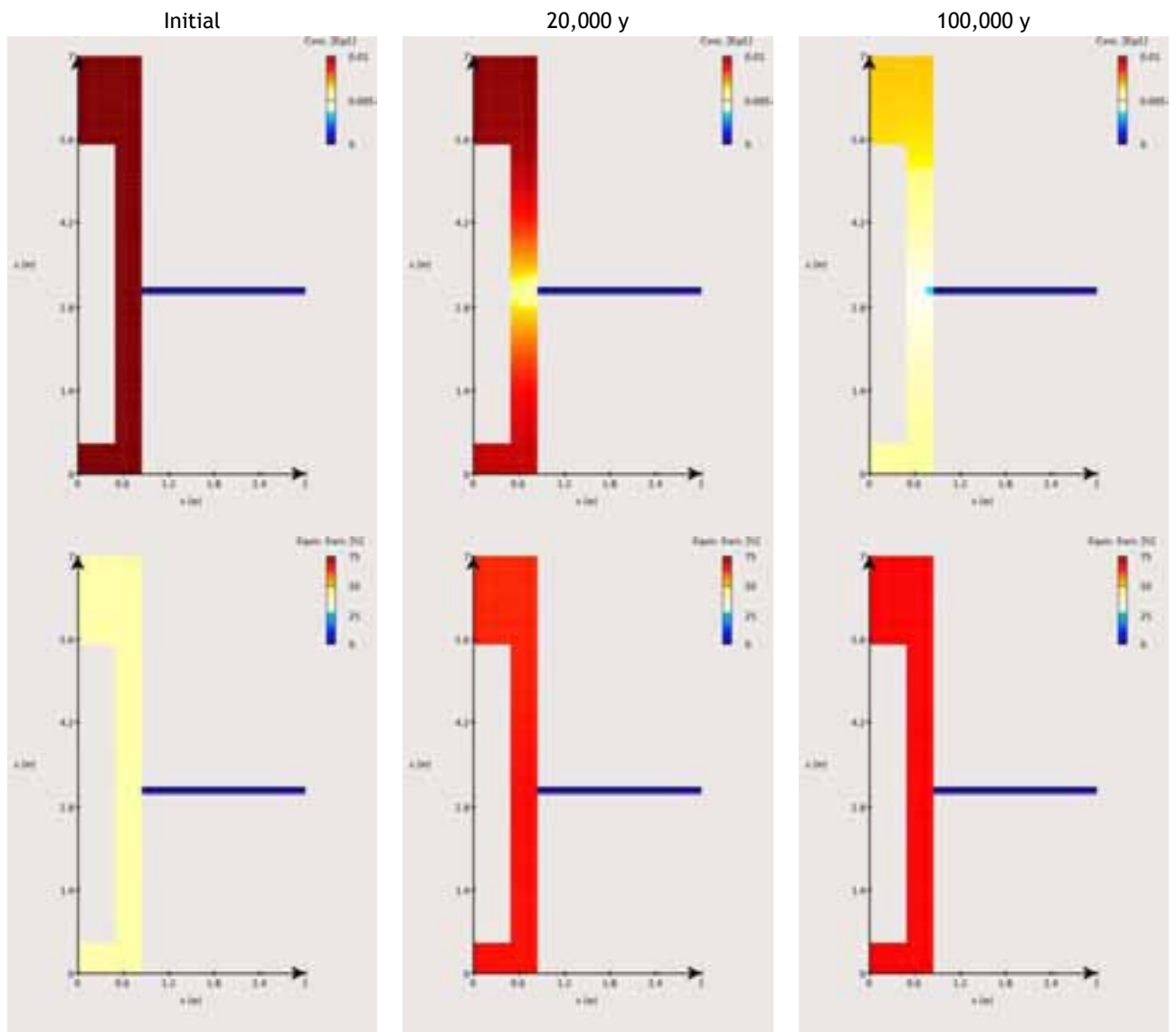


Figure 3-10. High-salinity water intrusion in Deponit CA-N bentonite: evolution of  $\text{DPN-OH}_2^+$  site concentration (top) and exchangeable Ca population (bottom) over 100,000 y.

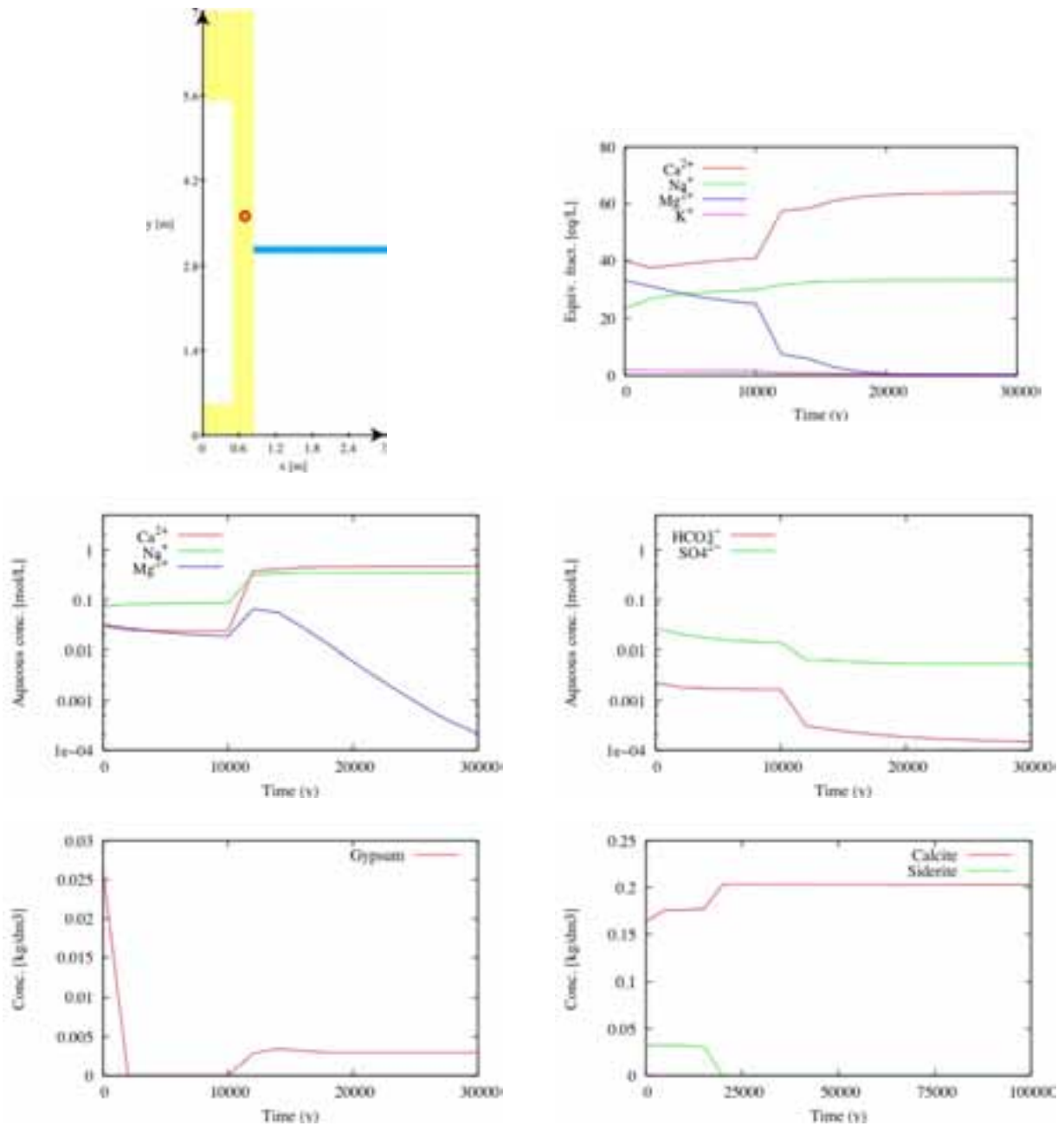


Figure 3-11. High-salinity groundwater intrusion in Deponit CA-N bentonite: evolution of pore water chemistry, cation exchange population and mineralogy in the bentonite, 50 cm above the fracture level.

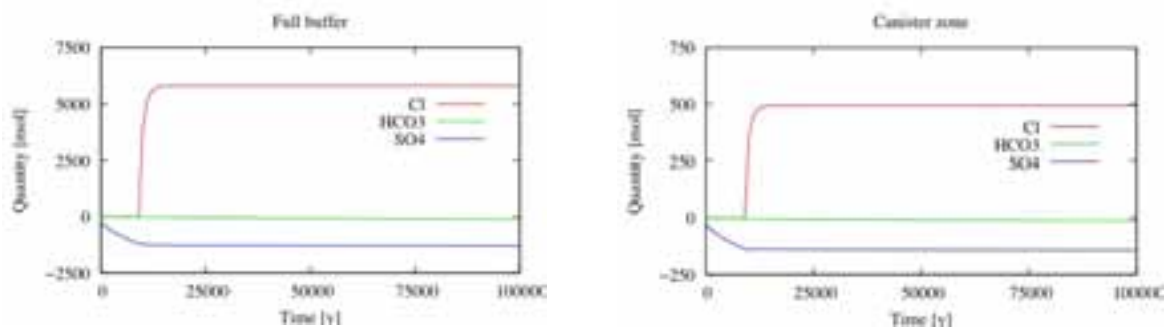


Figure 3-12. Evolution with time of cumulative flux of carbonate, chloride and sulfate ions in the full volume of the bentonite buffer and in the zone around the canister (5 cm width).

### 3.3 ICE-MELTING WATER INTRUSION, THE GRIMSEL GROUNDWATER

In the present simulation case, an ice-melting water coming from the fracture network is assumed to reach the buffer after 10,000 y up to 100,000 y, in replacement of the Forsmark groundwater considered in the reference case.

Figure 3-13 shows the evolution of pH and pe in the buffer over 100,000 y. The ice-melting water, contrasted with respect to the initial bentonite pore water, raises the pH in the entire buffer volume up to around 9 at 20,000 y and around 10 after 100,000 y of interaction. The pe drops from -2.6 to -6.5 in the full buffer volume, as a direct consequence of the concomitant shift of pH towards more alkaline values.

The modelling of the surface complexation (i.e. acid/base properties of the functional group at the clay surface) considers an electrostatic corrective term which is based on the double layer theory. The effect of the electrostatic term is sensitive to the ionic strength, especially at low ionic strength values as in the case of the Grimsel water type. If the corrective factor is turned off in the present calculations, the buffering capacity due to deprotonation of the surface sites is a bit more effective and the pH values are uniformly decreased by 0.3 pH unit.

The evolution of the exchangeable cation populations (Figure 3-14) proceeds in two steps: i) a significant evolution during the first 15,000 y after the intrusion of Grimsel groundwater (fixed Ca ratio increases in most of the buffer volume from 41 to 45-50% range of values while fixed Na ratio decreases from 24 to 15-10 %) and ii) a weak but continuous evolution over the remaining time of simulation, which still develops from the fracture to the other parts of the buffer (Ca and Na ratios reach respectively 80 and 5 % in the bentonite zone close to the fracture, against 50 and 15 % far from the fracture).

The Grimsel water type shows an undersaturation state for both gypsum and dolomite. As a consequence, gypsum which is partly dissolved during the first 10,000 y period of Forsmark groundwater inflowing, completely disappears from the entire bentonite after 10,000 y of interaction with Grimsel water (i.e. in 20,000 y simulation). Dolomite is also totally dissolved in the zones located 1.5 m from the fracture plane leading to calcite precipitation, but is only partly dissolved elsewhere. This mainly results from the first 10,000 y of Forsmark groundwater inflow (Figure 3-15). The contents of the other minerals are rather stable, except for a slight and slow dissolution of siderite in the vicinity of the fracture plane.

Two main cationic depletions due to diffusion from the buffer to the fracture control the mineralogical evolution, that of calcium and of magnesium. The Ca depletion leads to gypsum dissolution, while Mg depletion results in dolomite dissolution. Like in the reference case, the dissolution of dolomite is partly compensated by the precipitation of calcite. There is globally, over the whole simulation period, a replacement of Na by Ca in the exchanger with an intensification of this process at proximity of the fracture plane. The proportions of fixed cations tend to those of Deponit CA-N exchanger in strict equilibrium with the Grimsel water chemistry (i.e. 95% fixed Ca, 4% Na, 1% Mg, 0.1% K). The propagation within bentonite is in this case very slow since weakly mineralized water with low absolute concentrations in aqueous cations requires more time to change the cation exchange populations than more mineralized water.

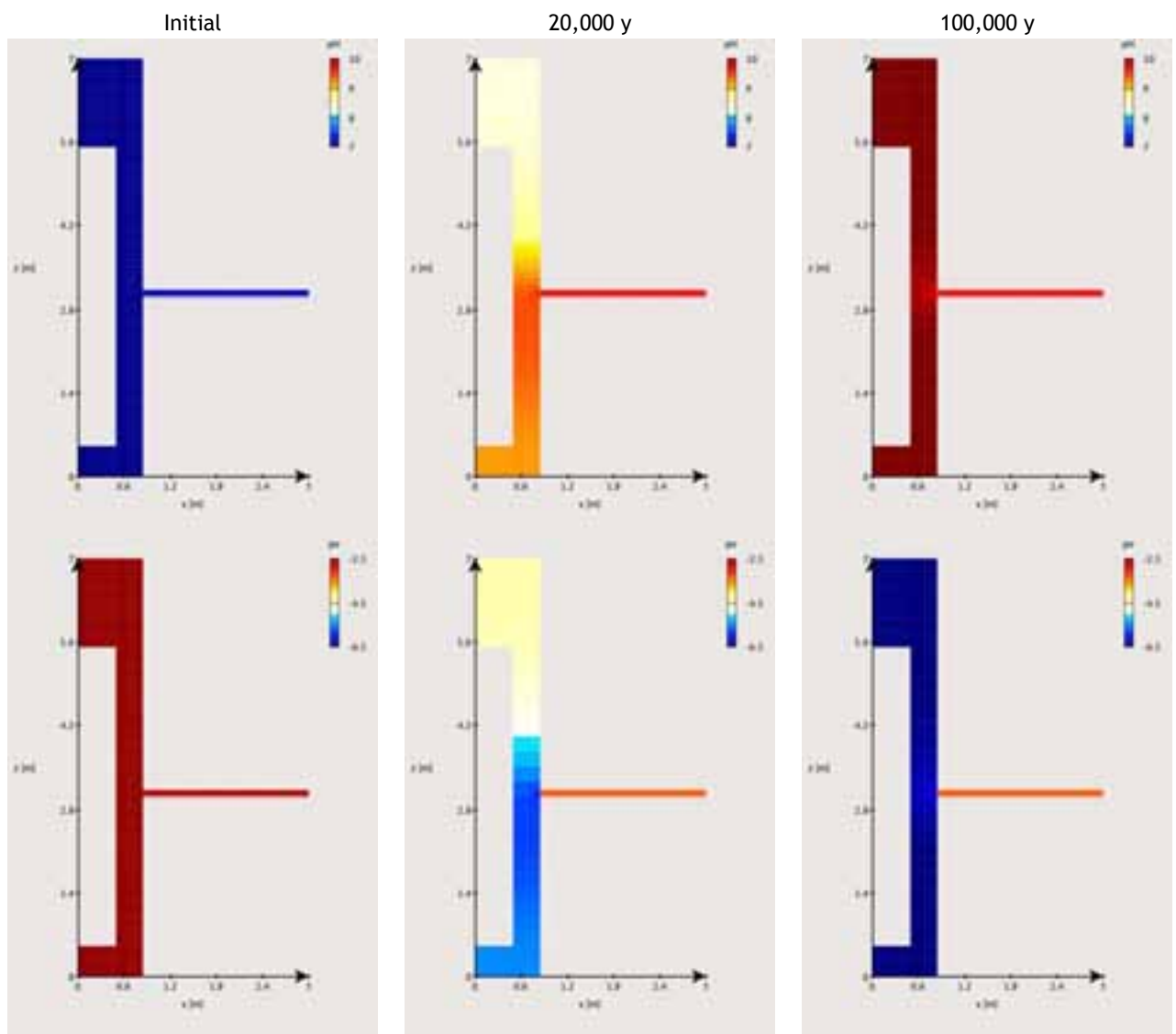


Figure 3-13. Ice-melting water intrusion in Deponit CA-N bentonite: evolution of pH and pe over 100,000 y.

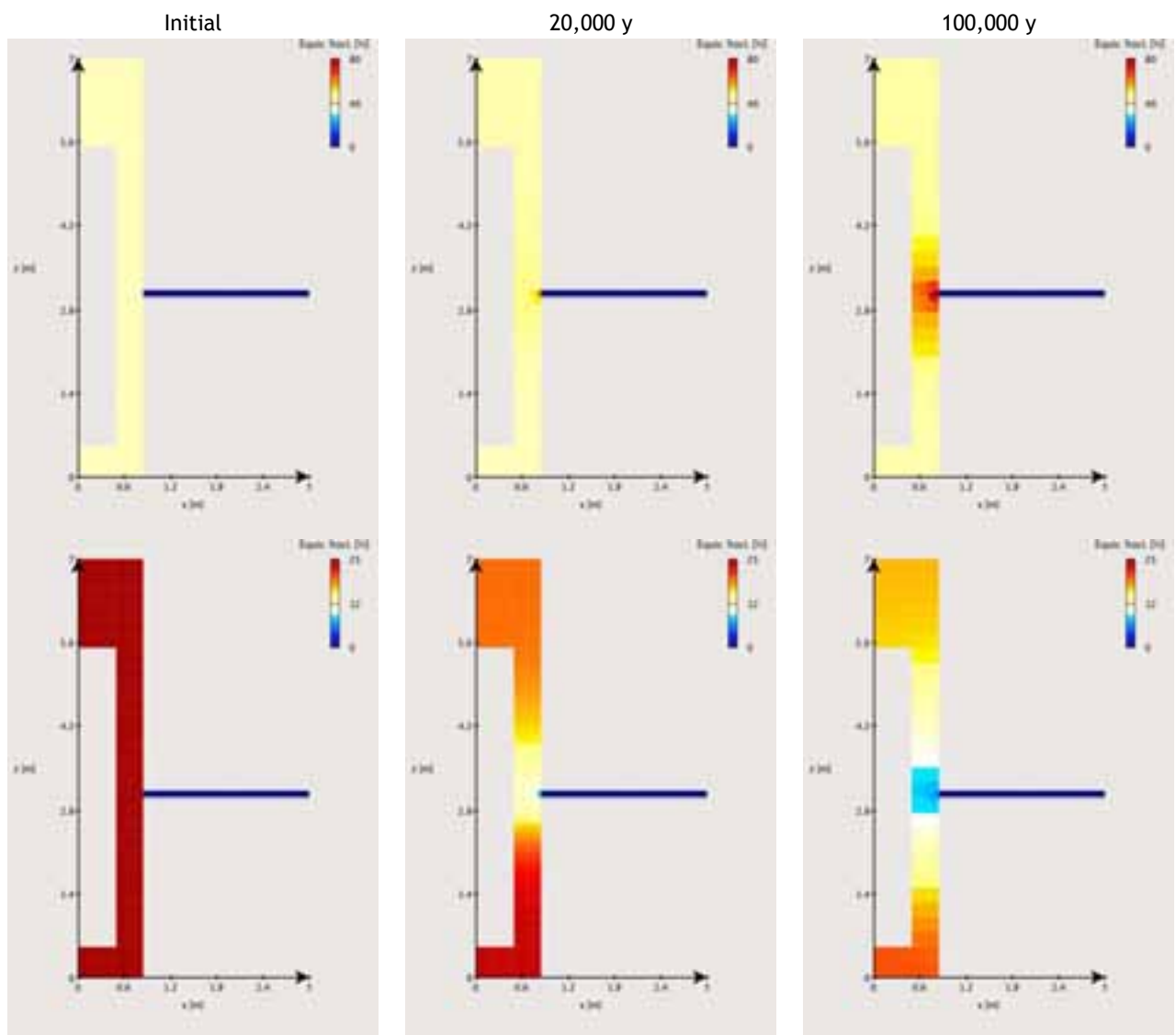


Figure 3-14. Ice-melting water intrusion in Deponit CA-N bentonite: evolution of exchangeable Ca (top) and Na (bottom) populations over 100,000 y.

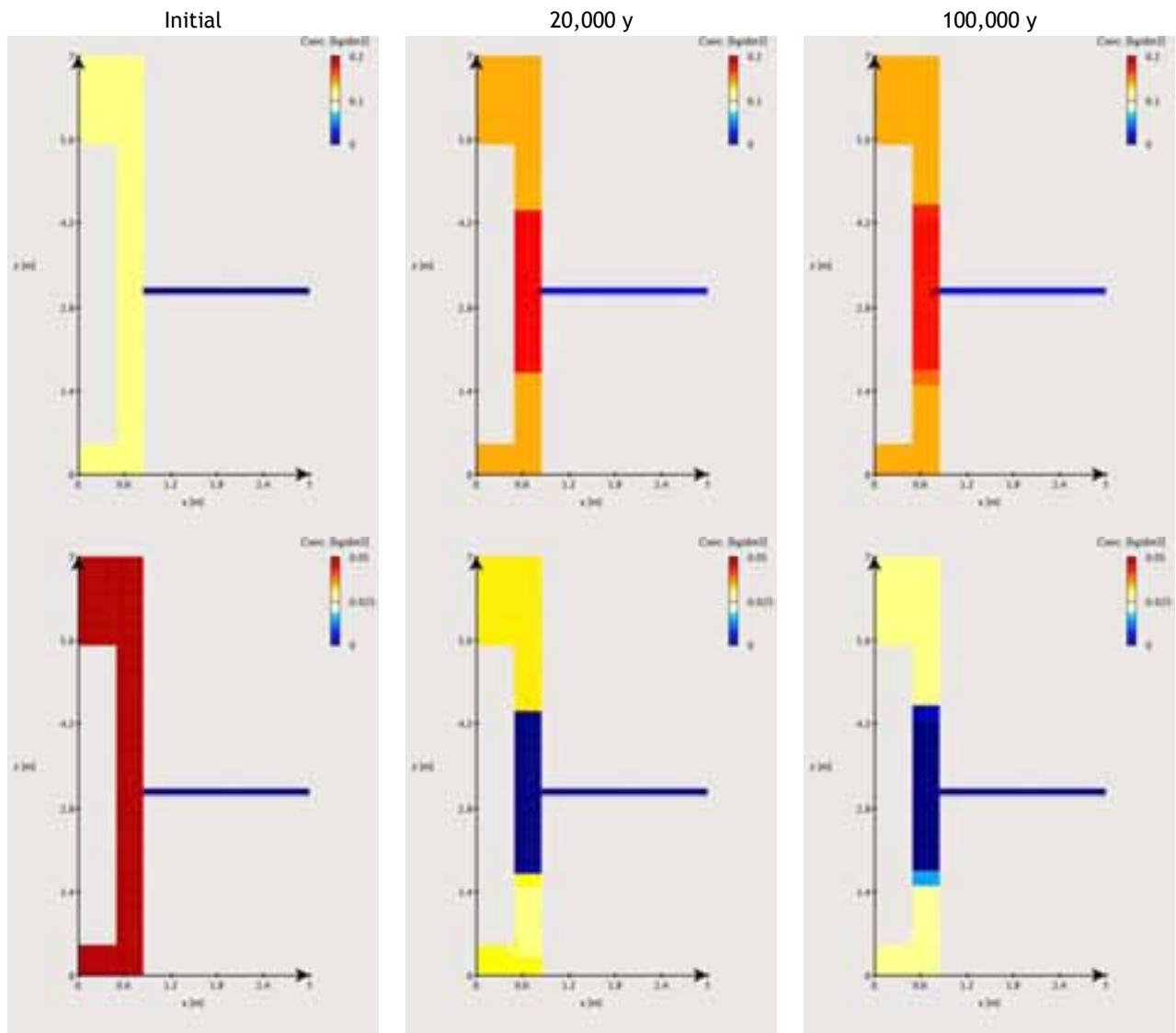


Figure 3-15. Ice-melting water intrusion in Deponit CA-N bentonite: evolution of calcite (top) and dolomite (bottom) over 100,000 y.

### 3.4 SENSITIVITY ANALYSIS

The reference case, i.e. the intrusion of Forsmark groundwater, is used for the sensitivity analysis to the equilibrium constant for gypsum. The other sensitivity analysis calculations are based on the high-salinity groundwater intrusion scenario because it yields to stronger geochemical perturbation and evolution compared to the reference case and therefore enhance the observed trends.

#### 3.4.1 GYPSUM EQUILIBRIUM CONSTANTS

The equilibrium constant (log K) for gypsum is found to vary depending on the thermodynamic database (TDB), as reported in Table 3-1. Though the discrepancies between these Log K values appear quite small, the behavior of gypsum calculated for the simulation cases treated in the present study is relatively sensitive to the selected Log K, as illustrated hereafter for the reference case with Deponit CA-N bentonite.

Figure 3-16 gives the gypsum concentrations calculated using either the Log K of 4.48 selected throughout the present study, or that of 4.85 chosen in Arcos *et al.* (2006), at different interaction times. The gypsum dissolution front propagates clearly faster with the lower Log K value. This explains the differences between both studies regarding the calculated times for a complete dissolution of gypsum in the entire buffer volume. However, the variations are less important when considering MX-80 bentonite, as the initial amount of gypsum is lower than in Deponit CA-N bentonite. At last, it is worth noting that these studies take into account the two boundary values of the Log K range. An intermediate value, i.e. that from the updated MINTEQ TDB, may have been more appropriate in view of the base calculation sets.

Table 3-1. Gypsum formation constant ( $\text{Ca}^{2+} + \text{SO}_4^{2-} + \text{H}_2\text{O} \rightarrow \text{CaSO}_4 \cdot \text{H}_2\text{O}$ ) from various thermodynamic databases.

TDB	Log K (25°C)	Reference
MinteqA2	4.85, updated 4.60	Allison <i>et al.</i> , 1991
Hatches-r10	4.60	Hatches, 1991
Nagra	4.58	Pearson and Berner, 1991
EQ3/6	4.48	Wolery, 1992

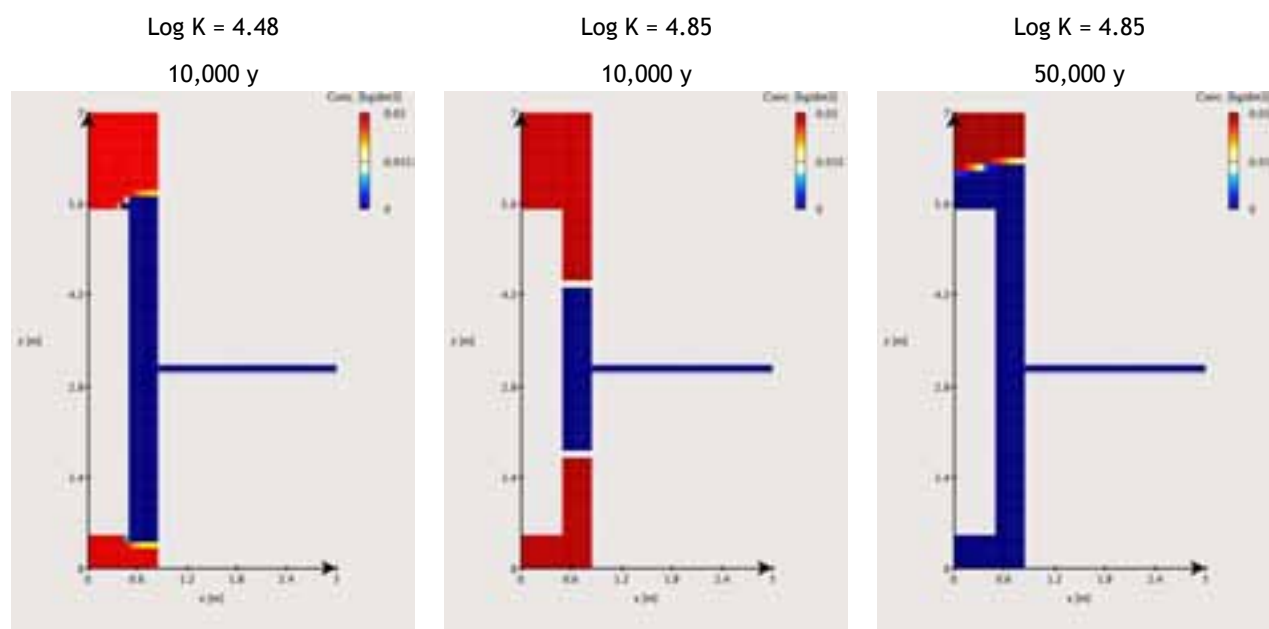


Figure 3-16. Influence of the Log K value selected for gypsum on the stability of this mineral: evolution of gypsum concentration at 10,000 and 50,000 y for the reference case with Deponit CA-N Bentonite.

### 3.4.2 ACTIVITY CORRECTION MODELS

The truncated Davies equation is commonly used to calculate ion activity in solution. This model is accurate up to an ionic strength of 0.5 mol/l. The B-dot equation, which is also an extended form of the Debye-Hückel equation, can be applied to a range of natural waters, including dilute fluids and dominant NaCl solution with ionic strength up to 3 mol/l. The high-salinity groundwater has an ionic strength of 1.7 mol/l, therefore well above the Davies theoretical threshold. On the other hand, its NaCl signature makes it suitable for the application of the B-dot approach.

In the present study, the truncated Davies model has been used for the reference case and the ice-melting water intrusion whereas the B-dot model has been assigned to any calculations dealing with the Laxemar groundwaters. It is worth noting, however, that a sensitivity calculation made with the truncated Davies model instead of the B-dot did not lead to any significant discrepancy in the modelling results.

### 3.4.3 NUMERICAL CONSIDERATIONS

#### *Iterative coupling scheme and time-step*

HYTEC code is based on a sequential iterative approach with possibly varying time-steps (see section 2.1.2) whereas PHAST code used in Arcos *et al.* (2006) considers a non iterative approach and takes into account a fixed time-step (Parkhurst *et al.*, 2004). A set of calculations has thus been launched in a non iterative sequential mode with fixed time-steps ranging from 0.1 y to 100 y. The corresponding results have been compared to those obtained by considering a normal sequential iterative approach with an adaptative time-step. For time-steps greater than 1 y, HYTEC either encountered fatal non-convergence problems or oscillation patterns without any physical meanings. The results obtained with non iterative constant time-steps of 0.1 and 1 y (i.e. analogue to PHAST) were in very good agreement with the those obtained with the sequential iterative approach (i.e. HYTEC in normal mode), as shown in Figure 3-17 for sharp oxidative dissolution fronts classically harder to tackle with.

#### *Grid size refinement*

As introduced in section 2.1, HYTEC is based on a finite volume spatial discretization method rather than a finite element (FE) approach. The FE approach lacks precision in the definition of an initial mass or concentration confined in a specific geometric area, due to the interpolation of concentration between adjacent nodes. This is schematically illustrated by Figure 3-18, which shows the mass-distribution over two elements in a one-dimensional system (assuming linear interpolation). FD and FV approaches, which use a constant concentration in each element, are precise with respect to this problem. The FV approach also provides a more precise solution in the case of a variable porosity. Mineral concentrations (which indirectly define the porosity) are calculated at exactly the same point where the hydrodynamic model uses the porosity, in the centre of a representative volume.

Notwithstanding the relevancy of the FV approach for reactive transport calculations, the quality and accuracy of a modelling study may depend on the refinement of the grid size (see for instance de Windt and Badreddine, 2007). The grid sizes shown in Figure 2-3 and Figure 2-4 were found to be operational, that is to say they offered a good accuracy for a reasonable CPU calculation time. To check that point a sensitivity analysis calculation was made with a number of nodes increased by a factor 4 (Figure 3-19). The pH profiles are slightly different but no difference can be noticed for the profiles of siderite dissolution. Globally, grid size refinement did not lead to any significant improvement in the system evolution simulation.

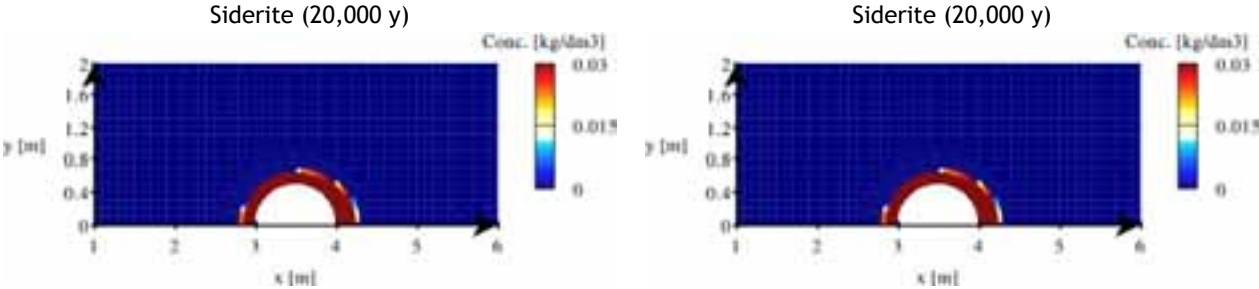


Figure 3-17. Highly-saline groundwater intrusion, modelling results obtained with an iterative sequential coupling and an adaptative time step (left) and with a non iterative sequential coupling and a fixed time step of 1 y (right).

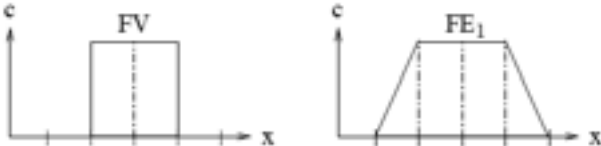


Figure 3-18. Illustration of mass distributions for FV and FE approaches. Too much mass is defined for uncorrected FE approach.

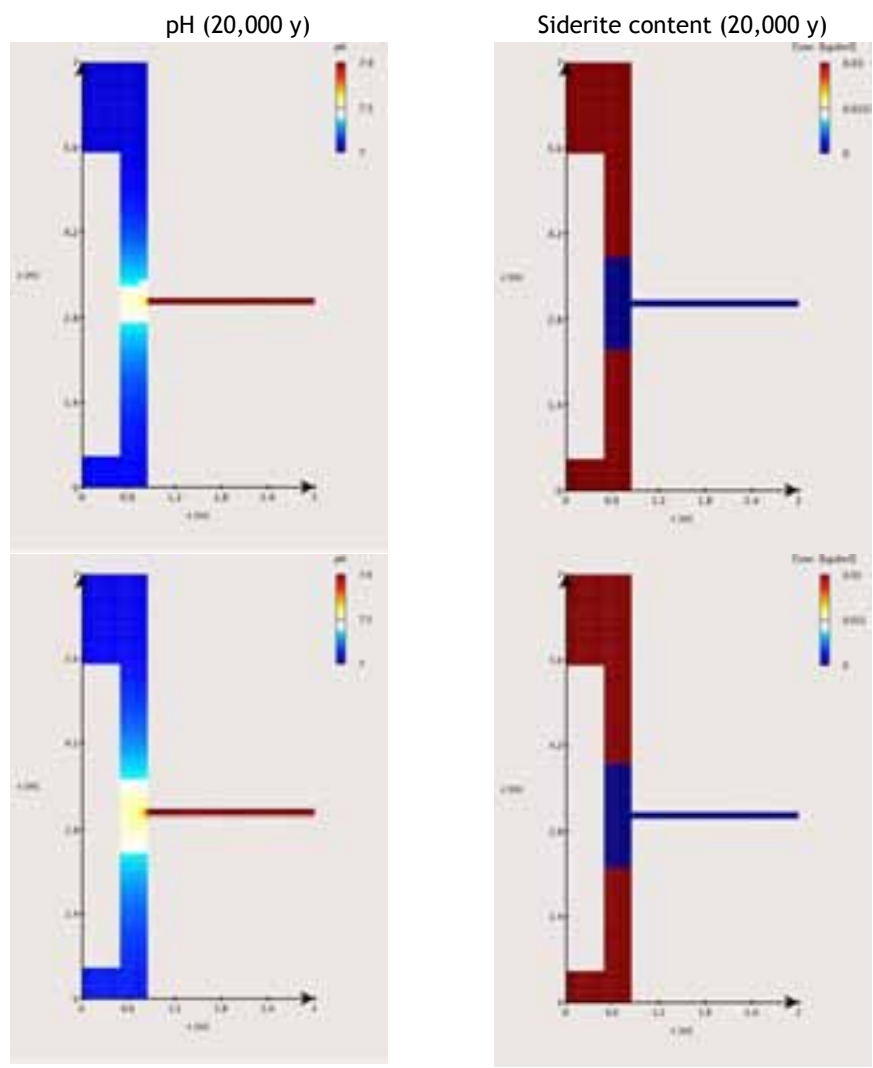


Figure 3-19. Highly-saline groundwater intrusion, the number of nodes is increased by a factor 4 between the top and bottom graphs.

## 4 MX-80 BENTONITE/GROUNDWATER LONG-TERM INTERACTIONS

### 4.1 REFERENCE CASE, THE FORSMARK GROUNDWATER

As observed with the Deponit CA-N bentonite, the intrusion of Forsmark groundwater into MX-80 bentonite induces a moderate evolution of pH and thus of  $p_e$ , which progressively develops from the bentonite zone at the fracture plane level to the whole buffer volume over the calculation period (100,000 y). Modelling results reported in Figure 4-1 show that pH increases from 7.0 to 7.2 at the most, trending in this way to reach the pH value of Forsmark groundwater, whereas  $p_e$  decreases from -3.15 to -3.3 accordingly.

The evolution of the exchangeable cation populations on montmorillonite shows an important fixation of Ca at the expense of Na (Figure 4-2): fixed Ca proportion increases from 18 to about 50 %, whereas the fixed Na decreases from more than 72 to 35 %. This process takes place progressively reaching a quasi steady-state over about 60,000 y at the top of the bentonite buffer, as shown in Figure 4-3. The mineral phases remain almost stable, except gypsum that completely disappears from the entire buffer volume after 5,000 y of interactions (Figure 4-4). A very slight (but continuous over 100,000 y) precipitation of calcite and siderite within bentonite near the fracture is nevertheless calculated.

Two major processes drive the above-described evolution: diffusion of aqueous sulfates from the buffer to the fracture and diffusion of Ca from the fracture to the buffer. Sulfates out-diffusion, due to its concentration initially about two times higher in the bentonite than in the Forsmark groundwater, leads to an aqueous sulfates depletion within the bentonite and subsequently to gypsum dissolution so as to counteract the depletion. In addition to gypsum dissolution, the gradient in aqueous Ca content, which is more than two times higher in the Forsmark groundwater than in the buffer, results in an increase in aqueous Ca within bentonite. As a consequence, Na initially sorbed in the montmorillonite exchanger is replaced by Ca (Figure 4-3). After gypsum dissolution, the in-diffusion of Ca in the buffer remains the only source for this aqueous species, thus the Na by Ca replacement proceeds slower. It is worth noting that in the present case, gypsum dissolves faster (5,000 y) than in the reference case with Deponit CA-N bentonite (25,000 y) due to i) a smaller amount of gypsum in the MX-80 bentonite and ii) a stronger concentration gradient in aqueous sulfates. The pH of the bentonite pore water is mainly controlled by the acid/base properties of the montmorillonite clay and the composition of the Forsmark groundwater.

As mentioned in section 2.4.3, an uncertainty exists regarding the composition of MX-80 bentonite, which may contain carbonate minerals (calcite and siderite). Calculations accounting for these minerals indicate a slight dissolution of calcite over the first 20,000 y (Figure 4-5) as aqueous carbonates diffuses out to counter the concentration gradient between the buffer and fracture waters. However, the in-diffusion of aqueous Ca interferes (in the opposite way) with this dissolution process, so that the dissolution of calcite is more pronounced in the bentonite parts far from the fracture than at the level of groundwater inflowing. This leads to a pH increase from 7.0 up to 7.5 in the part of the buffer far from the fracture (up to 7.2 near the fracture). Calcite dissolution stops when aqueous carbonate content within the buffer reaches the Forsmark groundwater one. Then, as aqueous

Ca goes on inflowing, though at a progressively lower rate, calcite slightly precipitates and thus influences the pH, which decreases down until the end of the simulation to the value of 7.2 in the whole buffer (Figure 4-6). These processes do not significantly change either the Na by Ca exchange ratio or the gypsum dissolution period.

At last, as in the reference case with the Deponit CA-N bentonite, the similarity between the redox state of MX-80 bentonite and Forsmark groundwater preserves the redox sensitive minerals from any significant alteration.

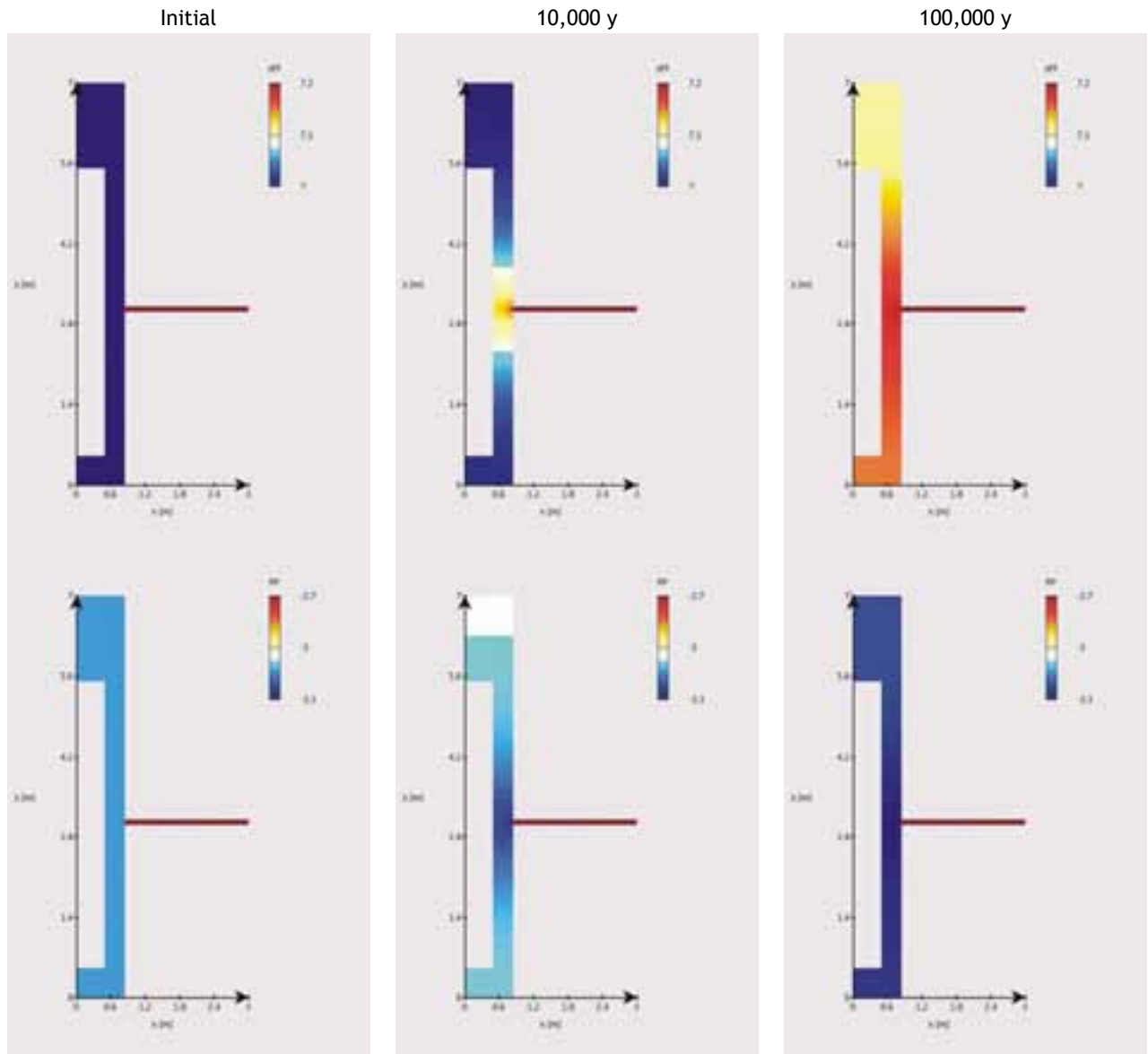


Figure 4-1. Reference case with MX-80 bentonite: evolution of pH and pe over 100,000 y.

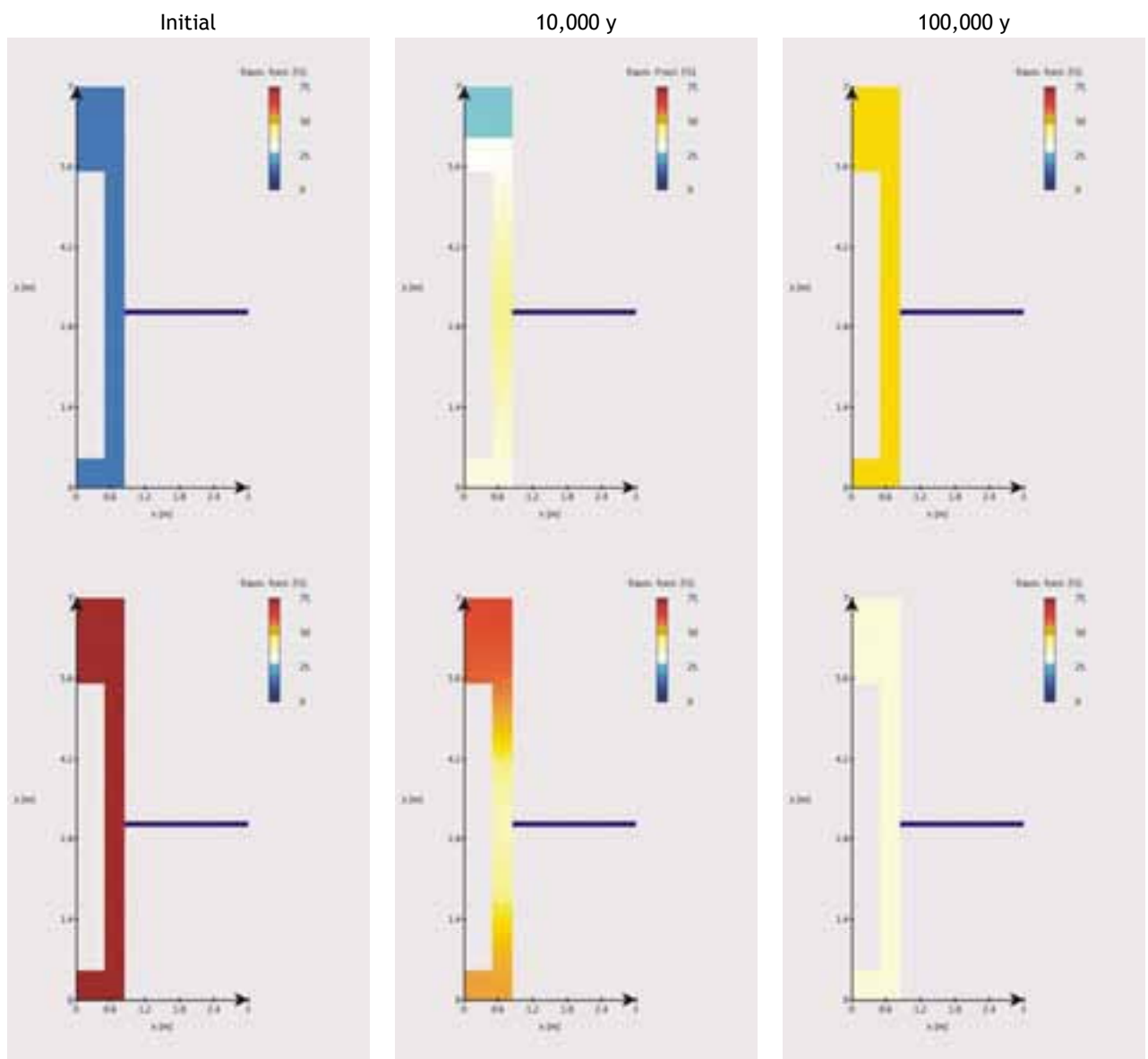


Figure 4-2. Reference case with MX-80 bentonite: evolution of exchangeable Ca (top) and Na (bottom) populations over 100,000 y.

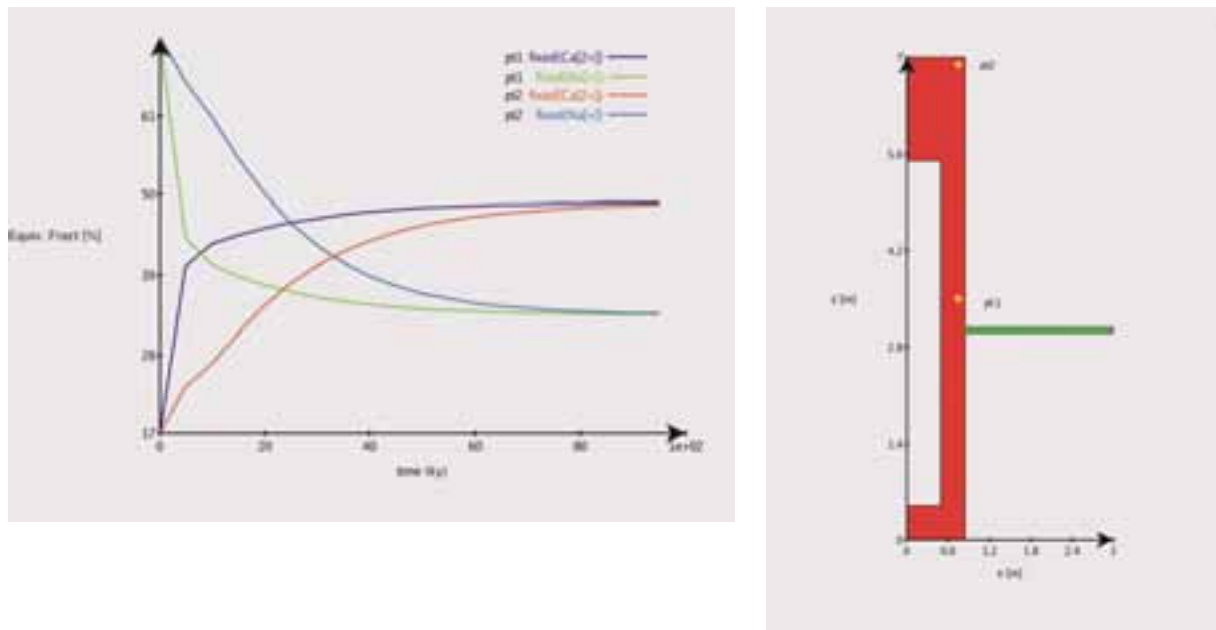


Figure 4-3. Reference case with MX-80 bentonite: evolution of exchangeable Na and Ca populations as a function of time over 100,000 y at two points, located at 0.5 and 3.9 m above the fracture level as defined in the figure on the right.

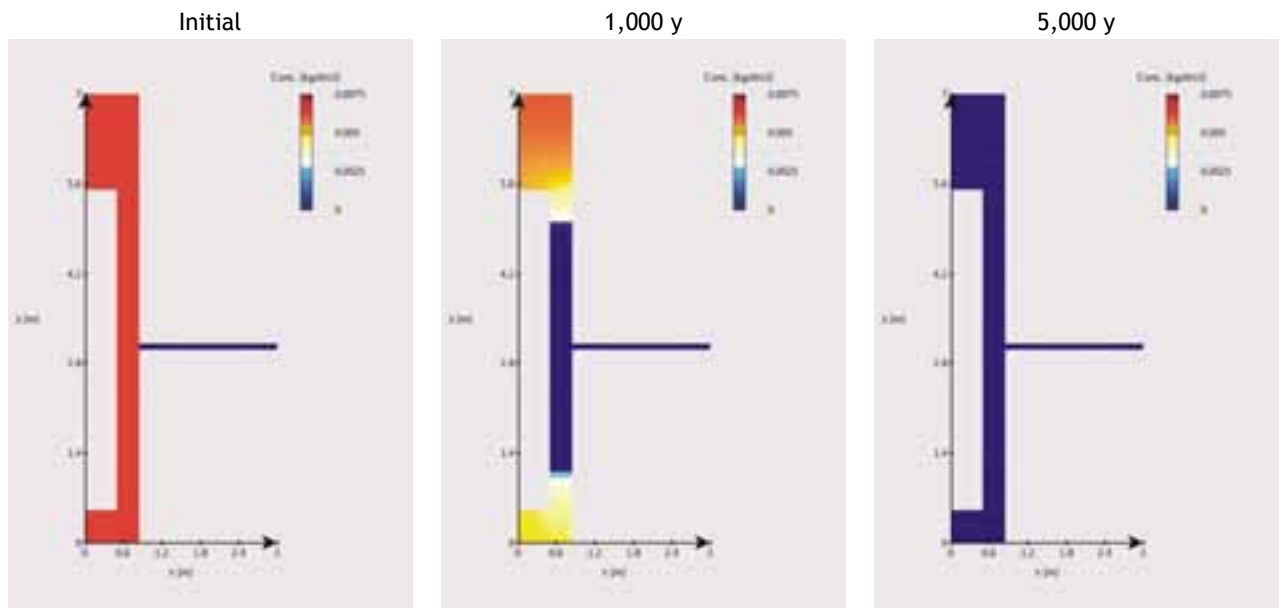


Figure 4-4. Reference case with MX-80 bentonite: evolution of gypsum content over 5,000 y.

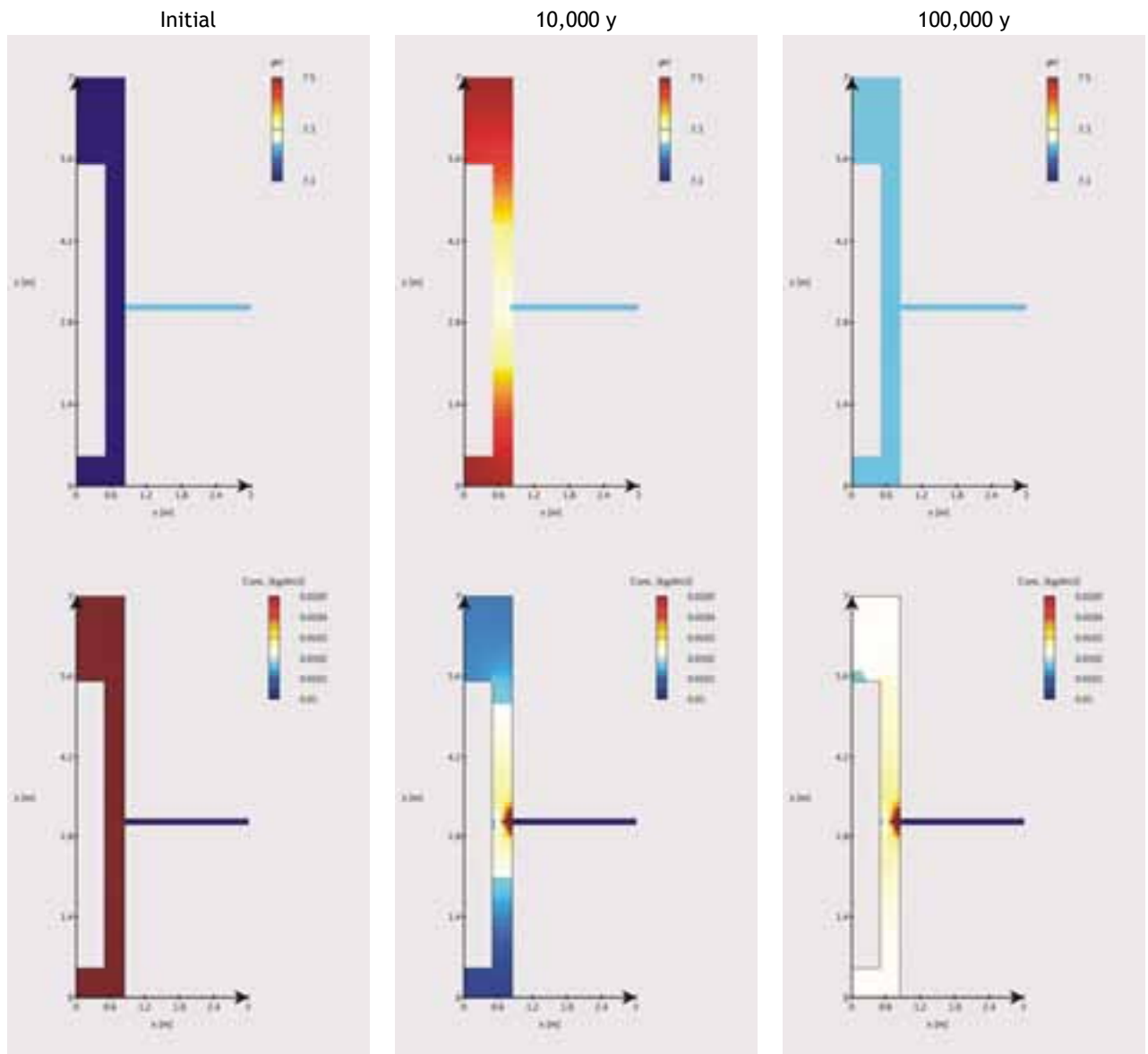


Figure 4-5. Reference groundwater intrusion in with MX-80 bentonite with carbonate minerals: evolution of pH and calcite content over 100,000 y.

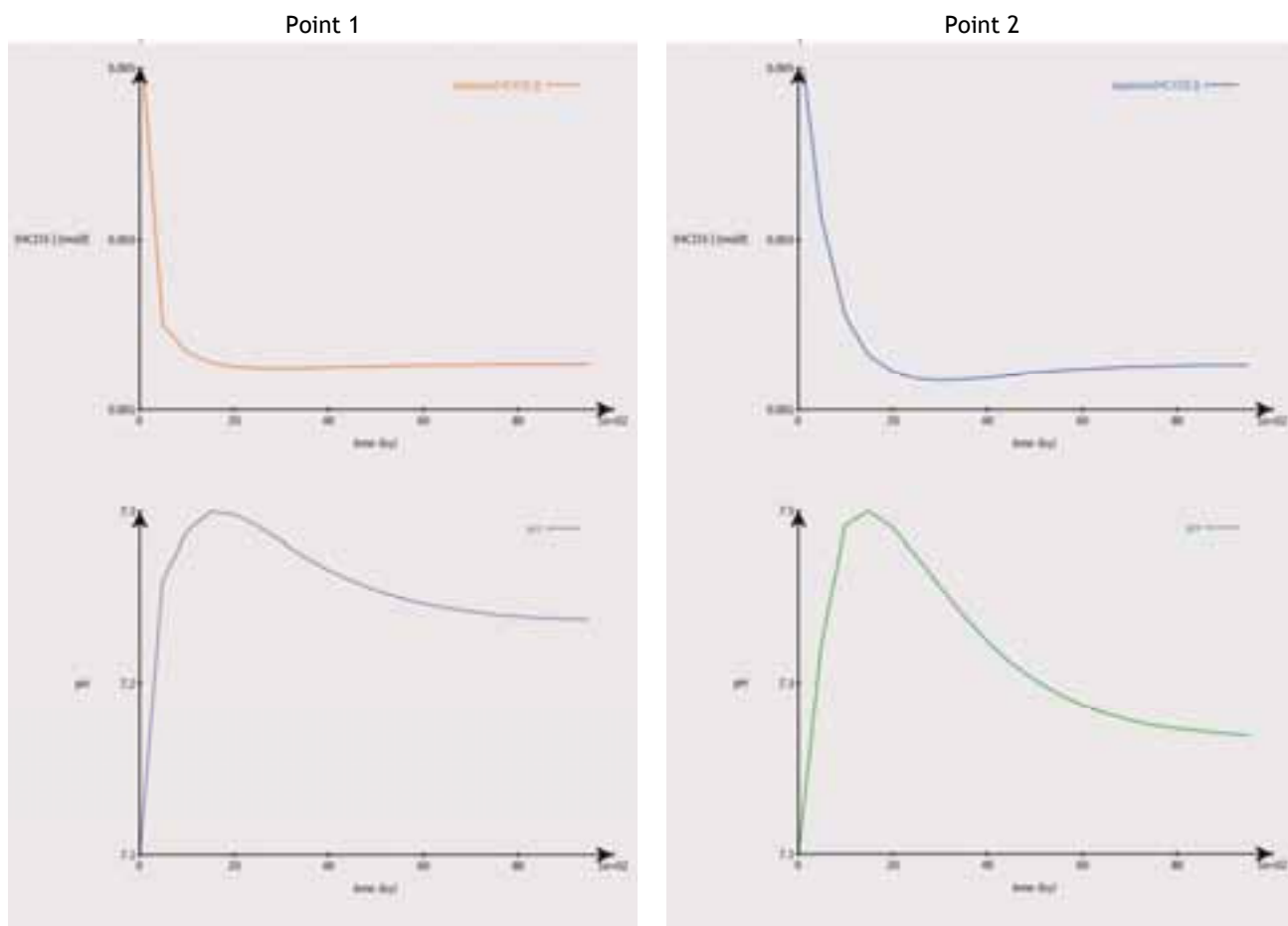


Figure 4-6. Reference groundwater intrusion in with MX-80 bentonite with carbonate minerals: evolution of aqueous carbonate concentration (top) and pH (bottom) at two points, located at 0.5 and 3.9 m above the fracture level as defined in Figure 4-3.

## 4.2 HIGH-SALINITY WATER INTRUSION, THE LAXEMAR GROUNDWATER

The model considers a circulation of Forsmark groundwater in the fracture network during the first 10,000 y, followed by a long-term intrusion of a highly-saline groundwater, the Laxemar groundwater. The first 10,000 y step of the system evolution is therefore strictly identical to that of the Forsmark reference case (see section 4.1). Some of the processes mentioned below regarding the interaction between MX-80 bentonite and Laxemar groundwater have been detailed in previous cases, notably the case with Deponit CA-N bentonite (see section 3.2). Their description is therefore abridged in the followings.

The intrusion of Laxemar groundwater into MX-80 bentonite leads to slight changes in pH and  $p_e$ , as shown in Figure 4-7. A slow increase in pH is observed close to the fracture, from 7.0 up to 7.5 over 100,000 y, while the other parts of the buffer remain at a pH of 7.0. pH is actually strongly buffered by the acid/base properties of the buffer. As in the previous cases,  $p_e$  slowly evolves according to pH.

Large amounts of Ca diffuse into the bentonite when the intrusion of Laxemar groundwater starts, since calcium concentration is 20 times higher in the Laxemar groundwater than in the Forsmark one. This process notably

increases the Na by Ca exchange in the buffer as illustrated in Figure 4-8. Ca fixed in montmorillonite reaches values close to 64 % in the whole buffer after 10,000 y of interaction with the Laxemar groundwater (i.e. 20,000 y of simulation). On the contrary, a depletion of aqueous Mg and K is observed, leading to a decrease of the fixed proportions in the exchanger (10 to 16 % of Mg fixed at the intrusion of Laxemar groundwater to 0 % after 20,000 y of simulation). The fixed Na population narrowly varies to a steady value of 36 %. This distribution of fixed cations is then maintained constant until the end of the simulation.

At last, it is worth mentioning that gypsum disappears from MX-80 bentonite during the interaction with the Forsmark groundwater but, on the contrary to the case with Deponit CA-N bentonite, this mineral does not precipitate as the Laxemar groundwater enters the system. The other mineral phases do not significantly evolve until the end of the simulation time.

Calculations taking into account calcite and siderite in MX-80 bentonite composition indicate a geochemical evolution of the buffer close to that observed for Deponit CA-N bentonite in interaction with Laxemar groundwater. Figure 4-9 shows that the pH of the buffer pore water increases over 100,000 y from 7.0 to 7.9 at the fracture plane level and to 7.4 far from the fracture, showing that equilibrium in terms of pH is not reached at the end of the simulation. The undersaturation of siderite leads to the complete dissolution of this mineral in the whole bentonite at 70,000 y. Calcite precipitation due to important Ca in-diffusion from the high-salinity groundwater compensate siderite dissolution (Figure 4-10). After this dissolution, calcite slightly dissolves until the end of the simulation. At last, one notes that gypsum and exchangeable cation populations evolve as observed for MX-80 bentonite without carbonates.

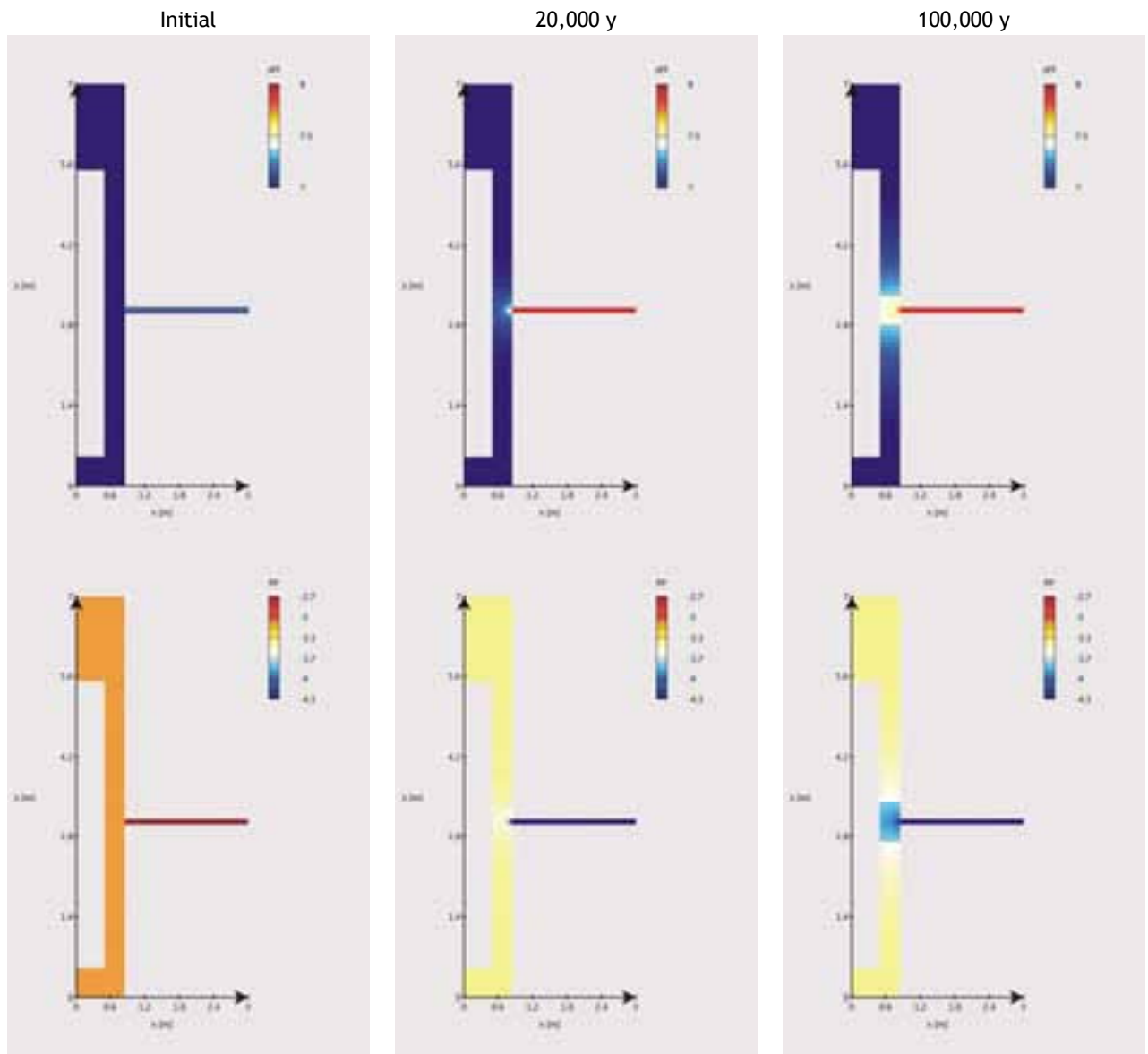


Figure 4-7. High-salinity water intrusion in MX-80 bentonite: evolution of pH and pe over 100,000 y.

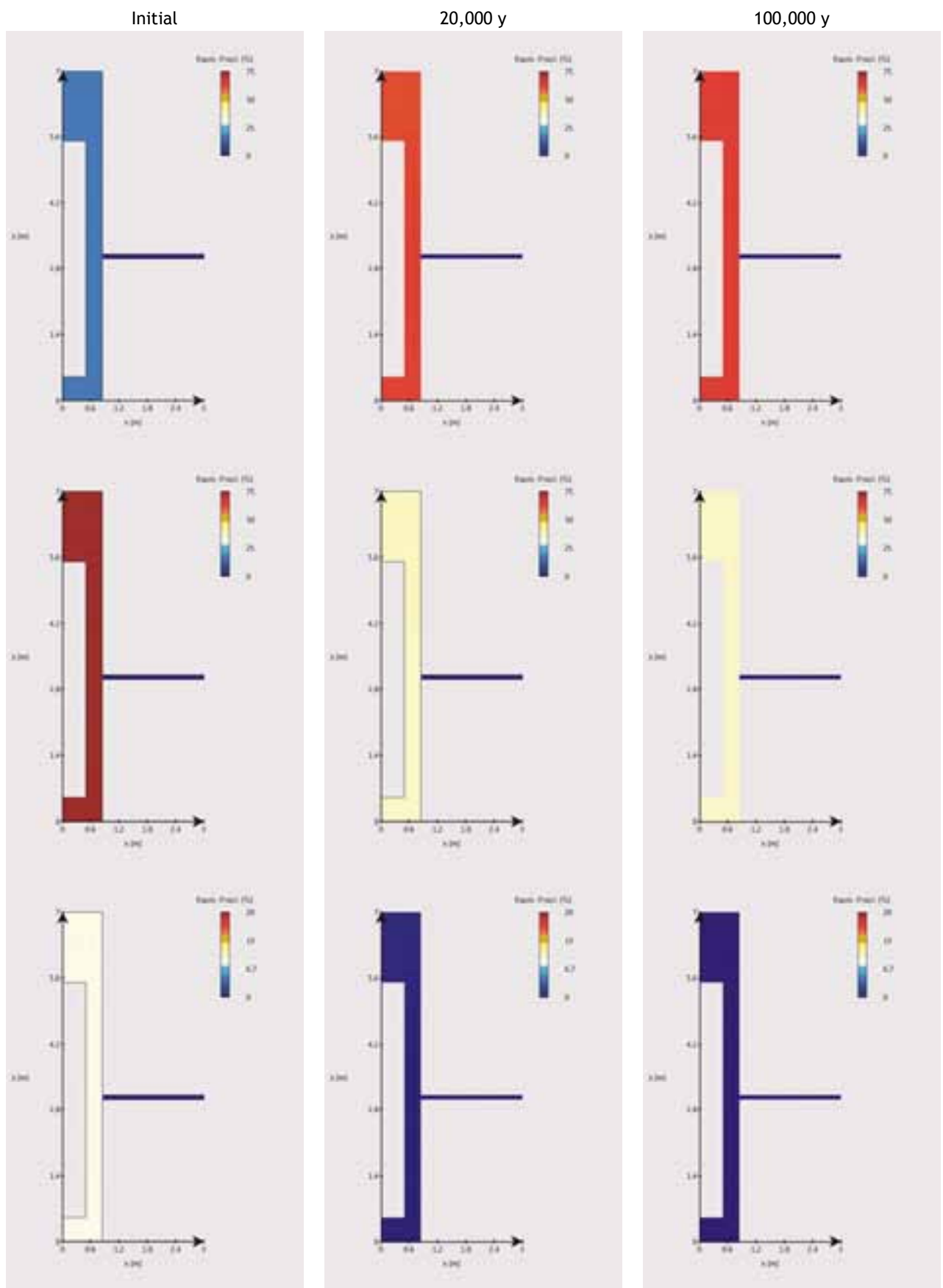


Figure 4-8. High-salinity water intrusion in MX-80 bentonite: evolution of exchangeable Ca (top), Na (middle) and Mg (bottom) populations over 100,000 y.

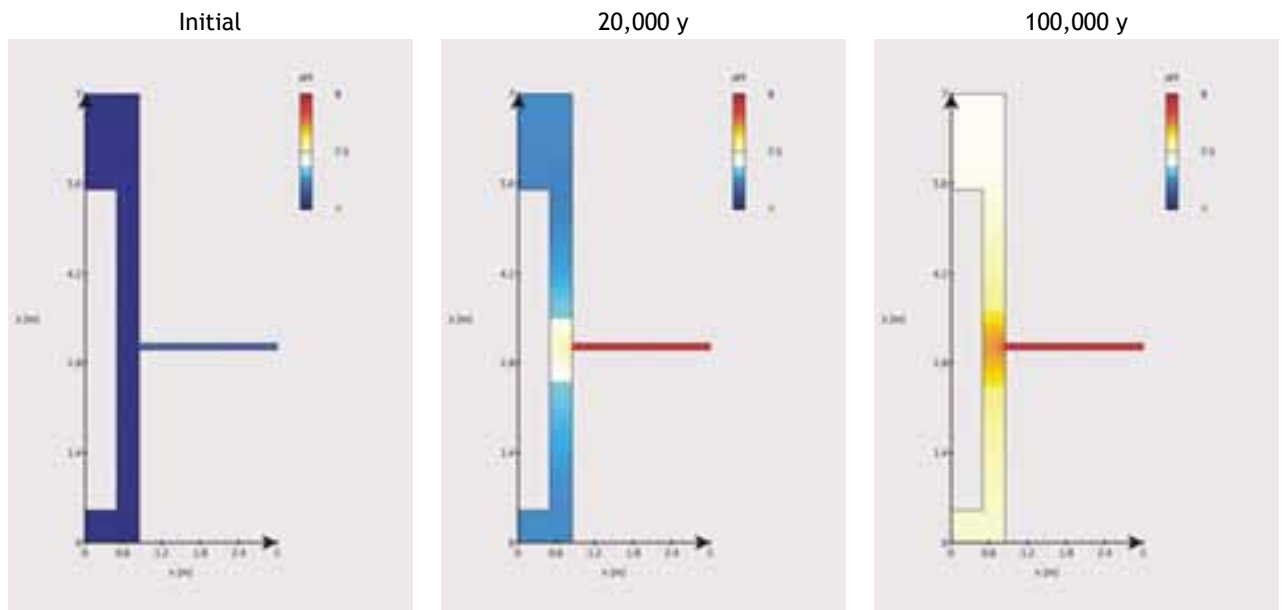


Figure 4-9. High-salinity water intrusion in MX-80 bentonite with carbonate minerals: evolution of pH over 100,000 y.

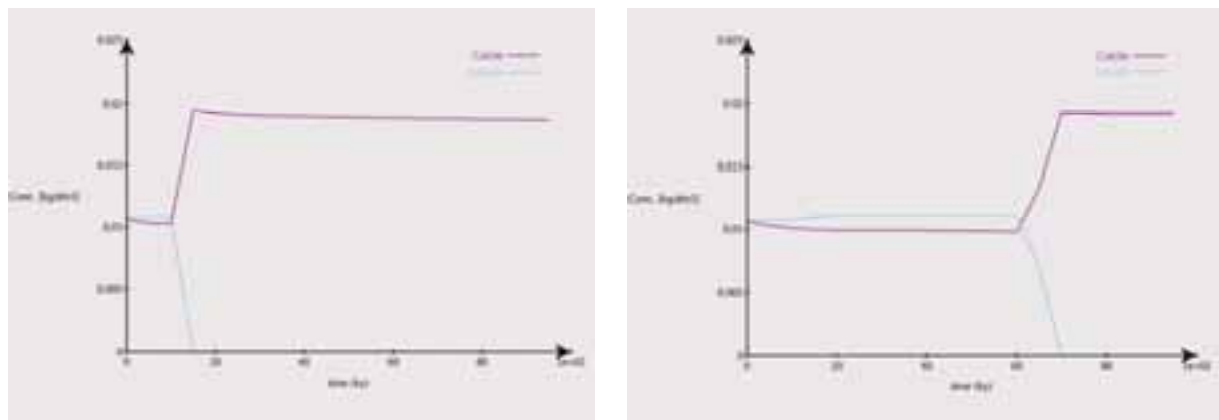


Figure 4-10. High-salinity water intrusion in MX-80 bentonite with carbonate minerals: evolution of calcite and siderite contents as a function of time over 100,000 y at two points, located at 0.5 m (left) and 3.9 m (right) above the fracture level as defined in Figure 4-3.

### 4.3 ICE-MELTING WATER INTRUSION, THE GRIMSEL GROUNDWATER

The present case assumes that an intrusion of ice-melting water in the near-field takes place via the fracture after a first 10,000 y period of Forsmark water inflowing, until the end of the simulation (100,000 y). The perturbation in pH and pe caused by such diluted water (ionic strength 0.001 mol/L, pH 9.6) slowly develops throughout the buffer over 100,000 y of interaction, without reaching a uniform state as shown in Figure 4-11. The pH of the bentonite pore water rises from 7.0 up to 9.5 at the level of the fracture, while a value of 8 is calculated at the top of the buffer. Accordingly, pe decreases from -3.15 to -5.9 within bentonite near the fracture and to -4.5 far from it. This pH increase is principally due to the diffusion of the high pH plume produced by the ice-melting water, delayed by the deprotonation of montmorillonite surface sites.

As in the reference case (intrusion of Forsmark groundwater), gypsum completely dissolves over the first 5,000 y while the other minerals remains stable during the whole simulation time. This dissolution process feeds the pore water with aqueous Ca, leading to Na by Ca replacement in the montmorillonite exchanger as illustrated in Figure 4-12. This ion exchange occurs on a rather uniform manner in the whole bentonite volume, increasing the fixed Ca proportion from 18 to 23 % whilst decreasing the fixed Na from 72 to 67 %. These proportions of exchanged cations are kept almost constant until the end of the simulation, except at the fracture level. In this particular zone, the Na by Ca exchange operates further, up to 82 % of fixed Ca against 12 % of fixed Na. These values tend to those of a MX-80 exchanger in strict equilibrium with the Grimsel water chemistry (same proportions as those given for Deponit CA-N bentonite). As previously mentioned, the propagation within the whole bentonite of the perturbation in terms of fixed cation ratios is very slow due to the very low concentrations in aqueous cations in Grimsel water.

In the presence of calcite and siderite in the MX-80 composition, the perturbation caused by the intrusion of diluted water is somewhat more marked (Figure 4-13). The pH rises up to 10.5 in the whole bentonite volume due principally to the complete dissolution of calcite. This dissolution of calcite also provides aqueous Ca into the bentonite pore water and by this way enhances the Na by Ca exchange reaction. Ca population in the exchanger thus reaches 50 % in a large part of the bentonite buffer at the end of the simulation. As mentioned in section 2.3, the effect of the electrostatic term is sensitive to the ionic strength, especially at low ionic strength values as in the case of the Grimsel water type. If the corrective factor in the surface complexation modelling is turned off in the present calculations, the buffering capacity due to deprotonation of the surface sites is a bit more effective and the pH values are uniformly decreased by 0.3 pH unit.

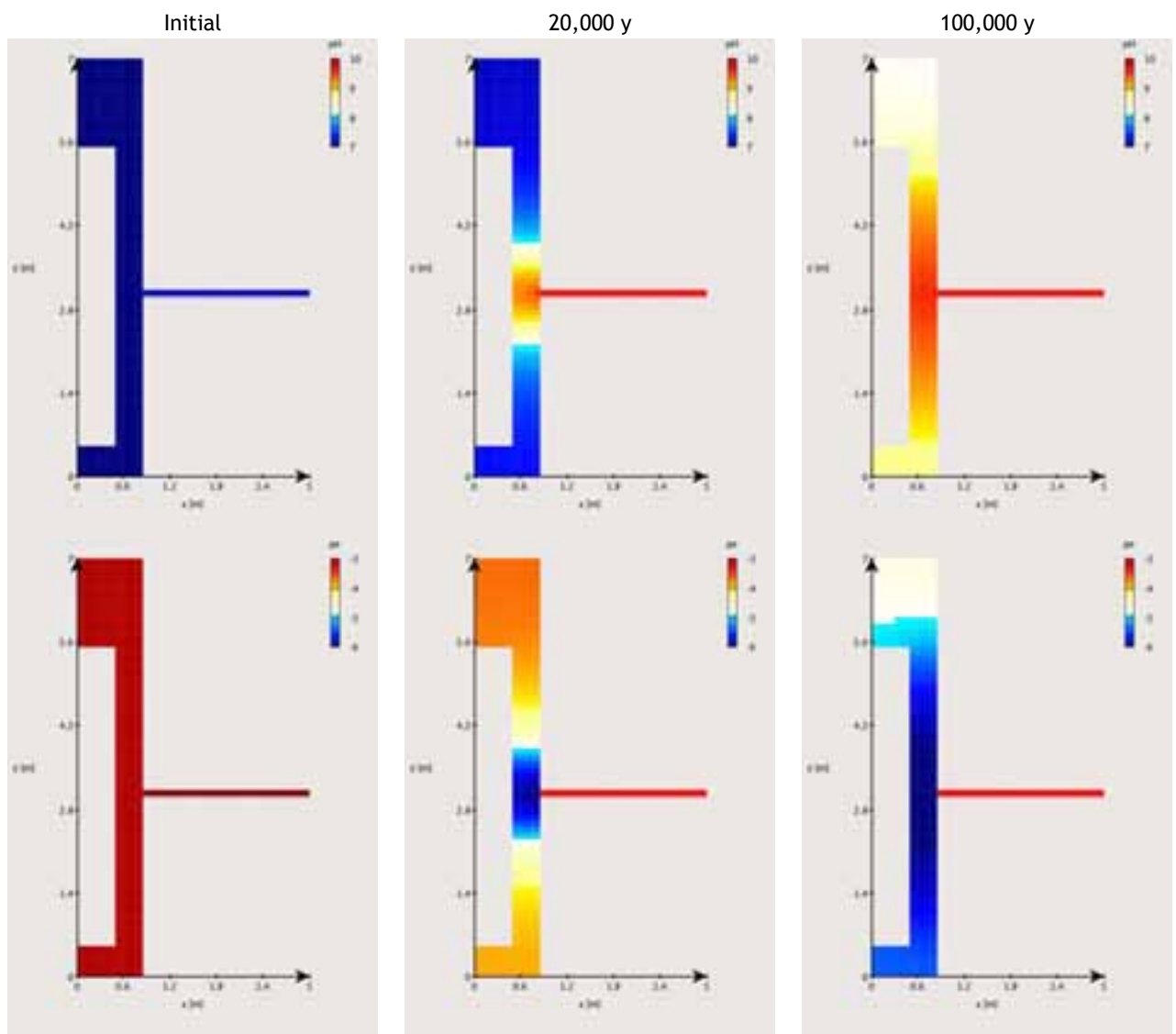


Figure 4-11. Ice-melting water intrusion in MX-80 bentonite: evolution of pH and pe over 100,000 y.

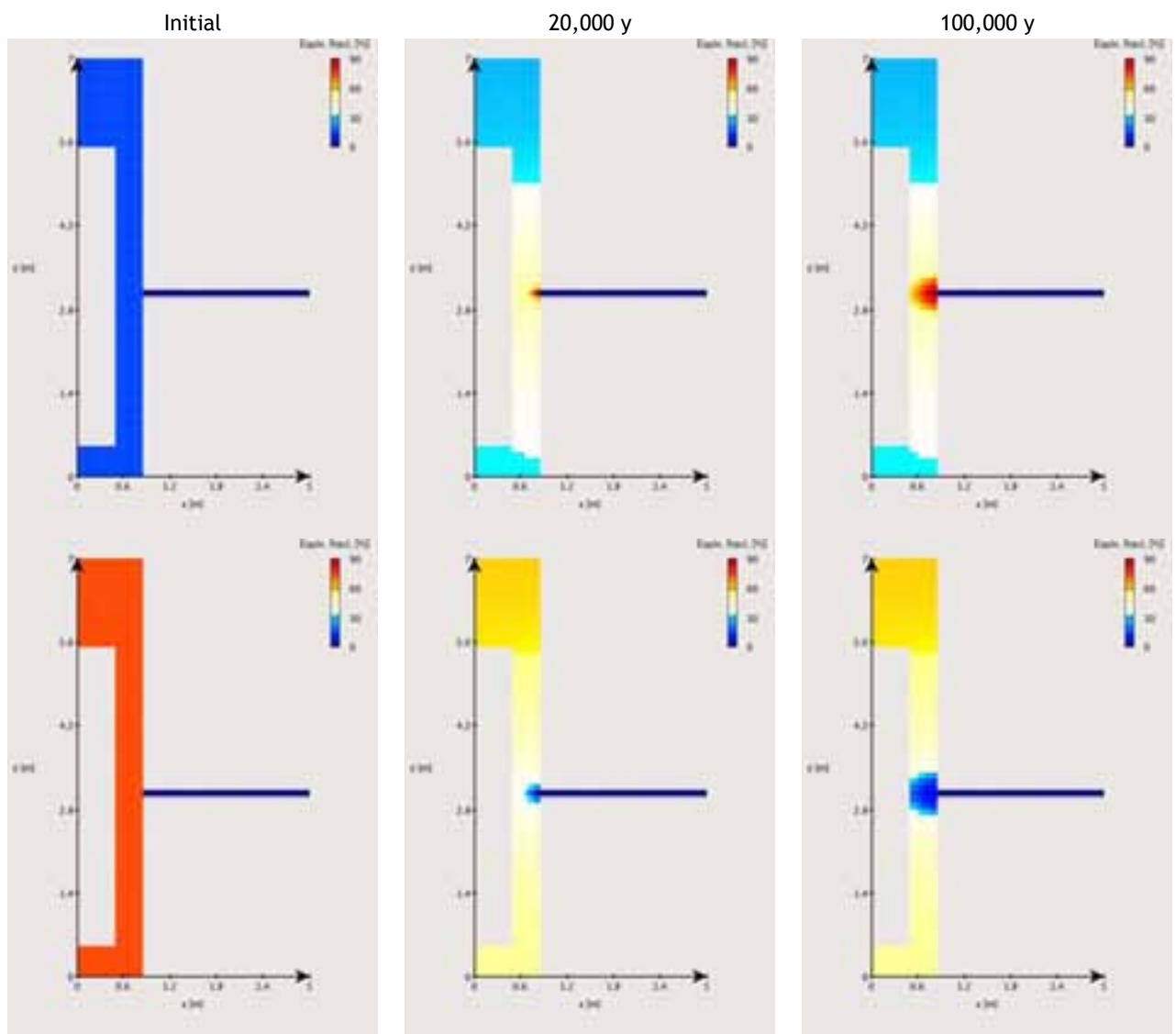


Figure 4-12. Ice-melting water intrusion in MX-80 bentonite: evolution of exchangeable Ca (top), Na (bottom) populations over 100,000 y.

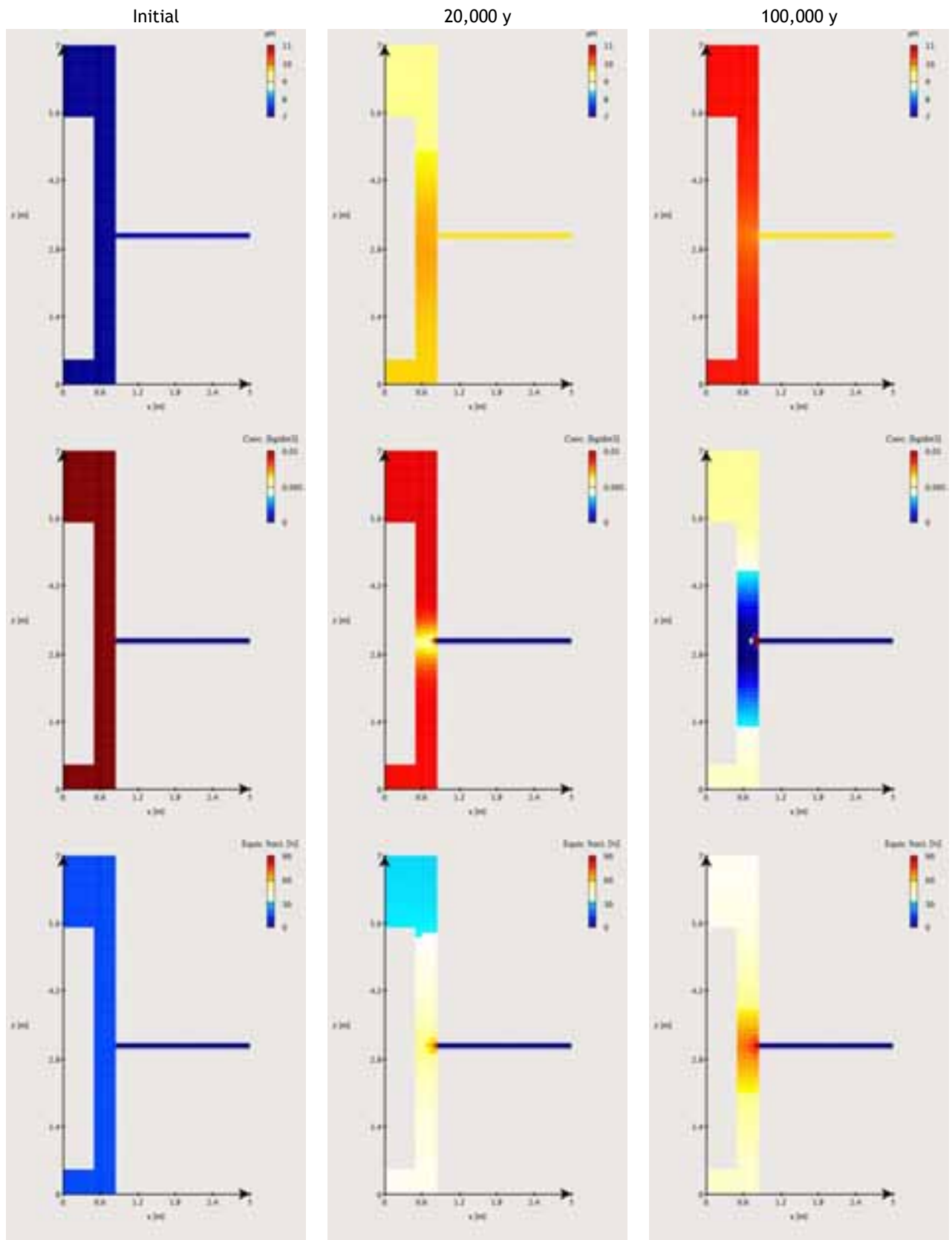
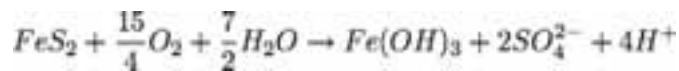


Figure 4-13. Ice-melting water intrusion in MX-80 bentonite with carbonate minerals: evolution of pH (top), calcite content (middle) and exchangeable Ca (bottom) over 100,000 y.

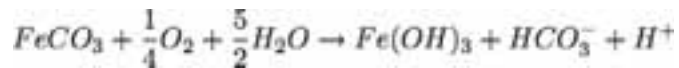
## 5 DURABILITY OF THE DEPOSIT CA-N REDOX BUFFERING CAPACITY

### 5.1 CONTEXT

The preservation of reducing conditions in the KBS-3 disposal contributes to a favourable chemical environment regarding radioelement mobility, notably in avoiding any kinds of oxidative dissolution of the uranium dioxide pellets and in minimizing the solubility of many radionuclides. The solid phases susceptible to buffer the redox potential in the Deponit CA-N are pyrite and siderite (Heath and Tweed, 1999; Beaucaire *et al.*, 2000), both of them being accessory minerals. In the case of oxic water intrusion, redox buffering is related to the oxidative dissolution of these two minerals, respectively (Appelo and Postma, 1996):



and



the ageing of Fe(OH)<sub>3</sub> (ferrihydrite) yielding goethite.

Pyrite is by far the most powerful mineral buffer because it contains two reducing agents, namely one ferrous iron for two sulfur species. There are 3.75 moles of dissolved oxygen reacting with 1 mole of pyrite. Siderite contains one ferrous iron, carbonate species having no reducing ability, and 0.25 mole of oxygen are consumed by mole of siderite only. Thermodynamically, sulfur is a stronger reducing agent than ferrous iron and is the first to react with oxygen. As an illustration, Figure 5-1 corresponds to the titration of a pyrite/siderite buffer by dissolved oxygen (calcite is in equilibrium too, and pH is fixed to 9). Pyrite is progressively dissolved and release ferrous iron which precipitate as siderite. Once all the sulfur content has reacted, the oxidative dissolution shifts to siderite dissolution. The redox potential is buffered to reducing conditions as long as pyrite and siderite are present, the pe value being lower in presence of pyrite.

The oxygen content of the Forsmark and Laxemar deep waters is almost nil. As a matter of fact, reducing conditions were permanently maintained over the simulated 100,000 y period in the interaction cases described in the previous sections. Even in the event of ice-melting water intrusion, many scavenging processes (e.g. bacteria, see Trotignon *et al.*, 2002) should bring the dissolved oxygen to zero. However, for purpose of performance assessment robustness (a *what if* approach), this section is devoted to the durability of the redox buffering capacity in case of an intrusion of oxidizing shallow waters. It essentially deals with oxidative dissolution processes of pyrite and siderite.

The preliminary intrusion of Forsmark groundwater during 10,000 y is disregarded in the modelling, that is to say that the oxidized diluted water interacts with the Deponit CA-N since the beginning of the calculations over 90,000 y. The formation of ferrihydrite was considered in all the simulations except for a sensitivity case, which is discussed at the end of this chapter. Increasing values of oxygen fugacity were considered in the simulations: fug O<sub>2</sub>(g) = 0.001, 0.04 and 0.2. The corresponding dissolved oxygen contents (at 15°C) worth 3e-6, 6e-5, 3e-4 mol/L respectively. The major part of the results discussed below was computed with the intermediate fugacity of 0.04

which assumes a 80 % consumption of the oxygen dissolved in a shallow water equilibrated with atmosphere. A fully saturated fugacity of 0.2 seems very unlikely from the one hand, and the oxidizing perturbation are expected to be quite weak for oxygen fugacities below 0.001 from the other hand. The above oxidative dissolution equations were set under kinetic control in the calculations according to the kinetic rate laws detailed in section 2.2.1. Figure 5-1 shows the corresponding global kinetic rate of dissolved oxygen consumption by pyrite and siderite. The rate is given per year and takes into account the evolution of the mineral reactive surface. Pyrite reactivity is weakly dependent on pH but significantly decreases with oxygen fugacity, whereas siderite reactivity is constant over the considered pH range (8-10) and is not dependent on oxygen fugacity. Pyrite and siderite oxygen consumption rates are equivalent for fugacity values above 0.01. Below this threshold, the oxidative dissolution rate of siderite is the greatest.

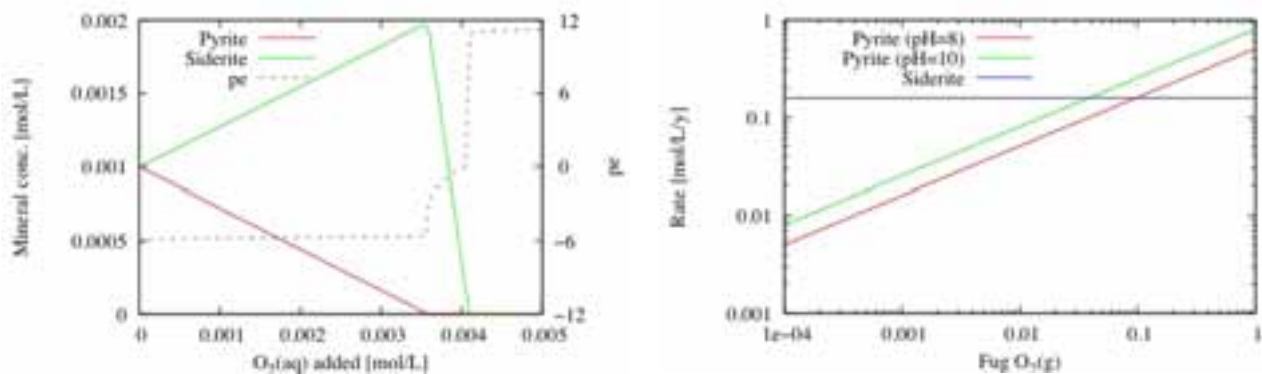


Figure 5-1. Titration of a siderite/pyrite buffer by dissolved oxygen assuming thermodynamic equilibrium (left); kinetic rate of oxygen consumption by siderite and pyrite according to pH and oxygen fugacity (right).

## 5.2 INTRUSION OF ICE-MELTING WATER WITH INCREASING OXYGEN CONTENTS

Figure 5-2 shows the evolution of pH, pe and the penetration of dissolved oxygen content in buffer over 90,000 y (without considering a first 10,000 y period of Forsmark groundwater inflowing). The decrease of pe in the full buffer volume is a direct consequence of the concomitant increase of pH. The zone of influence of the oxidizing perturbation is restricted to the fracture periphery, even after 90,000 y. These observations indicate that the redox potential is efficiently buffered (around -6) on the very long-term. It is interesting to note that the protons released by the oxidation of pyrite and siderite do not shift the pH towards more acidic domains.

Figure 5-3 corresponds to a cross-section through the bentonite buffer, highlighting the interdependency between the redox state (pe), the redox-buffering minerals (pyrite and siderite) and the secondary formation of ferric hydrous phases right in those zones which become fully depleted in pyrite and siderite. There is a sharp contrast/front between the reduced and the oxidized zones and ferrihydrite (Fe(OH)<sub>3</sub>) can indeed precipitate in oxidizing conditions only. One also notes that the dissolution fronts of pyrite and siderite are close to each others.

The corresponding two-dimensional profiles are given in Figure 5-4 and Figure 5-5, where one clearly notes again the progressive dissolution of pyrite and siderite yielding precipitation of secondary ferrihydrite (at 90,000 y).

As mentioned, the siderite and pyrite dissolution profiles show a close relationship with dissolved oxygen and ferrihydrite precipitation profiles. Such a relationship is a bit more complex when goethite is allowed to precipitate (Figure 5-5, bottom graphs). Although the extension of the pe plume is unchanged, one notes a more delocalized alteration zone characterized by a deeper front of siderite dissolution and goethite formation. This is due to the greater pe-pH domain of goethite stability compared to ferrihydrite, as represented in the Pourbaix/pe-pH diagrams of Figure 3-4 calculated for a chemical composition representative of the Deponit CA-N pore water. Siderite almost disappears from the diagram once goethite is considered.

Coming back to the pyrite/siderite/ferrihydrite paragenesis, Figure 5-6 compares the extension of the pyrite dissolution fronts at 90,000 y as a function of the oxygen fugacity. The oxidizing perturbation could be neglected as soon as the fugacity is below one thousandth, i.e. approximately 0.001. On the other side of the fugacity range, a water in equilibrium with atmosphere induces a more pronounced perturbation front within the bentonite up to a distance of 50 cm from the fracture. All in all, the perturbation remains relatively well localized, even after 90,000 y, partly because the initial dissolved oxygen content is low (i.e.  $3 \times 10^{-4}$  mol/L maximum) by comparison to the pyrite/siderite content (ca. 0.8 mol/L), and partly because the oxygen diffusive transfer is slow within the buffer (a perfect tracer, introduced in the Grimsel fracture water at a constant concentration, needs between 1,500 and 2,500 y to fully fill the buffer pore volume). However, local canister corrosion could not be disregarded in the case of intrusion of atmosphere-equilibrated waters though the occurrence of such an event seems unlikely.

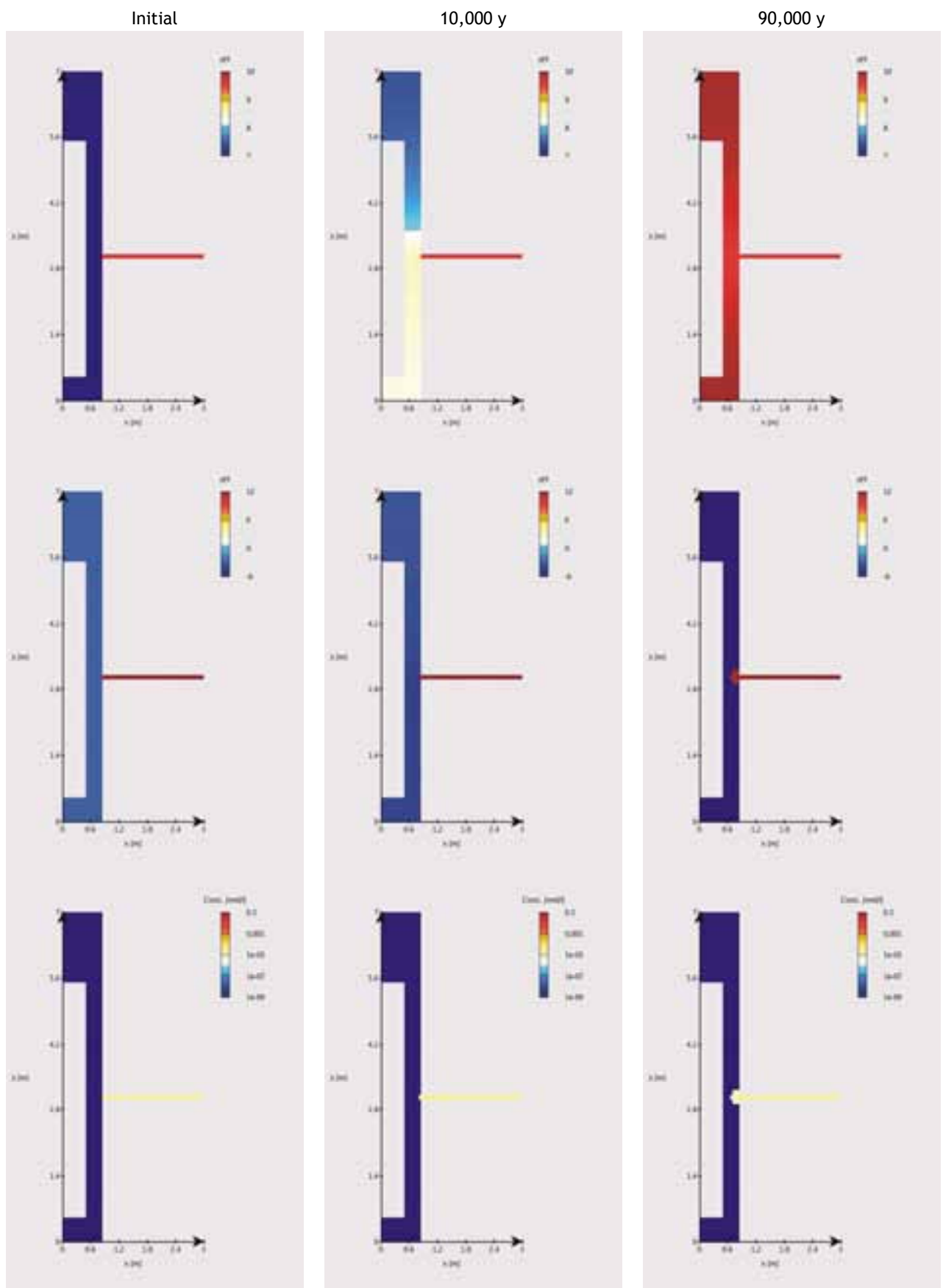


Figure 5-2. Ice-melting groundwater intrusion in Deponit CA-N bentonite ( $fug O_2 = 0.04$ ), evolution of pH (top), pe and the dissolved oxygen content over 90,000 y.

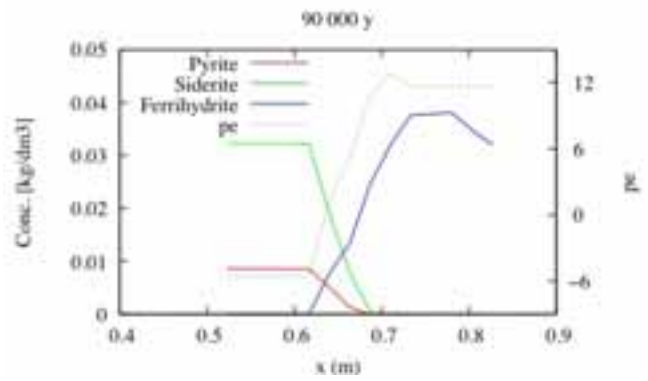
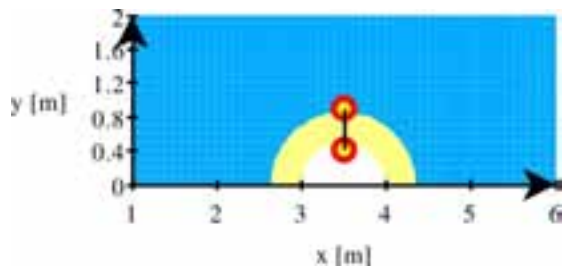


Figure 5-3. Ice-melting groundwater intrusion in Deponit CA-N bentonite ( $fug O_2 = 0.04$ ), cross-section through the bentonite buffer showing the interdependency between the redox state (pe) and the redox-poising minerals.

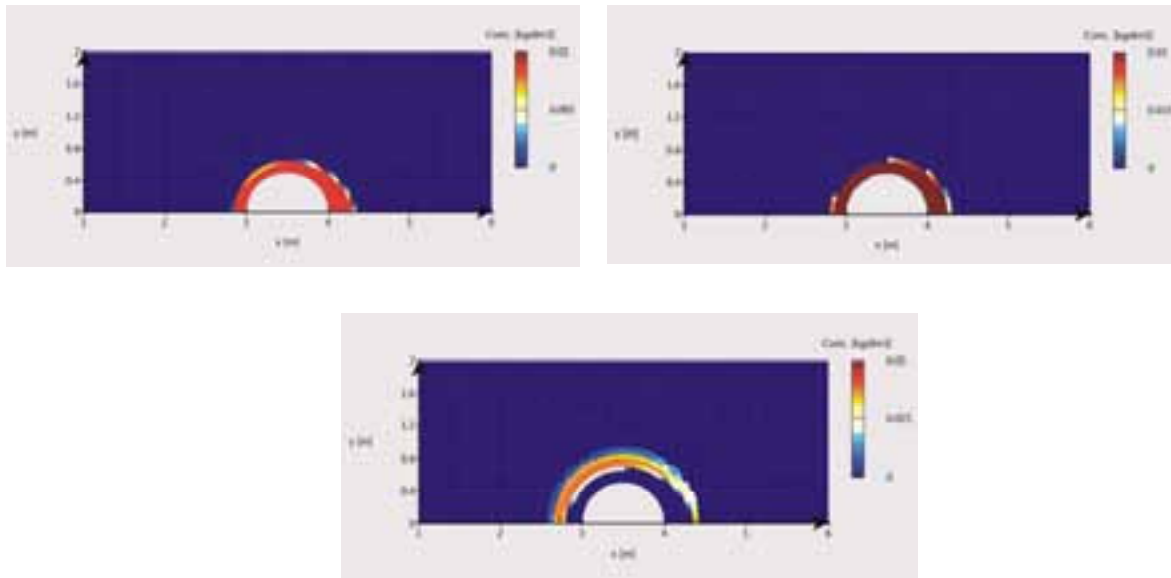


Figure 5-4. Ice-melting groundwater intrusion in Deponit CA-N bentonite ( $fug O_2 = 0.04$ ), progressive dissolution of pyrite and siderite yielding precipitation of secondary ferrihydrite (at 90,000 y).

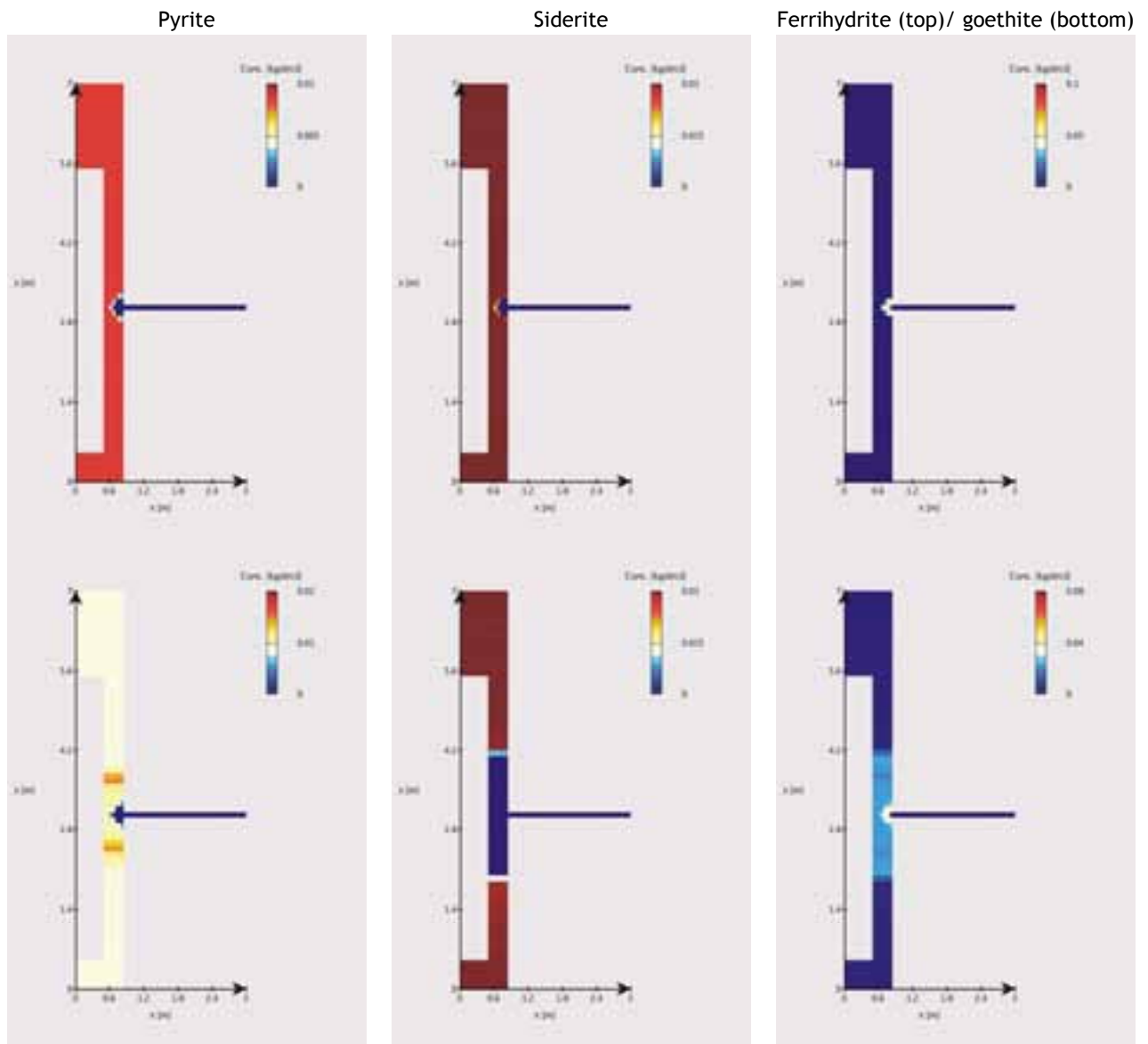


Figure 5-5. Ice-melting groundwater intrusion in Deponit CA-N bentonite ( $fug O_2 = 0.04$ ), pyrite, siderite and secondary iron-mineral contents calculated at 90,000 y considering either ferrihydrite (top) or goethite precipitation.

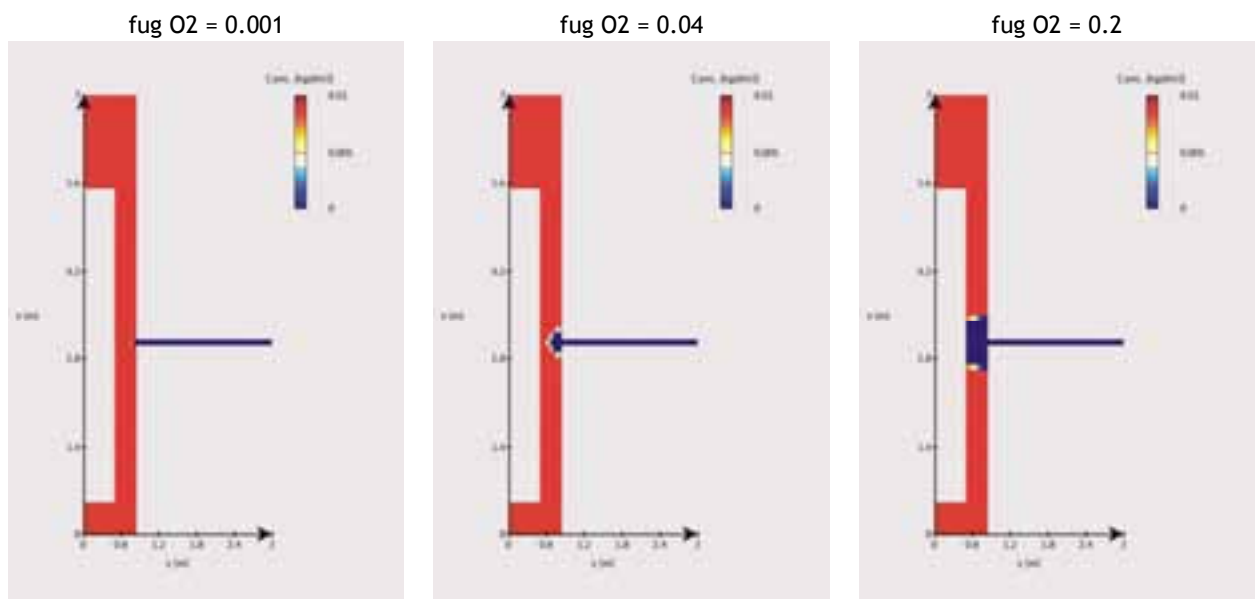


Figure 5-6. Ice-melting groundwater intrusion in Deponit CA-N bentonite, extension of the pyrite dissolution front at 90,000 y as a function of the oxygen fugacity.

## 6 THERMAL EFFECT ON MX-80 BENTONITE

Radioactive decay of radionuclides contained in spent fuel results in a heat production and thus in a temperature field in the near field of deposition holes. As given in Figure 6-1, temperature of the inner and outer borders of the buffer (i.e. on the waste-package side and on the host rock side) could reach maximum values respectively around 80°C and 65°C after 10 to 30 y of spent fuel disposal. Simulations were thus performed so as to assess the effect of such a rise in temperature on the geochemical evolution of MX-80 bentonite (without or with carbonates) interacting with the reference Forsmark groundwater.

In this set of calculations, a constant thermal gradient is accounted for as illustrated in Figure 6-2, with a temperature fixed at 80°C at the buffer inner border and 65°C at its outer border over a 1,000 y simulation period, as in Arcos *et al.* (2006). It is worth noting that the expected thermal stage is shorter, therefore this modelling should overestimate the thermal effect on bentonite. Table 6-1 gives MX-80 bentonite pore water composition resulting from initial equilibrium calculations at a temperature of 80°C. In addition to the minerals previously accounted for at 15°C, other secondary minerals as anhydrite and hematite are allowed to precipitate. The former is more stable at high temperatures than gypsum and the latter is always more stable than ferrihydrite but kinetically hindered at low temperatures. In this respect, it is worth noting the full replacement of gypsum by anhydrite at temperatures between 65 and 80°C. In addition to this, dolomite and hematite slightly precipitate. The main consequence of this is a lower concentration in aqueous sulfates and carbonates in the MX-80 bentonite pore water for the range 65-80°C than at 15°C. Furthermore, the temperature gradient has a direct effect on pH distribution along a horizontal cross-section, the higher the temperature the lower the pH.

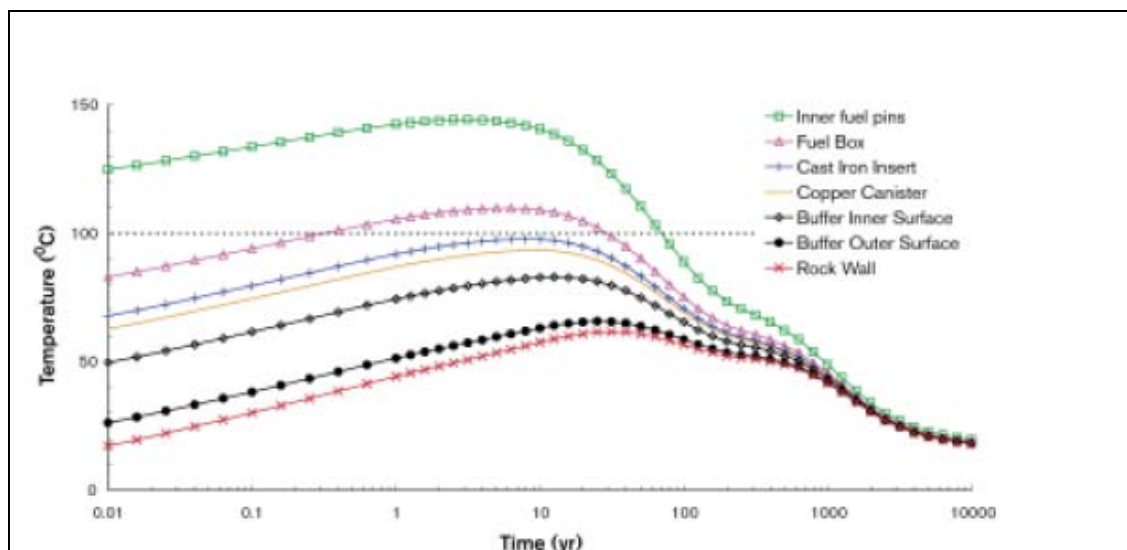


Figure 6-1. Thermal evolution of the near field (Arcos *et al.*, 2006).

Table 6-1. Chemical composition of MX-80 bentonite pore water at 80°C and 15°C.

		MX-80 without carbonates		MX-80 with carbonates	
		15	80	15	80
Temp.	°C	15	80	15	80
pH	-	7.0	6.9	7.0	5.9
pe	-	-3.15	-3.60	-3.15	-2.37
Eh	V	-0.18	-0.25	-0.18	-0.16
I	mol/L	0.29	0.23	0.29	0.23
Na	mol/L	2.1e-1	2.1e-1	2.1e-1	2.1e-1
K	mol/L	1.4e-3	1.4e-3	1.4e-3	1.4e-3
Ca	mol/L	1.0e-2	1.0e-2	1.0e-2	1.0e-2
Mg	mol/L	5.6e-3	5.6e-3	5.6e-3	5.6e-3
Fe	mol/L	1.1e-5	1.1e-6	1.0e-4	7.6e-5
SiO <sub>2</sub>	mol/L	6.0e-5	5.5e-4	6.0e-5	5.5e-4
HCO <sub>3</sub> <sup>-</sup>	mol/L	1.5e-3	5.0e-4	4.0e-3	5.1e-3
Cl <sup>-</sup>	mol/L	1.5e-1	1.5e-1	1.5e-1	1.5e-1
SO <sub>4</sub> <sup>2-</sup>	mol/L	3.8e-2	1.0e-2	3.8e-2	1.0e-2

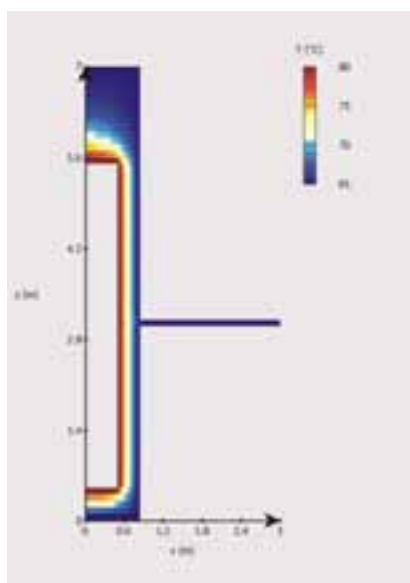


Figure 6-2. Constant temperature field modelled over 1,000 y. The temperature of the bentonite inner border is set at 80°C while that at its outer border is set at 65°C.

When Forsmark groundwater inflows, the pH decreases gradually in the buffer at the fracture level from 6.9 to 6.5 (pH of Forsmark groundwater at 65°C) over the simulation period, while pe increases from -3.6 to -3.2. Note that a pH value of 6.5 still corresponds to a neutral to slightly alkaline conditions for this temperature range. This pH decrease is controlled by the inflow of aqueous carbonates in the buffer (Figure 6-3). Far from the fracture level, pH and pe are still close to their initial value at 1,000 y.

The Na by Ca replacement is not significant far from the fracture level, but is more pronounced close to the fracture, where exchangeable Ca population increases from 18 to 28 % (Figure 6-4).

The in-diffusion of aqueous carbonates leads to precipitation of carbonate minerals, located essentially in the warmer zones: dolomite precipitates in the warmer zones but dissolves in the cooler zones as shown in Figure 6-5; calcite and hematite slightly precipitates in the warmer zones. Forsmark groundwater being undersaturated with respect to anhydrite, this mineral completely dissolves within bentonite at the fracture plane level in a very first step (not illustrated here). Farther from the fracture, anhydrite dissolves in the cooler zones and slightly precipitates in the warmer zones. However, the diffusion of Forsmark groundwater into the MX-80 bentonite leads to a progressive dissolution of this precipitated anhydrite over the simulation period as shown in Figure 6-5. The other mineral that shows an evolution due to the considered temperature field is quartz, which dissolves close to the canister and slightly precipitates in the cooler zone far from the fracture. No change of porosity is observed over the simulation period.

In the presence of carbonate minerals in the MX-80 bentonite, initial equilibrium calculations (Table 6-1) lead to the entire replacement of calcite by dolomite and to a lower initial pH value (5.9). The results obtained when simulating Forsmark groundwater inflows are globally similar to those previously described for MX-80 bentonite without carbonate minerals. The slight differences that can be pointed out are: a slight pH increase from 6.0 to 6.2 close to the fracture due to the intrusion of Forsmark groundwater (pH 6.5), and siderite dissolution due to aqueous carbonate out-diffusion allowing pyrrhotite and hematite to precipitate and also to the thermal effect (dissolution around the canister) (Figure 6-6).

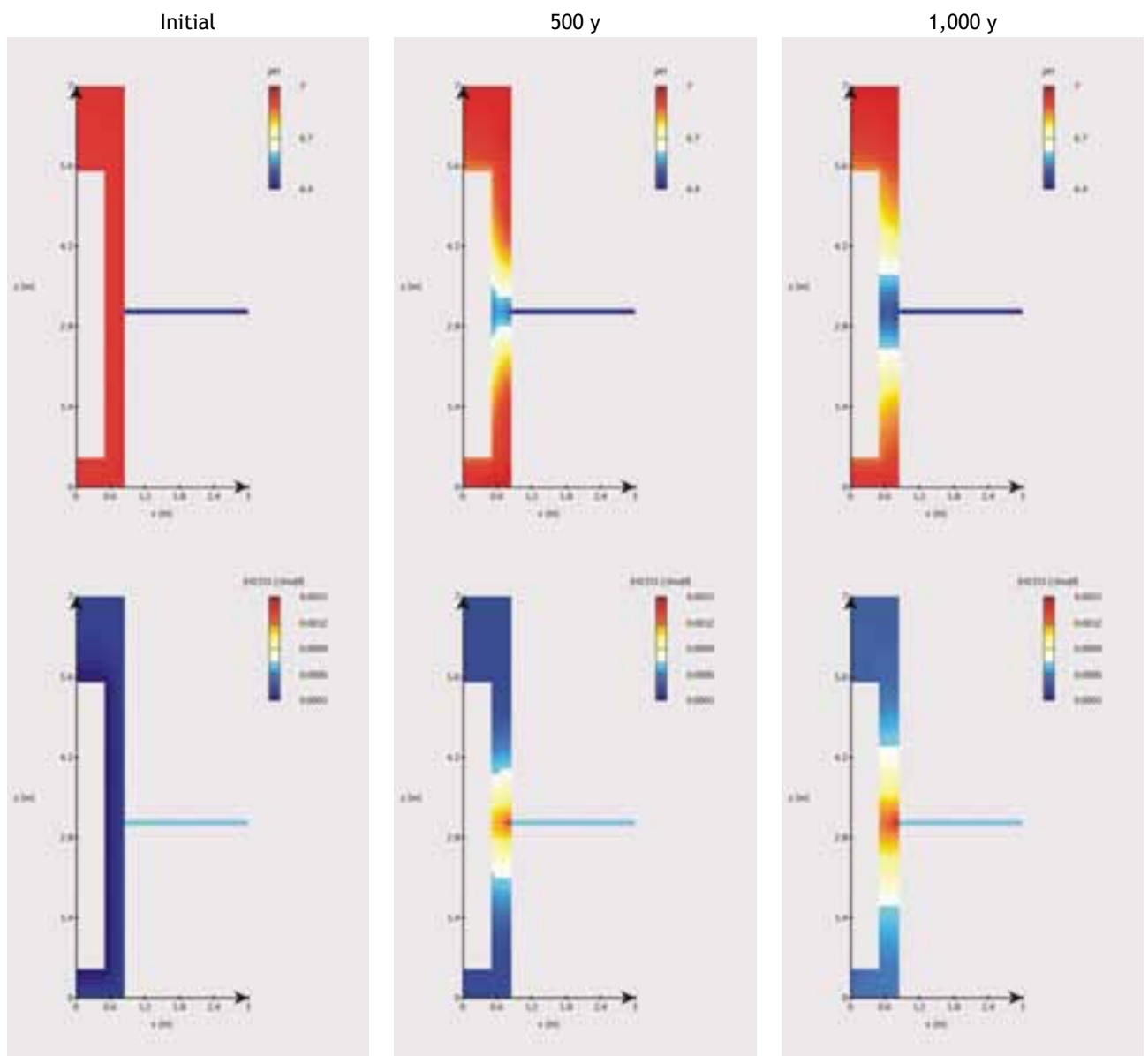


Figure 6-3. Thermal effect on MX-80 bentonite without initial carbonate minerals: evolution of pH and aqueous carbonate contents over 1,000 y.

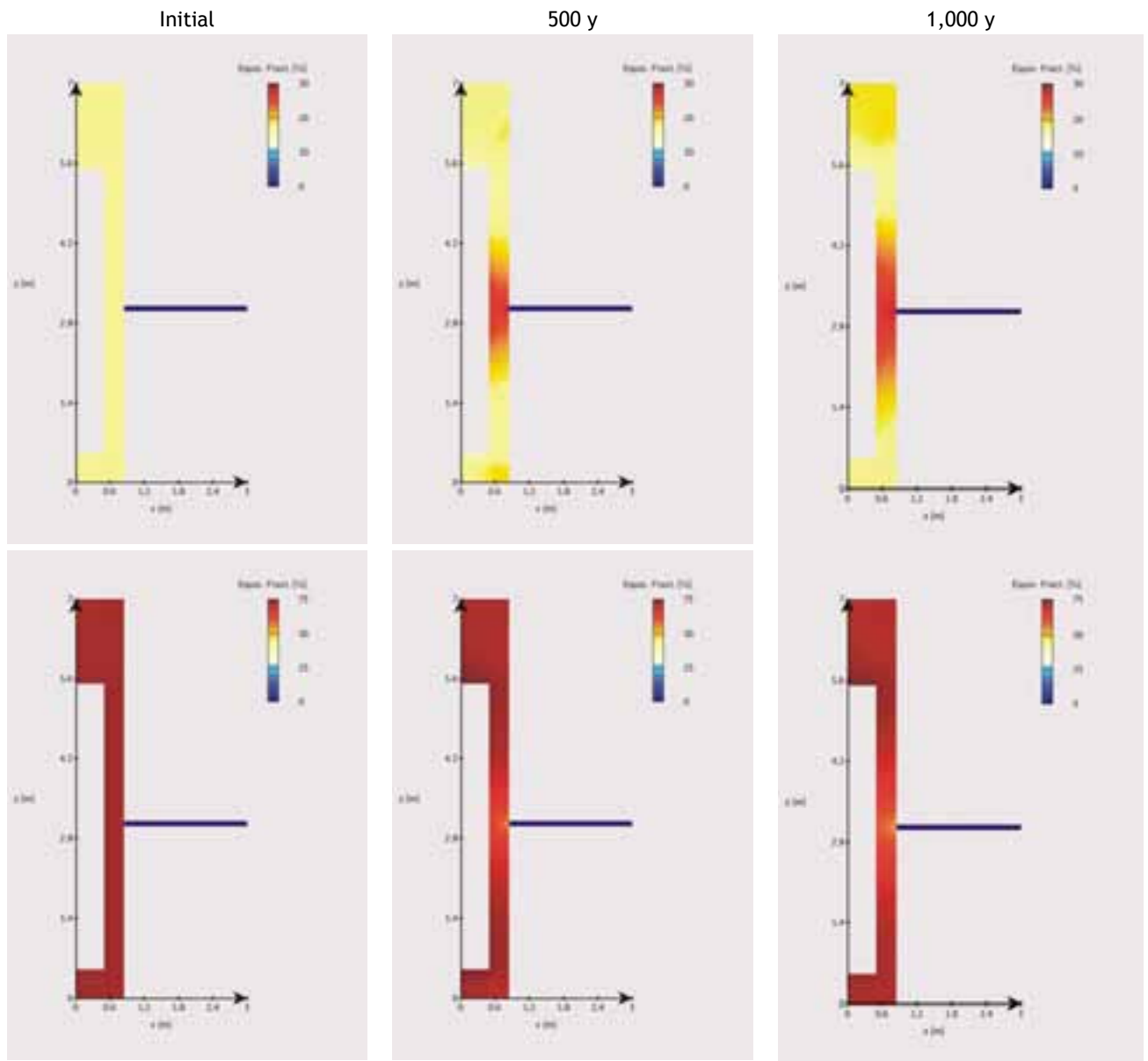


Figure 6-4. Thermal effect on MX-80 bentonite without initial carbonate minerals: evolution of exchangeable Ca (top) and Na (bottom) populations over 1,000 y.

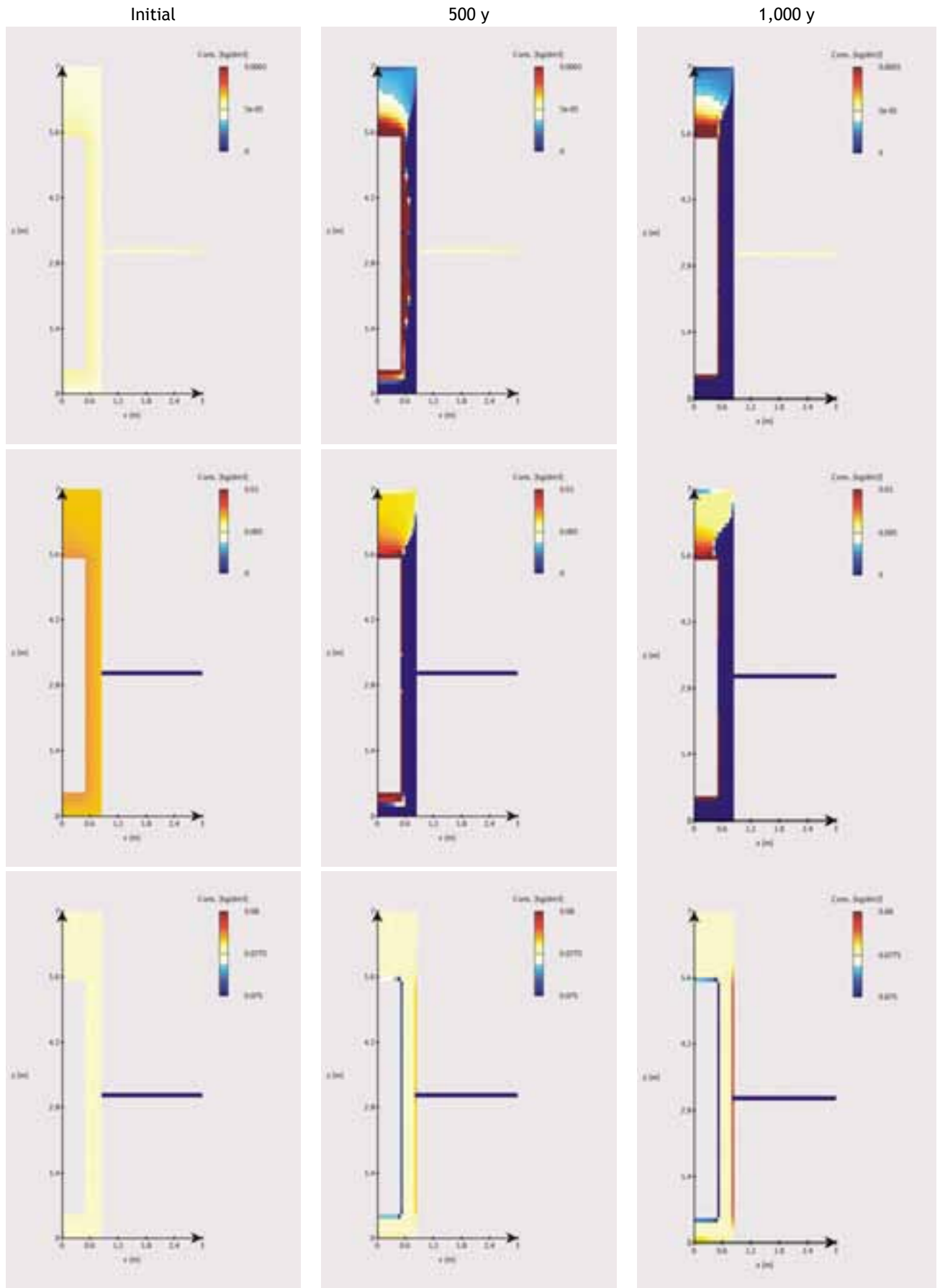


Figure 6-5. Thermal effect on MX-80 bentonite without initial carbonate minerals: evolution of dolomite (top), anhydrite (middle) and quartz (bottom) contents over 1,000 y. Note that for a better observation, scale bars have been limited to a very narrow range.

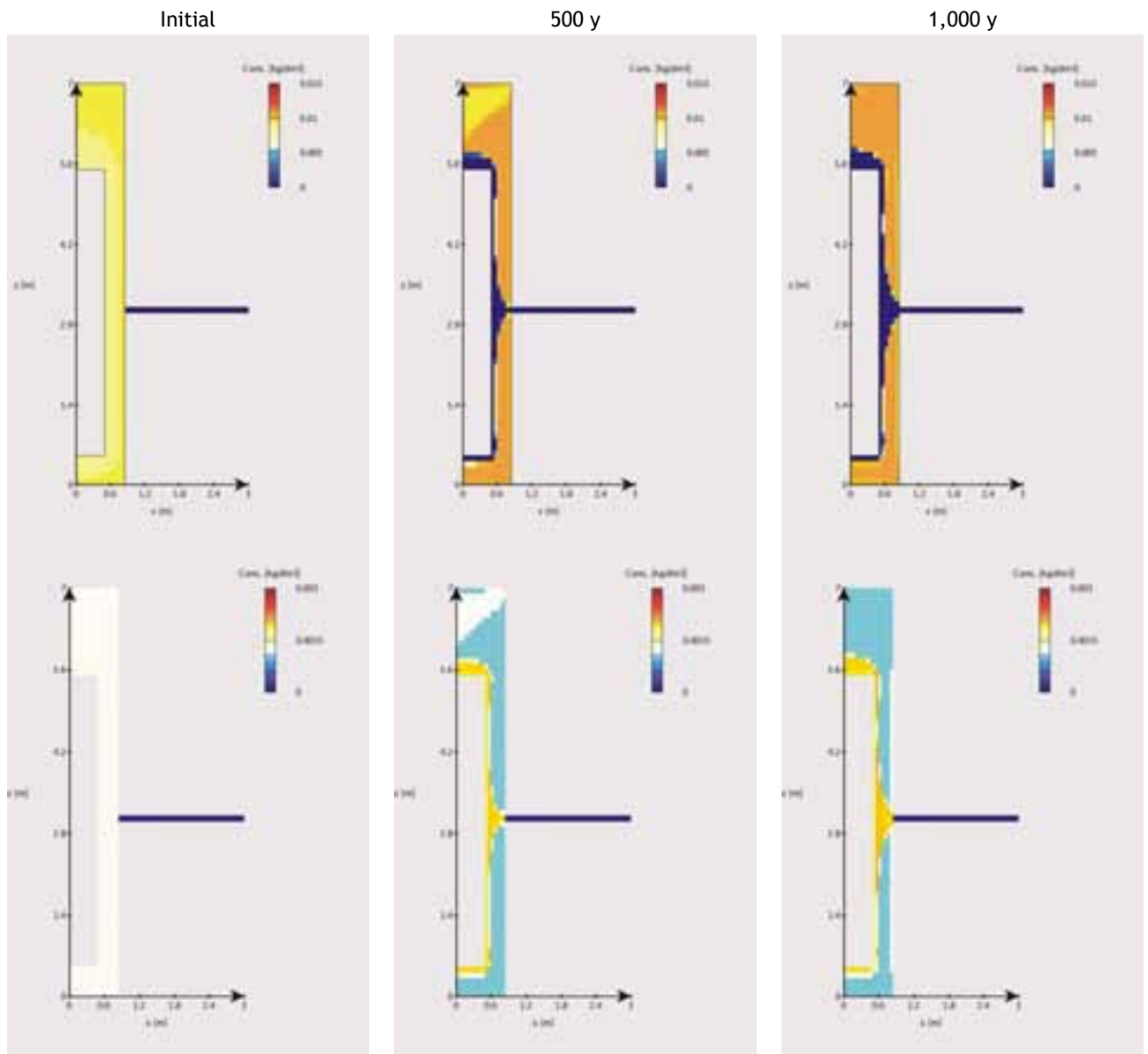


Figure 6-6. Thermal effect on MX-80 bentonite with carbonate minerals in its initial composition: evolution of siderite (top) and pyrrhotite (bottom) contents over 1,000 y.

## 7 SUMMARY AND CROSS-COMPARISON OF SIMULATED CASES

Generally speaking, as described in the previous sections, most of the processes that govern the geochemical evolution of either Deponit CA-N or MX-80 bentonite due to the inflow of waters are common to both bentonites. First, the diffusive properties of these bentonites, which are considered as a continuous medium surrounding the canister, are responsible for the initially slow propagation of the perturbations, which further slow down with time as concentration gradients diminish. The variation in solute concentrations between the bentonite pore waters and the considered entering groundwaters induces the diffusion of aqueous chemical species either in or out from the bentonite and thus produces the observed reactions of dissolution-precipitation and/or of cation exchange. The main results in terms of geochemical evolutions of both bentonites can be summarized for each type of considered inflowing water as follows (note that a summary table is reported in appendix).

When interacting with the reference Forsmark groundwater, both bentonites reach a uniform geochemical steady state throughout their entire volume over the 100,000 y simulation period. The interaction induces weak changes in the pH of the bentonite pore waters (0.3 unit maximum). The fixed cation proportion is also moderately modified to reach similar ratios in both bentonites (about 50 % Ca, 35 % Na, 15 % Mg). Gypsum and dolomite when present are entirely dissolved, while calcite precipitates more or less markedly. The geochemical characteristics of the bentonites are thus only slightly modified. However, it is worth keeping in mind that their initial state is calculated using this Forsmark groundwater, so as to fit (at best) the experimentally determined geochemistry. This explains, in addition to the relatively non aggressive chemistry of Forsmark water with respect to bentonite, that the calculated evolutions remain slight.

The intrusion of the high-salinity Laxemar groundwater leads to a comparatively higher perturbation in both bentonites. The pH increases by around one unit maximum near the fracture plane, reaching in this case that of the Laxemar water (7.9). However, the rise in pH smoothens farther in the bentonite volume, since the alkaline pH plume is efficiently buffered by the deprotonation reaction on the montmorillonite surface. The fixed cation ratios in both bentonite exchangers are changed relatively quickly and thus uniformly modified at the end of the simulation into a predominant calcic form (about 65 % Ca, 35 % Na). When carbonates are present in the bentonite composition, some dissolution (dolomite, siderite) and precipitation (calcite, gypsum) reaction occur, in addition to the mineralogical alteration due to the first 10,000 y of Forsmark water inflowing.

The interaction between the bentonites and the diluted Grimsel water results in an even more pronounced geochemical evolution. The calculated pH values over the whole simulation period rise by several units, either in the whole bentonite volume or locally up to 10.5 near the fracture plane for MX-80 buffer. The cation exchangers turn globally into a more calcic population but on a much contrasted manner depending on the bentonite zones, with a fixed Ca ratio up to about 80 % near the fracture plane for both bentonites. Actually, the exchange process requires important volumes of Grimsel water to reach a steady-state due to the low amounts of solutes available in such weakly mineralized water. The mineralogical transformation are similar to those produced by the Forsmark or Laxemar groundwaters, though some variations are observed, such as a partial dissolution of dolomite present in Deponit CA-N bentonite (steady-state not reached regarding this mineral) and a total dissolution of calcite when present in MX-80 bentonite.

In all these interaction cases,  $p_e$  strictly varies in accordance to pH. The groundwaters are all under reducing state and their diffusion within the bentonite does not yield to neither significant change in the redox conditions nor to any significant destabilization of redox sensitive minerals (pyrite or pyrrhotite; siderite), except for siderite in the “Deponit CA-N/Laxemar water” interaction case (though not formally linked to a redox process). Reducing conditions were permanently maintained over the simulated 100,000 y period. Another remark is that the calculated porosity rise due to mineralogical alteration do not exceed 2 % (i.e. a maximum porosity of 45 % compared to 43 % initially) whatever the calculation case.

Some specificity is nevertheless observed in the behaviour of both bentonites. On the one side, MX-80 bentonite is found out to provide a more efficient pH buffer by deprotonation reaction compared to Deponit CA-N bentonite, but this is no more longer verified if carbonates are initially present in MX-80 and calcite governs the pH changes. On the other side, the variations in fixed cation populations are less pronounced in Deponit CA-N than in MX-80 bentonite, the latter being initially poorer in fixed Ca.

In addition to the previous set of interaction cases, a hypothetical intrusion of ice-melting oxidizing water was studied in view of estimating the durability of the Deponit CA-N redox buffering capacity. The ice-melting water was equilibrated with oxygen fugacities ranging from 0.001 to 0.2 for a sensitivity analysis. The solid phases susceptible to buffer the redox potential in the Deponit CA-N bentonite are pyrite and siderite, pyrite being by far the most powerful buffer. The  $p_e$  value is found to be efficiently buffered (around -6 at pH 10) by the dissolution of these both minerals on the very long-term, so that half of the bentonite thickness at the fracture level is still under strongly reducing conditions after 100,000 y for a 0.04 oxygen fugacity. It is worth noting that the extension of the perturbation was found to be a bit larger when goethite was selected as the secondary ferric phase instead of ferrihydrite. Taken as a whole, the oxidizing perturbation could be neglected as soon as the oxygen fugacity is below 0.001. On the other side of the fugacity range (0.2), water in equilibrium with atmosphere induces a more pronounced perturbation front within the whole bentonite thickness up to a distance of 50 cm from the fracture plane.

Regarding the influence of the thermal transient during the first hundreds of years, conservative conditions have been considered in a first attempt, with a constant thermal gradient simulated throughout the fracture plane domain, the buffer boundaries being set at 80 (inside) and 65°C (outside). With these thermal conditions, rather limited changes are calculated in the MX-80 bentonite geochemistry when interacting with Forsmark groundwater. The pH remains slightly alkaline (6.5 in the considered temperature range). Some minerals dissolve (anhydrite, dolomite) or precipitates (quartz) in the cooler zones whilst they show the inverse behaviour (respectively precipitate or dissolve) in the warmer zones close to the canister. Anhydrite, more stable than gypsum at this range of temperatures, dissolves in the whole bentonite volume in a further stage. Na by Ca replacement is observed in a volume localized around the fracture.

The simulations carried out in the present study can be further commented with respect to those reported in Arcos et al. (2006). As a preliminary statement, it is worth underlining that Arcos and co-authors have presented a high quality and complete modelling work, whatever in the way to model the geometries and the geochemical components, the relevance of the alternative simulated cases or the analyses of the calculation results.

The reactive transport codes used in both modelling work, i.e. HYTEC and PHAST are globally similar in the implemented theories and in their functionalities. The main difference concerns the iterative coupling scheme. However, a non iterative constant time-steps approach analogue to that used in PHAST has been shown to produce results very close to those obtained with a sequential iterative approach as usually applied with HYTEC.

The main trends in geochemical evolutions of Deponit CA-N and MX-80 bentonites due to the intrusion of the three main types of waters, i.e. reference, high-salinity and diluted water, are found to be globally similar in both studies. This agreement obviously builds confidence in such type of modelling work. Nevertheless, some divergence can be drawn up when analysing some processes in more details. In particular, the following issues can be pointed out:

- The selected values for the equilibrium constant of gypsum and dolomite are lower in Arcos *et al.* (2006) than those selected in the present study. Both mineral phases appear therefore less stable in the present work, i.e. the times needed to reach their complete dissolution are shorter. As an illustration, in the reference case with Deponit CA-N bentonite, dolomite dissolves completely near the fracture zone in 25,000 y in the present calculations, whereas in Arcos *et al.* (2006), dolomite has not entirely disappeared from this zone after 60,000 y of simulation. Regarding gypsum, times of dissolution are globally 4 times shorter in the present study than in Arcos and co-authors' work for both bentonites (about 20,000 y vs. 60,000 y for Deponit CA-N bentonite; about 5,000 y vs. 20,000 y for MX-80 bentonite). Actually, lowest and highest values reported in thermodynamic databases for the equilibrium constant have been used in one and the other study whereas an intermediate value might have been more relevant. For dolomite, the constant selected for the present study, so as to precisely reproduce the adsorbed cation population, probably results in an overestimated dissolution process;
- The rises in pH due to the interactions with Laxemar and Grimsel groundwater are found to be more intense than in Arcos *et al.* (2006), by about 0.4 unit. As mentioned in section 3.3 and 4.3 related to the interaction with diluted Grimsel groundwater, this difference in pH may partly be explained by the electrostatic correction for the double layer, which may be disabled so as to reduce the sensitivity of the model to the ionic strength of waters. In this case, the bentonite pH value (9.9) drops (to 9.6) when the electrostatic correction is disabled (to be compared to 9.3 in Arcos *et al.* 2006). Actually, no change in pH is observed in the case of saline waters as high ionic strengths reduce the electrostatic effects.

In addition, other differences e.g. in the simulation grids (2D-cylindrical versus 3D) or in the simulation periods (100,000 y versus 60,000 y) may also explain some slight discrepancies in the reported evolutions with time. However, this should not hinder the fact that both studies agrees on the overall evolutions, which remain moderate.

## 8 CONCLUSION

The purpose of the present study is to model the geochemical evolution of the buffer in the KBS-3 disposal concept, due to the intrusion of different types of water via a fracture intersecting a disposal borehole. Various scenarios have been simulated using the reactive transport modelling code HYTEC and a similar layout to that reported in Arcos *et al.* (2006). Deponit CA-N and MX-80 bentonites were considered as potential buffers interacting with either a reference (Forsmark), a high-salinity (Laxemar) or an ice-melting (Grimsel) groundwater. In addition, a focus was given to the thermal effect on the basis of the MX-80 bentonite / Forsmark case, as well as to the durability of the redox buffering capacity for the Deponit CA-N bentonite / ice-melting groundwater case.

The sets of simulation performed in the present study indicate that globally, the intrusion of the considered groundwaters should not affect drastically the geochemistry of neither the Deponit CA-N nor the MX-80 bentonite on the long-term. Moreover, some of the calculated evolutions appear to be very slow, so that bentonites are still in a transient stage at the end of the 100,000 y simulation period.

Regarding the chemical and hydraulic containment properties of both bentonites in interaction with the considered waters, the calculated evolutions point out that:

- pH may reach quite high values (up to 10.5) but does not exceed the criterion value (11) reported by SKB (SKB, 2006) with regards to the chemical stability of bentonite. Moreover, pe remains reducing. Thus one can expect in a first approach that the effect of the calculated geochemical evolution on radionuclide mobility should globally remain low;
- The aqueous concentrations in chloride remains below the requirement assigned by SKB (SKB, 2006), i.e. below 3 mol/L with respect to chloride corrosion of canister;
- The dissolution of accessory minerals is either partially or totally counterbalanced by precipitation of secondary phases, so that the calculated porosity changes are lower than 2 %. This should not be significant with respect to the hydraulic containment provided by the bentonites;
- The montmorillonite exchanger becomes more charged with fixed Ca cations, especially in the case of the intrusion of Grimsel groundwater (albeit localized around the fracture plane). This may reduce the swelling pressure of the bentonite. In this respect, it would be interesting to quantify the potential maximum decrease in swelling capacity by ad hoc experiments and to make sure that this does not significantly affect the overall bentonite containment performance.

The main trends in geochemical evolutions of both bentonites highlighted by the present study are in good agreement with the results presented in Arcos *et al.* (2006). Nevertheless, some differences have been pointed out, which principally are:

- Lower times of dissolution for gypsum and dolomite in the present study, due to a different selection of the equilibrium constant value for each of those minerals;
- A more intense increase of pH with ice-melting groundwater in the present work.

Furthermore, the possible contrast between the bentonite geochemical properties near a fracture plane and far from it also rises a further questioning on the potential consequences of this difference with regard to containment properties. In particular, one can mention the potential for a local oxidative corrosion of the canister if oxidizing water penetrates the buffer via the intersecting fracture, though this outcome should be balanced with the likelihood of the scenario.

At last, it is worth remembering that some important hypotheses have been made in the present simulation work in terms of scenario, notably a fracture plane intersecting a deposition hole combined with the intrusion of high-salinity, diluted and oxidizing waters. The likeliness of these settings should be kept in mind when addressing the influence of such phenomena in a safety assessment. Furthermore, the present study was performed considering assumptions and parameter values selected in Arcos *et al.* (2006) for SKB as requested by SSI. The results presented herein should therefore be understood with the soundness of these input conditions. They appeared globally rational but have not been thoroughly reviewed by IRSN. Nevertheless, some related issues, which might be further assessed so as to reinforce this modelling study, can be pointed out. As mentioned in Arcos *et al.* (2006), the stability of montmorillonite (though this lead to the issue of secondary minerals that will form as montmorillonite dissolves), the potential effect of thermo-hydraulic processes during the initial transient phase with regards to their effects on the corrosion-aggressive ion concentrations and the sensitivity of the results to the fracture representation (geometry and water flowing rate) worth being tackled. The possible influence of a hydraulic short-cut around (e.g. due to a spalled zone) or within bentonite would also be interesting to investigate as 'what if' cases.

## 9 REFERENCES

- Allison, J.D., Brown, D.S. and Novo-Gradac, K.J. (1991). MINTEQA2/PRODEF2, A Geochemical Assessment Model for Environmental Systems: Version 3.0 User's Manual. EPA/600/3-91/021. U.S. EPA, Athens, GA, 30605.
- Appelo, C.A.J. and Postma, D. (1996). *Geochemistry, groundwater and pollution*, Balkema Eds, Rotterdam (NL).
- Arcos, D., Grandia, F. and Domènech, C. (2006). Geochemical evolution of the near field of a KBS-3 repository, Technical Report TR-06-16, SKB (S).
- Beaucaire, C., Pitsch, H., Toulhoat, P., Motellier, S. and Louvat, D. (2000). Regional fluid characterization and modelling of water-rock equilibria in the Boom clay formation and in the Rupelian aquifer at Mol, Belgium, *Appl. Geochem.* 15, 667-686.
- Bradbury, M.H. and Baeyens, B. (1998). A Physicochemical Characterisation and Geochemical Modelling Approach for Determining Pore water Chemistries in Argillaceous Rocks, *Geochim. Cosm. Acta* 62, 783-795.
- De Windt L., Pellegrini, D. and van der Lee, J. (2004). Coupled modeling of cement/claystone interactions and radionuclides migration, *Journal of Contaminant Hydrology* 68, 165-182.
- De Windt, L. and Badreddine, R. (2007). Modelling of long-term dynamic leaching tests applied to solidified/stabilised waste, *Journal of Waste Management* (in press).
- Duckworth, O.W. and Martin, S.T. (2004). Role of molecular oxygen in the dissolution of siderite and rhodochrosite, *Geochim. Cosm. Acta* 68, 607-621.
- Hatches, 1991. Hatches-r10, database for radio chemical modelling. Tech. rep., NEA.
- Heath, T.G. and Tweed, C.J. (1999). A model for redox control in a cementitious repository, *Mat. Res. Soc. Symp. Proc.* 556, 1245-1252.
- Helferich, F. (1995). *Ion exchange*, Dover Publication, New York (USA).
- Köhler, S.J., Dufaud, F. and Oelkers, E.H. (2003). An experimental study of illite dissolution kinetics as a function of pH from 1.4 to 12.4 and temperature from 5 to 50°C, *Geoch. Cosm. Acta* 67(19), 3583-3594.
- Lagneau, V. (2003). R2D2 - Reactive Transport and Waterflow on an Odd Dimension 2 grid, Technical Report LHM/RD/03/05, Ecole des Mines de Paris (F).
- Neretnieks, I. (2006). Flow and solute transport in a zone damaged due to spalling, Technical Report R-06-91, SKB (S).
- Parkhurst, D.L., Kipp, K.L., Engesgaard, P. and Charlton, S.R. (2004). PHAST—A program for simulating groundwater flow, solute transport, and multicomponent geochemical reactions, U.S. Geological Survey, *Techniques and Methods* 6-A8, 154 p.
- Pearson, F.J., Berner, U. (1991). Nagra thermochemical data base: I. Core data. Report NTB 91-17, Nagra, Wettingen, Switzerland.
- Read, D., Glasser, F.P., Ayora, C., Guardiola, M.P., Sneyers, A. (2001). Mineralogical and microstructural changes accompanying the interaction of Boom Clay with ordinary Portland cement. *Adv. Cement Res.* 13(4), 175-183.
- Savage, D., Noy, D. and Mihara, M. (2002). Modelling the interaction of bentonite with hyperalkaline fluids. *Appl. geoch.* 17, 207-223.
- Trotignon, L., Michaud, V., Lartigue, J.E., Ambrosi, J.P., Eisenlohr, L., Griffault, L., de Combarieu, M. and Dumas, S. (2002). Laboratory simulation of an oxidizing perturbation in a deep granite environment, *Geochim. Cosm. Acta* 66, 2583-2601.

- SKB (2004). Interim process report for the safety assessment SR-Can, Technical Report R-04-33.
- SKB (2006). Lon-term safety for KBS-3 repositories at Forsmark and Laxemar - a first evaluation. Main report of the SR-Can project, Technical Report TR-06-09.
- van der Lee, J. and De Windt, L. (2002). CHESS Tutorial and Cookbook, Updated for Version 3.0, rapport ENSMP LHM/RD/02/13.
- van der Lee, J., De Windt, L., Lagneau, V. and Goblet, P. (2003). Module-oriented modeling of reactive transport with HYTEC. *Comp. Geosc.* 29, 265-275.
- van der Lee, J. (2005). Reactive transport modelling with HYTEC - Users guide and tutorial, Technical Report LHM/RD/05/30, Ecole des Mines de Paris (France).
- Wersin, P. (2003). Geochemical modelling of bentonite pore water in high level waste repositories, *J. Cont. Hydr.* 61, 405-422.
- Williamson, M.A. and Rimstidt, J.D. (1994). The kinetics and electrochemical rate-determining step of aqueous pyrite oxidation, *Geochim. Cosm. Acta* 58, 5443-5454.
- Wolery, T. (1992). EQ3/6, a software package for geochemical modelling of aqueous systems: package overview and installation guide, report UCRL-MA-110662 PT I, Lawrence Livermore National Laboratory (USA).

## APPENDIX

Summary table of the simulation results obtained in the present study

	Deponit CA-N	MX-80 (without carbonates)
Forsmark	<p>pH/pe tend to Forsmark values over 100,000 y.</p> <p>Exchangeable cation occupancy:</p> <p>Na : 24 % → 35 %</p> <p>Mg : 33 % → 13 %</p> <p>Ca : 41 % → 50 %</p> <p>Gypsum dissolves in 25,000 y and dolomite in 85,000 y.</p>	<p>pH reaches Forsmark values in 50,000 y.</p> <p>pe : -3.15 → -3.3</p> <p>Exchangeable cation occupancy:</p> <p>Na : 72 % → 35 %</p> <p>Mg : 8 % → 13 %</p> <p>Ca : 18 % → 50 %</p> <p>Gypsum dissolves in 5,000 y.</p>
Laxemar	<p>pH : 7.0 → 7.5 (7.9 close to the fracture);</p> <p>pe : -2.6 → -3.5</p> <p>Exch. cation occupancy:</p> <p>Na : 24 % → 35 %</p> <p>Mg : 33 % → 0 %</p> <p>Ca : 41 % → 65 %</p> <p>Siderite and dolomite dissolve whereas secondary calcite precipitates. Gypsum moderately dissolves, pyrite more stabilized.</p>	<p>pH: 7.0 → 7.0 (7.5 close to the fracture)</p> <p>pe: -3.15 → -3.3 (-3.6 near the fracture)</p> <p>Exch. cation occupancy:</p> <p>Na : 72 % → 36 %</p> <p>Mg : 8 % → 0 %</p> <p>Ca : 18 % → 64 %</p> <p>Gypsum and calcite do not precipitate after Laxemar groundwater intrusion in the buffer.</p>
Grimsel	<p>pH : 7.0 → 10 after 100,000 y (close to the fracture) ;</p> <p>pe : -2.6 → -6.5</p> <p>Exch. cation occupancy:</p> <p>Na : 24 % → 10-15 % (25,000 y)</p> <p>Ca : 41 % → 45-50 % (25,000 y)</p> <p>Gypsum completely dissolves in 20,000 y and dolomite dissolves in zones located 1.5 m from the fracture plane leading to calcite precipitation over 100,000 y.</p>	<p>pH : 7.0 → 8 (9.5 close to the fracture)</p> <p>pe : -3.15 → -4.5 (-5.9 close to the fracture)</p> <p>Exch. cation occupancy:</p> <p>Na : 72 % → 62 % (12 % close to the fracture)</p> <p>Mg : 8 % → 13 % (6 % close to the fracture)</p> <p>Ca : 18 % → 23 % (82 % close to the fracture)</p> <p>Gypsum dissolves in 5,000 y.</p>
	<p>Grimsel/Oxidative perturbation:</p> <p>pH reaches 10 after 100,000 y</p> <p>pe controlled by pyrite and siderite dissolution.</p> <p>Secondary Fe(OH)<sub>3</sub> precipitates.</p>	<p>Forsmark/Thermal stress (simulation over 1,000 y):</p> <p>pH : 6.9 → 6.5 ; pe : -3.6 → -3.2</p> <p>Exch. cation occupancy:</p> <p>Na : 72 % → 57 %</p> <p>Mg : 8 % → 13 %</p> <p>Ca : 18 % → 28 %</p> <p>Gypsum initially transforms into anhydrite at high temperature, which slightly precipitates in the warmer zones and dissolves in the cooler zones. Dolomite precipitates in the warmer zones and dissolves in the cooler zones.</p>

## ABSTRACT

Elements of the SR-Can project relative to piping and erosion phenomena of bentonite components of a KBS-3 repository are analysed with regard to the experience feedback available at IRSN and consisting in experimental results obtained on samples at the UJF-Grenoble between 2000 and 2004. A synthesis of these tests is presented, with a closer attention to the Argillite/Bentonite tests during which phenomena of erosion occurred. The reference evolution of a KBS-3 repository, the resaturation and swelling kinetics of backfills and buffers and the possibility for a buffer to swell upwards the backfill have been considered. According to the reviewed documents, IRSN notes that the SR-Can project tackles the piping and erosion phenomena with local modellings and “rough estimates”, the latter being based on 3 “key” parameters: the water inflow in an underground opening, the concentration of bentonite in pipe water and the duration of the phenomena. IRSN considers that the reviewed elements do not evidence enough the conservatism of the parameters value, especially for the duration of the phenomena. Additional experimental results, at small and large scale, may be necessary.



# TABLE OF CONTENTS

<b>1 INTRODUCTION.....</b>	<b>82</b>
<b>2 CONDITIONS OF APPEARANCE OF EROSION .....</b>	<b>82</b>
2.1 HYDRO-MECHANICAL BEHAVIOUR OF CONTACT INTERFACES BETWEEN DIFFERENT MATERIALS.....	82
2.2 ROCK/MORTAR TESTS.....	82
2.3 ARGILLITE/BENTONITE TESTS .....	83
<b>3 PIPING AND EROSION OF BUFFER AND BACKFILL IN THE SR-CAN PROJECT .....</b>	<b>84</b>
3.1 REFERENCE EVOLUTION .....	84
3.2 RESATURATION AND SWELLING KINETICS OF BACKFILL AND BUFFER.....	84
3.3 PIPING AND EROSION OF BUFFER AND BACKFILL .....	85
<b>4 CONCLUSION .....</b>	<b>87</b>
<b>REFERENCES .....</b>	<b>89</b>

# **1 INTRODUCTION**

Between 2000 and 2004, IRSN studied the hydro-mechanical behaviour and the evolution of the hydraulic transmissivity of contact interfaces between different materials possibly involved in the sealing of an underground geological repository. A lot of tests have been performed by “Université Joseph Fourier” of Grenoble (UJF). A synthesis of the experimental results, with a closer attention to the Argillite/Bentonite tests for which phenomena of erosion could be observed, is presented in chapter 2. In chapter 3, IRSN has assessed the phenomenological issues related to the piping and erosion of buffer and backfill presented by SKB in the TR-06-09 report, chapters 9.2.4, 9.3.8 and 9.3.9, with the support of the experience feedback obtained through the above mentioned tests when relevant. IRSN has also put in perspective these issues and the associated remaining uncertainties with regard of the development of long term evolution scenarios presented by SKB in chapters 10, 11 and 12. IRSN underlines that its conclusions presented in chapter 4 are drawn from a restricted number of chapters analysed in the TR-06-09 report. Some remarks drawn by IRSN may thus require a more in depth discussion with SSI/SKI and SKB in order to possibly account for additional information that could better highlight some aspects of the review.

## **2 CONDITIONS OF APPEARANCE OF EROSION**

### **2.1 HYDRO-MECHANICAL BEHAVIOUR OF CONTACT INTERFACES BETWEEN DIFFERENT MATERIALS**

The tests performed at UJF consisted in tightening one against the other two pieces of various materials with the use of a press and to assess the evolution of the hydraulic transmissivity of the interface versus the applied normal stress. The purpose of the normal stress applied was to simulate the differed convergence of an excavation around a sealing plug or the inflation of a swelling core. The press used, a direct shear box (see Buzzi *et al.* (2006), Figure-1), is normally used to study rock joints. Regarding normal stress, its ability is of 100 kN on a sample of about 63 mm diameter. An associated hydraulic device can inject water up to 20 MPa of water pressure but in practice, the tests were limited to about 8 MPa of water pressure because of leaktighness difficulties. The injection hole of water is located in the middle of the sample and is about 5 mm diameter (Buzzi *et al.* (2006), Fig-5).

### **2.2 ROCK/MORTAR TESTS**

A first campaign of tests was performed on Rock/Mortar interfaces. The rock was an Argillite of the Toarcian age from the IRSN site of Tournemire. It has a clay fraction of 70 % (kaolinite, illite, smectite...), is nearly saturated in its natural state and is highly anisotropic. Because it seemed difficult to introduce graves into such small samples, a mortar was preferred to a concrete; it was a Rapidex 712 Mortar from Lanko. The influence of parameters such as the orientation of the bedding of the Argillite part of the sample, the orientation of the mortar pouring... was studied. Since the tested interfaces were true contacts of Argillite and Mortar and not replicas, the comparison of results could have been affected by a difference of initial roughness between different samples. This difficulty was solved by creating an artificial but reproducible roughness. Regular grooves were made on the Argillite part of the sample by hand, with the use of a saw, before creating the interface. This first campaign showed that among the studied parameters, the transmissivity of an interface was mostly affected by a relative initial lateral

displacement of the two parts of a sample. Such a lateral offset limits the aperture reduction and reduces the ability of the interface to close hydraulically. These results are described with more details in (Buzzi *et al.*, 2007).

## 2.3 ARGILLITE/BENTONITE TESTS

A second campaign has been performed on Argillite/Bentonite interfaces, on which focus is given hereafter. The results are detailed in Buzzi *et al.* (2006). Very few tests of this type were found in the literature. The bentonite being much less stiff than the rock and very water sensitive, this campaign was more difficult to carry on.

A special membrane, made of aluminium for mechanical purposes and elastomer to prevent leakage, had to be designed for the tests (Buzzi *et al.* (2006), Fig-3). Such a membrane maintains the bentonite in quasi oedometric conditions and allows water collection. The mechanical properties of the membrane, settled between the two parts of the sample, had to be characterised before the tests to be accounted for into the mechanical analysis of the results of the tests.

The Argillite was the same as previously described, from the IRSN site of Tournemire. The bentonite was a natural calcic bentonite FZ0 from BentoFrance, with 70-80 % of montmorillonite, 12-15 % of illite, 4-5 % of kaolinite, 2-5 % of calcite and 2-5 % of quartz. Bentonites mixed with sands or crushed rocks are often considered as potential materials for the engineered barriers or backfills of underground geological repositories. This campaign was especially dedicated to study the influence of the mixture composition on the hydraulic transmissivity of the interface. A first test (7BR90) evidenced that if both bentonite and Argillite were initially smooth, no water flow is detectable, even for high water injection pressure. An artificial but reproducible roughness was made by hand on the rock part of the sample with the use of a small saw (Buzzi *et al.* (2006), Fig-5). Thus, the water flow was localised into a groove and was not isotropic.

Different mixtures, with a mass fraction of bentonite ranging from 50 % to 90 %, were prepared for the bentonite part of the samples. The additives were sand and crushed rock. The mixtures were composed at the optimum water content. Bentonite/cement mixtures were also investigated but their behaviour quickly appeared to be different from the behaviour of mixtures with inert additives, the cement creating brittle bonds turning the mixture into a quasi brittle material, even for low cement contents.

A typical result obtained with a bentonite/inert-additive mixture (sand or crushed rock) is presented in Buzzi *et al.* (2006), Fig-8. The intrinsic transmissivity of the interface decreases with the increase of the normal stress applied and below  $10^{-16} \text{ m}^3$ , the interface was considered as closed. This happens for all the tests for a normal stress value between 3 and 5 MPa, which is low compared to rock joints or rock/mortar interfaces where about 10 MPa were needed for the same result. Cycles 1 and 2 in Buzzi *et al.* (2006), Fig-8 also show that the interface does not reopen immediately when the normal stress decreases. To continue the test beyond the closure of the interface (cycle 3 in Buzzi *et al.* (2006), Fig-8), the water pressure was increased till the water flows again, which damaged the interface (see Buzzi *et al.* (2006), Fig-13b). Thereafter, the behaviour of the interface was the same as for the previous cycles and for all the tests, closure of the interface occurred again for higher values of normal stress applied, even after one or two such degradations.

Many studies carried on the mechanical or hydraulic behaviour of bentonite mixtures show that the bentonite content can affect the properties of the mixture. However and so long the additive is inert (sand or crushed rock), the tests performed at UJF do not show any major effect of the composition of the bentonite part of the sample on the intrinsic transmissivity of the interface. Also, no modification of the argillite part of the samples due to the water flow was observed, maybe because of the short duration of the tests. On the opposite, the tests evidenced that the bentonite part of the samples was very sensitive to water within the interface zone (all the bentonite parts of samples were damaged by water during the tests) and that the initial transmissivity of an interface depends a lot on the initial pressure and flow rate of the water.

## **3 PIPING AND EROSION OF BUFFER AND BACKFILL IN THE SR-CAN PROJECT**

### **3.1 REFERENCE EVOLUTION**

The TR-06-09 report, chapter 12.3, indicates that the main function of the buffer is to prevent advective transport and to ensure that diffusion will be the dominant mechanism of transport. The ability of the buffer to assume this function mainly depends on its density, which may decrease during the buffer saturation due to piping/erosion, buffer expansion into the deposition tunnel or during glacial conditions due to colloid release/erosion process. SKB indicates that the colloid release/erosion process *“is poorly understood”, “has by far the highest impact on density in the reference evolution and [...] is the only factor that causes any considerable alteration of buffer density over the one million year assessment period”*.

The reference evolution considers that some tens of canisters fail during the one million year assessment period due to buffer colloid release/erosion leading to buffer advection and thus enhanced corrosion. From the analysis of this reference evolution, SKB concludes *“that the buffer is expected to function as intended until intruded by dilute glacial groundwater, after which there is little confidence that advection is prevented in many of the deposition holes. After several glaciations, there is little confidence that advection is prevented in any deposition holes. Thus, the main consideration is corrosion rates post-glaciation in the full set of deposition holes”*.

### **3.2 RESATURATION AND SWELLING KINETICS OF BACKFILL AND BUFFER**

The TR-06-09 report, chapter 4.2.5, indicates that the copper canisters are placed into buffers made of blocks of bentonite settled into deposition holes. *“SKB has not made a final selection of a buffer material”* but two materials, a Na-bentonite (MX80 type) and a Ca-bentonite (Deponit CA-N), are mentioned. Chapter 4.2.7 indicates that the backfill of the deposition tunnels would be made of precompacted blocks and that pellets would fill the remaining gaps. Two materials are considered for the backfill: a natural swelling clay (e.g. Friedland clay) associated with pellets of the same material or a mixture of the bentonite selected for the buffer with crushed rock (30/70) associated with bentonite pellets. Accounting for the allowed variations in density, chapter 4.2.8 indicates that the swelling pressure of the buffer may vary between 4.5 MPa and 13 MPa. Chapter 9.3.9 indicates a value *“slightly above 3 MPa”* for the backfill. Since the water for wetting is mainly coming through fractures, the delays for reaching saturation depend on the site. The expected saturation times are (TR-06-09, chapter 9.3.8):

- At Forsmark: 6-8 years for the 30/70 mixture and 40-50 years for Friedland clay for the backfills; 10 years to 50-100 years for the buffers.
- At Laxemar: 2-3 years for the 30/70 mixture and ~20 years for Friedland clay for the backfills; ~10 years for the buffers.

The TR-06-09 report, chapter 9.3.8, indicates that “*the tunnel backfill will generally become saturated faster than the buffer*” and chapter 9.3.9 mentions as “*additional*” and “*unlikely*” the case where “*the buffer swells before the backfill*”. SKB mentions that in that case, “*the [buffer] upward swelling may be more complicated and difficult to calculate*”. IRSN notes that the saturation kinetics mentioned above do not draw completely aside the possibility for a buffer to saturate before the backfill. Moreover, IRSN considers that heterogeneous rehydration of backfill and buffer (in space and time) can not be ruled out. Its consequence on swelling kinetic of both components and on their confinement properties should be further investigated as mentioned by TR-06-09, chapter 10.5.7. As a consequence, IRSN believes that the buffer upward swelling possibility may have been better accounted for in the derivation of the long term evolution scenarios as it is in chapter 12.3.1.

### 3.3 PIPING AND EROSION OF BUFFER AND BACKFILL

IRSN notes that piping and associated erosion was observed at Äspö HRL in the “*Long Term Test of Buffer Material*” (LOT) and the “*Large Scale Gas Injection Test*” (Lasgit). Regarding the “*calcic*” or “*sodic*” nature of the bentonite, (Push, 1983) indicates that “*Na-bentonite clay that propagates through the rock joints should be very sensitive to erosion*” and the tests performed at UJF evidenced that the zones in contact of a calcic bentonite with a rock are also very sensitive to erosion, whatever the mass fraction of sand or crushed rock (see Buzzi *et al.* (2006), Fig-13). The UJF samples were prepared at the optimum water content and compacted two times at 6 MPa.

The TR-06-09 report, chapter 9.2.4, proposes rough estimates of the mass loss of buffers and backfills due to piping/erosion phenomena and considers that these losses are small compared to the initial deposited masses (less than 1%). IRSN notes that these estimates directly depend on 3 “*key*” parameters:

1. A typical water inflow in a “*wet*” underground opening. For the rough estimates, SR-Can considers:
  - 0.1 litre/minute for the deposition holes, this value being “*an above average [...] at Äspö and a high inflow at Forsmark*”. Chapter 12.3.2 presents this value as the limit over which “*the buffer will not be able to seal and a channel (pipe) will be formed*”. SR-Can adds that grouting is required to achieve water flows less than 0.1 l/min;
  - 1 litre/minute for a “*wet deposition tunnel section corresponding to one deposition hole*”.

IRSN considers that the conditions of appearance of erosion are not necessary limited to a value of maximal water inflow but could also depend on other parameters such as the exact composition and form (blocks, pellets...) of the materials, the chemical nature of the groundwater (Push, 1983), other hydro-geological parameters, *etc.* Experiments are necessary to clarify these conditions and may possibly lead to improve the acceptance criteria of the different devices of a repository.

2. The concentration of bentonite in pipe water. Chapter 9.2.4 considers 10 g/l as “a *pessimistic maximum value*” since it would be “*an upper value observed in the very early stage of piping experiments*”. However, chapter 12.3.2 mentions an uncertainty of about a factor “*two up or down*”. IRSN notes that the considered value may thus be not conservative and considers that this value may depend on other parameters as already evoked at the previous point. Experiments, at small or large scale, under conditions as close as possible of expected ones, will certainly be required to precise the concentration of bentonite in pipe water.
3. A rough estimate of duration. SR-Can supposes that the erosion stops when the hydrostatic pressure is restored in a tunnel section and considers 100 days as a rough estimate. IRSN points out that this assumption supposes that the natural hydraulic pressures of the site do not lead to erode the bentonite components on the long term. IRSN also underlines that the duration of 100 days to restore the hydrostatic pressures is unclear because of its apparent contradiction with the saturation duration reminded above (i.e. several tens to hundreds of years). IRSN agrees when SKB mentions (chapter 12.3.2) that “*the time it takes to restore the hydraulic pressure in the tunnel*” is a “*key uncertainty*”. As a consequence, IRSN considers that SKB should better justify the estimation of the duration of erosion phenomena.

Regarding the backfill, the TR-06-09 report, chapter 9.2.4, indicates that “*piping is more likely to occur [...] since it is more likely to be intersected by fractures with sufficiently high water flow*”. IRSN underlines that the backfill near the rock face is filled with low density pellets and in touch with a potential “Excavation Damaged Zone” (EDZ) where the flow rate may be affected. SR-Can adds that “*the swelling pressure of the backfill will never be sufficiently high to resist the 5 MPa difference in water pressure between the groundwater in the rock and the open repository. Instead, the water inflow may not be stopped until a water tight plug is placed at the end of the tunnel and full water saturation is reached in the backfill*”. IRSN notes that the steadiness of the backfill relies on the time necessary to restore a hydrostatic pressure. IRSN considers that this time will also depend on the behaviour of the plugs closing the deposition tunnels. There will be a competition between the kinetics of erosion of the engineered barriers and their swelling, influencing the global hydro-geological behaviour of the repository. The study of the ability for the plugs and buffers to withstand piping/erosion during this time is thus of first importance. IRSN considers that numerical simulations of these coupled phenomena can quickly become very complex and that *in situ* experiments are certainly necessary to increase the confidence in the modelling.

The rough estimates mentioned here above only address the “global” aspect of erosion. The TR-06-09 report indicates that “*however, the loss [of mass] will occur locally close to the point of water inflow*” and provides a calculation (Börgesson and Hernelind, 2006) that considers the hole eroded into a buffer by 12 weeks of localized water inflow and shows that the buffer can clog the hole and locally restore, in front of the fracture, a swelling pressure of 2 MPa after 2.2 years (see TR-06-09, fig. 9-53). IRSN underlines that this calculation does not show that the erosion would stop because of the bentonite penetration into the fracture (which would stop the water inflow) but supposes that the erosion stops after 12 weeks because of the gradients restoration. IRSN also points out that the 2.2 years needed by the buffer to clog the hole and restore a swelling pressure in front of the fracture is much longer than the considered duration of erosion (12 weeks). Consequently, IRSN considers that this calculation is not completely convincing.

IRSN agrees that the modelling of the swelling and penetration of bentonite into a fracture simultaneously with its erosion is a very difficult concern. To illustrate it, IRSN refers to the calculations carried out in (Buzzi, 2006) to interpret the tests performed at the UJF. The Fig-17 in Buzzi *et al.* (2006) shows the mesh used for the mechanical study of a few millimetres of sample. It is refined up to 3688 elements to permit large strain calculations. The Fig-19 in Buzzi *et al.* (2006) shows the simulated penetration of the bentonite into a groove with respect to the normal stress applied on the sample. Parameters as clay/rock frictional coefficients are accounted for. From these mechanical results, the free spaces remaining for the water flow are assessed and meshed for hydraulic calculations (from 160000 to 650000 elements). The Fig-20 in Buzzi *et al.* (2006) shows that simulated and experimental results are very close, so long erosion is negligible. To account for erosion, its mechanism has to be understood. It is generally admitted that in presence of water, the bentonite forms a "gel" which is supposed to behave as a Bingham fluid. The water flow erodes it if the shearing stress due to the water flow on the gel exceeds a certain limit. The calculations mentioned in Buzzi *et al.* (2006), performed till the limits of appearance of erosion, suggest a "limit shear" ranging from 350 Pa to 550 Pa for these tests (Buzzi, 2004). Measures performed on the samples indicated a water content of the gel ranging from 150 % to 200 % (for a bentonite which Atterberg liquid limit  $W_L \approx 120$  %). For comparison, Pusch (1983) obtains, with another bentonite and experimental device, values ranging from about 900 Pa for 500 % of water content till 1700 Pa for 300 %, depending on the nature of the fluid. On a Laponite bentonite, Buzzi (2004) mentions values ranging from 20 to 1000 Pa. Indeed, the value of the "limit shear"  $\tau_L$  depends on the exact nature of the bentonite, the water composition, the water content of the gel, *etc.* The previous mentioned orders of magnitude illustrate the high variability of this very influent parameter.

As a consequence, considering the complexity of the evoked phenomena, IRSN considers that the SKB approach using rough estimates to tackle the "global" aspect of the problem is relevant in a first approach. IRSN underlines that the results directly depend on 3 "key" parameters (maximal water inflow, bentonite concentration in pipe water and duration), which conservatism could be better justified, notably regarding the duration of the phenomena. Experiments, at small or large scale, under conditions as close as possible of actual ones, will certainly be necessary. Regarding the "local" aspects of the problem, IRSN considers that the coupled modelling of swelling, penetration into a fracture and erosion of a bentonite can quickly become very complicated. Experimental validations are necessary to enhance confidence in the modelling. At last, the question of the duration of the phenomena could bring in the hydro-geological behaviour of the site, which would require a large scale experiment so as to be convincing.

## **4 CONCLUSION**

In the first instance, IRSN emphasises that, in the TR-06-09 report, SKB presents a relevant compilation of processes and related uncertainties associated with the erosion and piping of backfill and buffer components. Possibility for buffer expansion into the deposition tunnel is also addressed. IRSN notes that the lack of knowledge and further investigations to be performed are listed by SKB in various chapters and especially in the chapters 9.2, 9.3, 9.4 and 10. SR-Can project proposes simplified modelling of the combined piping and erosion processes which is a satisfactory first approach, given both the complexity of the above phenomena and the associated remaining uncertainties at this stage of the SR-Can project. But IRSN considers that those rough estimates rely on

combination of rather “idealistic” hydration processes (in time and space) and estimation of “key” parameters values that do not really reflect the uncertainties mentioned by SKB itself. IRSN observes an apparent discrepancy between the description of the processes and related uncertainties in chapter 9 and their treatment in the long term evolution scenarios. The reasons for ruling out some perturbations should be better explained. More precisely, IRSN believes that at this feasibility stage of the SR-Can project, the treatment of mechanical perturbations due to buffer expansion and erosion in long term evolution scenarios may have been more conservative in order to account for remaining uncertainties. In a further stage considering progress achieved in characterisation and process understanding and/or modelling, long term scenario would be possibly derived in a less conservative manner, i.e. more realistic and providing safety margins.

IRSN believes also that several points may be better detailed in the next SR-Site project which concern:

- the influence of heterogeneous (in time and space) resaturation of backfill and plugs (at the end of backfilled tunnels) on the conditions required for stopping the piping and erosion processes,
- the influence of heterogeneous (in time and space) resaturation of backfill and buffer on swelling behaviour of those components and their resulting long term containment properties,
- the intensity and duration of the erosion and piping considering repository hydrogeological conditions and coupling with swelling.

## REFERENCES

Buzzi, O. (2004): Hydromécanique du contact entre géomateriaux. Expérimentation et modélisation. Application au stockage de déchets nucléaires. Thèse, Université Joseph Fourier, Grenoble, France.

Buzzi, O., M. Boulon, F. Deleruyelle, F. Besnus (2006): Hydromechanical Behaviour of Rock-Bentonite Interfaces Under Compression. *Rock Mechanics and Rock Engineering*, DOI 10.1007/s00603-006-0099-2.

Buzzi, O., J. Hans, M. Boulon, F. Deleruyelle, F. Besnus (2007): Hydromechanical study of rock-mortar interfaces. *Physics and Chemistry of the Earth* 32 (2007) 820-831.

SKB TR-06-09: "Long-term safety for KBS-3 repositories at Forsmark and Laxemar - a first evaluation", Sweden.

Pusch, R. (1983): Stability of bentonite gels in crystalline rock - physical aspects. Technical Report TR-83-04, SKB, Sweden.



**2008:01 Myndigheternas granskning av SKB:s preliminära säkerhetsbedömningar för Forsmark och Laxemar**

Avdelningen för kärnteknik och avfall och SKI  
Maria Nordén, Övind Toverud, Petra Wallberg, Bo Strömberg, Anders Wiebert, Björn Dverstorp, Fritz Kautsky, Eva Simic och Shulan Xu 90 SEK

**2008:02 Patientstråldoser vid röntgendiagnostik i Sverige – 1999 och 2006**

Avdelningen för personal- och patientstrålskydd  
Wolfram Leitz och Anja Almén 110 SEK

**2008:03 Radiologiska undersökningar i Sverige under 2005**

Avdelningen för personal- och patientstrålskydd  
Anja Almén, Sven Richter och Wolfram Leitz 110 SEK

**2008:04 SKI:s och SSI:s gemensamma granskning av SKB:s Säkerhetsrapport SR-Can Granskningsrapport**

Avdelningen för kärnteknik och avfall  
Björn Dverstorp och Bo Strömberg 110 SEK

**2008:05 SKI:s Expert Evaluation of the Swedish Nuclear Fuel and Waste Management Company's Safety Assessment SR-Can –Report of the Safety Assessment Methodology Review Team**

Avdelningen för kärnteknik och avfall  
Budhi Sagar, et. al 110 SEK

**2008:06 Review of SKB's Safety Assessment SR-Can: –Contributions in support of SKI's and SSI's review by external consultants**

Avdelningen för kärnteknik och avfall  
Pierre Glynn et. al. 110 SEK

**2008:07 Modelling of long term geochemical evolution and study of mechanical perturbation of bentonite buffer of a KBS-3 repository**

Avdelningen för kärnteknik och avfall  
François Marsal, Laurent de Windt, Delphine Pellegrini, Frédéric Deleruyelle and Christophe Serres 110 SEK



**STATENS STRÅLSKYDDSinSTITUT, SSI**, är en central tillsynsmyndighet som verkar för ett gott strålskydd för människan och miljön, nu och i framtiden.

SSI sätter gränser för stråldoser till allmänheten och för dem som arbetar med strålning, utfärdar föreskrifter och kontrollerar att de efterlevs. SSI håller beredskap dygnet runt mot olyckor med strålning. Myndigheten informerar, utbildar och utfärdar råd och rekommendationer samt stöder och utvärderar forskning. SSI bedriver även internationellt utvecklingsarbete.

Myndigheten, som sorterar under Miljödepartementet, har 110 anställda och är belägen i Solna.

**THE SWEDISH RADIATION PROTECTION AUTHORITY (SSI)** is a central regulatory authority charged with promoting effective radiation protection for people and the environment today and in the future.

SSI sets limits on radiation doses to the public and to those that work with radiation. SSI has staff on standby round the clock to respond to radiation accidents. Other roles include information, education, issuing advice and recommendations, and funding and evaluating research.

SSI is also involved in international development cooperation. SSI, with 110 employees located at Solna near Stockholm, reports to the Ministry of Environment.



*Statens strålskyddsinstitut*  
Swedish Radiation Protection Authority

**Address:** Statens strålskyddsinstitut; S-171 16 Stockholm

**Besöksadress:** Solna strandväg 96

**Telefon:** 08-729 71 00, **Fax:** 08-729 71 08

**Address:** Swedish Radiation Protection Authority  
SE-171 16 Stockholm; Sweden

**Visiting address:** Solna strandväg 96

**Telephone:** + 46 8-729 71 00, **Fax:** + 46 8-729 71 08

[www.ssi.se](http://www.ssi.se)